# FAULT DIAGNOSIS SCHEMES FOR THREE-PHASE INDUCTION MOTOR

Thesis submitted in partial fulfillment of the requirements
for the award of the degree of

**DOCTOR OF PHILOSOPHY**
**IN**
**ELECTRICAL ENGINEERING**

by

**NEERUKONDA RAMA DEVI**

**Roll No. 700813**

**Supervisor**

**Prof. D. V. S. S. Siva Sarma**


**DEPARTMENT OF ELECTRICAL ENGINEERING**
**NATIONAL INSTITUTE OF TECHNOLOGY**
**WARANGAL-506004**
**TELANGANA, INDIA**
**JANUARY 2017**

Department of Electrical Engineering

National Institute of Technology

Warangal


# CERTIFICATE

This is to certify that the present dissertation work entitled **"Fault Diagnosis Schemes for Three-Phase Induction Motor"** which is being submitted by Smt. Neerukonda Rama Devi (Roll No. 700813), is a bonafide work submitted to National Institute of Technology, Warangal in partial fulfilment of the requirement for the award of the degree of Doctor of Philosophy in the Department of Electrical Engineering. To the best of my knowledge, the work has not been submitted elsewhere for the award of any degree.

Dr. D. V. S. S. Siva Sarma
(Supervisor)
Professor
Department of Electrical Engineering
National Institute of Technology
Warangal - 506004
Telangana, India.

# Approval Sheet

This Thesis entitled **"Fault Diagnosis Schemes for Three-Phase Induction Motor"** by NEERUKONDA RAMA DEVI is approved for the degree of Doctor of Philosophy.

Examiners

_____

_____

_____

Supervisors

_____

_____

_____

Chairman

_____

Date:_____-

# Declaration

This is to certify that the work presented in the thesis entitled **"Fault Diagnosis Schemes for Three-Phase Induction Motor"** is a bonafide work done by me under the supervision of **Prof. D. V. S. S. Siva Sarma** and was not submitted elsewhere for the award of any degree.

I declare that this written submission represents my ideas in my own words and where others' ideas or words have been included, I have adequately cited and referenced the original sources. I also declare that I have adhered to all principles of academic honesty and integrity and have not misrepresented or fabricated or falsified any idea / data / fact / source in my submission. I understand that any violation of the above will be a cause for disciplinary action by the Institute and can also evoke penal action from the sources which have thus not been properly cited or from whom proper permission has not been taken when needed.

(Signature)

**N. Rama Devi**

(Name of the student)

(Roll No: 700813)

Date: 11/01/2017

*Dedicated to*

***my teachers, who taught me***

***and***

***my family, who taught me as well***

# Acknowledgements

To begin with, I am grateful to the Almighty for everything destined for me. I am indebted deeply to my parents for all the sacrifice they have made for nurturing me during my formative years and throughout my career. I am equally indebted to my husband, my lovely children, my mother-in-law and my father-in-law for their untiring care and unwithered affection for me.

I am ever grateful to **Prof. D. V. S. S. Siva Sarma**, my research supervisor; but for his unreserved help and support this thesis work couldn't have come to submission. He has been a constant source of inspirational guidance. I am indebted to the academic discipline and scholastic patience he has brought to bear while dealing with me and my endeavor.

I express my sincere thanks to **Prof. P. V. Ramana Rao**, my previous guide, for his support and care during the course of my Ph.D. work.

I wish to acknowledge my sincere gratitude to DSC members **Prof. N. Viswanathan**, Head of the Department, **Prof. B. K. Murthy** and **Dr. C. B. Rama Rao** for their help, feedback, cooperation and encouragement during the course of my Ph.D. work. I also thank all my teachers and other faculty members of Department of Electrical Engineering for their help and support in my efforts. I would like to express my sincere thanks to my fellow research scholars **Mr. Varma, Mr. Vara Prasad, Smt. Pujitha** and all others for their support.

I thank **Sri M. Seshagiri Rao, President, Bapatla Education Society**, for his dynamic leadership and for promoting research activities in the campus of Bapatla Engineering College. Thanks are also due to the other members of the governing body and the management committee for their

supporting role. I would like to thank our principal **Prof. N. Sudhakar**, for all his endeavors in grooming the college and for creating good academic ambience on the campus.

I am deeply indebted to all the **faculty and staff** of the Department of Electrical and Electronics Engineering, Bapatla Engineering College who have been with me all the time encouraging. I would also like to profusely thank all the other faculty and staff of the college who directly or indirectly made my stay at the college successful, happy and enjoyable.

This thesis was typeset with LaTeX* by the author

*LaTeXis a document preparation system developed by Leslie Lamport as an extension of Donald Knuth's TeX typesetting system.

# Abstract

With the advent of power electronics devices, the usage of ac motors, particularly, induction motors in variable speed drives have increased due to flexible speed control strategy. Majority of industrial drives are driven by induction motors because of its ruggedness and less maintenance. Motors experience various abnormal operating conditions that lead to their failure. These failures not only damage the equipment, but also severely interrupt to the processes involved in the industry, causing revenue loss. Thus, the detection and diagnosis of fault condition at the inception stage is of great practical significance. In general, fault diagnosis schemes concentrate on sensing specific failure modes in one of three induction motor components i.e. stator, rotor and bearings. One of the most difficult problem related to three-phase induction motors is the identification of stator incipient faults at the time of inception. These faults usually starts with winding insulation failure, which occurs due to overheating, thermal stress, insulation deterioration etc. In particular, an undetected stator inter-turn fault may progressively lead to a line to ground fault in the stator winding. Hence, early detection of stator inter-turn fault is essential for improving motor reliability, to reduce the cost of breakdown and to avoid catastrophic failures of motors. For these reasons, there has been a

continually increasing interest in the area of fault detection and diagnosis of induction motor. Both technical and economical consideration necessitates the development of a new computer-based diagnostic system to detect, classify, identify and locate the faults through condition monitoring. Typically, sensors are added to motors to detect specific faults, which include thermal and proximity sensors for bearing failures, accelerometers for vibrations, etc. An ideal diagnostic procedure should take the minimum measurements needed from a machine and by analysis extract a feature, so that its condition can be inferred to give a clear indication of incipient failure modes in minimal time. In this thesis the condition monitoring of induction machines have been carried out by using three phase currents which are typically available at motor control centre.

From the perspective of long-term research on the fault diagnosis of electrical machines, it appears that recent focus has been on the use of signal processing and artificial intelligent in order to improve the performances of traditional model-based methods. An effective algorithm should be able to take variations in fault signature amplitude, line current noise level, frequency offset, and phase offset into consideration to avoid missing or false alarms. Still there is no on-line monitoring method widely applied in industries and accepted in the motor fault diagnosis community. Hence, the development of any on-line monitoring method should be capable of diagnosing various faults and detection of deterioration of the inter-turn insulation prior to a fault besides being cost effective. In this thesis two fault detection algorithms are presented for low voltage induction motors based on Discrete Wavelet Transform and Stationary Wavelet Transform for detection of various stator winding faults and

supply side faults. To classify various disturbances, identify the stator winding insulation faults and severity level of stator inter-turn fault, two types of classification algorithms are presented based on feed forward neural network and modular neural network.

# Table of Contents

**Certificate** ii

**Approval Sheet** iii

**Declaration** iv

**Dedication** v

**Acknowledgements** vi

**Abstract** viii

**List of Figures** xvi

**List of Tables** xxix

**List of Abbreviations and Symbols** xxxi

**1 Introduction** 1

1.1 Overview . . . . . 1

1.2 Literature Survey on Fault Diagnosis . . . . . 6

1.2.1 Model Based Methods . . . . . 7

1.2.2 Model-Free Methods . . . . . 10

1.2.2.1 Signal Monitoring Methods . . . . . 10
1.2.2.2 Signal Analysing Methods . . . . . 11
1.2.2.2.1 Time Domain Analysis: . . . . . 12
1.2.2.2.2 Frequency Domain Analysis: . . 12
1.2.2.2.3 Time-Frequency Domain Analysis: . . . . . 13
1.2.3 Classification Methods . . . . . 15
1.3 Summary of Various Monitoring Techniques . . . . . 16
1.4 Motivation . . . . . 18
1.5 Contributions . . . . . 20
1.6 Organization of the Thesis . . . . . 22

**2 Modelling of Stator Winding in 3-Phase Induction Motor for Fault Diagnosis-Validation 24**

2.1 Introduction . . . . . 24
2.2 Modelling of 3-phase Induction Motor . . . . . 24
2.3 Distributed Model Parameters . . . . . 27
2.3.1 Stator First Turn Leakage Inductance ($\eta\ L_{ls}$): . . . . 27
2.3.2 Total Stator to Frame Capacitance per Phase ($C_{sf-total}$): . . . . . 27
2.3.3 Stator Turn to Turn Winding Capacitance ($C_{sw}$): . . . 29
2.3.4 Stator Turn to Turn Damping Resistance in Winding ($R_{sw}$): . . . . . 29
2.3.5 Stator Initial Frame to Ground Damping Resistance ($\mu Rs$): . . . . . 30
2.4 Experimental Setup for DM and CM Test . . . . . 30

2.5 Estimation of Parameters . . . . . 33
2.6 Model Validation . . . . . 36
2.7 Conclusions . . . . . 41

**3 Fault Detection Schemes** **42**
3.1 Introduction . . . . . 42
3.2 Various Stator and Supply Side Faults in a 3-Phase Induction Motor . . . . . 42
3.2.1 Stator Faults . . . . . 43
3.2.2 Unbalanced Supply . . . . . 44
3.2.3 Single-Phasing . . . . . 45
3.2.4 Under Voltage . . . . . 46
3.3 Wavelet Transform . . . . . 46
3.3.1 Discrete Wavelet Transform (DWT) . . . . . 48
3.3.2 Stationary Wavelet Transform (SWT) . . . . . 49
3.4 Proposed Fault Detection Scheme using DWT . . . . . 51
3.4.1 Validation of Proposed Fault Detection Scheme using DWT . . . . . 52
3.5 Proposed Fault Detection Scheme using SWT and DWT . . 63
3.5.1 Validation of Proposed Detection Scheme . . . . . 73
3.5.1.1 Experimental Setup . . . . . 73
3.5.1.2 Simulation Models for Stator Faults . . . . 73
3.5.1.3 Experimental and Simulation Results for a 3-hp Induction Motor . . . . . 77

3.5.1.4 Comparison between Experimental and Simulation Results for a 3-hp Induction Motor . . . . . 91
3.5.1.5 Experimental Results for a 10-hp Induction Motor . . . . . 93
3.6 Conclusions . . . . . 99

**4 Classification of Various Disturbances of a 3-Phase Induction Motor Using Wavelet and Modular Neural Network 100**
4.1 Introduction . . . . . 100
4.2 Features for Disturbance Classifier . . . . . 101
4.3 ANN Structures for Disturbance Classifier (ANN-1) . . . . . 112
4.3.1 Training and Testing of ANN based Disturbance Classifier . . . . . 114
4.4 MNN Structure for Disturbance Classifier(MNN-1) . . . . . 118
4.4.1 Training and Testing of MNN based Disturbance Classifier . . . . . 119
4.5 Comparison of Performance between ANN-1 and MNN-1 . 120
4.6 Conclusions . . . . . 121

**5 Classification of Stator Phase Faults 123**
5.1 Introduction . . . . . 123
5.2 Extraction of features for phase fault classification . . . . . 123
5.3 ANN structure for phase fault classifier (ANN-2) . . . . . 128
5.3.1 Training and Testing of ANN-2 . . . . . 129
5.4 MNN structure for phase fault classifier (MNN-2) . . . . . 131
5.4.1 Training and Testing of MNN-2 . . . . . 131

5.5 Comparison of performance between ANN-2 and MNN-2 for stator phase fault classification . . . . . 132
5.6 Conclusions . . . . . 133

**6 Identification of Faulty Phase and Estimation of Severity Level for Stator Inter-Turn Faults 135**
6.1 Introduction . . . . . 135
6.2 Features used for identification of faulty phase and estimation of fault severity . . . . . 136
6.3 Proposed ANN based classifier for identification of faulty phase and estimation of fault severity of stator inter-turn faults 143
6.3.1 Training and testing of the proposed ANN based method (ANN-3) . . . . . 144
6.4 Proposed MNN based classifier for identification of faulty phase and estimation of fault severity of stator inter-turn faults 146
6.4.1 Training and testing of the proposed MNN based classifier (MNN-3) . . . . . 147
6.5 Comparison of performance between ANN-3 and MNN-3 for fault classification . . . . . 149
6.6 Conclusions . . . . . 150

**7 Conclusions and Future Scope 151**
7.1 Conclusions . . . . . 151
7.2 Future Scope . . . . . 155

**Bibliography 156**

# List of Figures


1.1 Various applications and root causes of stress on a three-phase induction motor . . . . . 3
1.2 Typical failures of induction motor . . . . . 3
1.3 Stator winding insulation faults . . . . . 5
1.4 Maintenance procedures in industries and their features . . . 6
1.5 Analytical redundancy model-based fault detection, isolation, and reconfiguration . . . . . 9
1.6 Mapping between monitoring parameters and analysing techniques to detect the faults . . . . . 19
1.7 Road map for research work . . . . . 22

2.1 Lumped parameter model . . . . . 25
2.2 Distributed parameter model . . . . . 26
2.3 3-phase induction motor distributed model . . . . . 26
2.4 Physical representation of stator winding capacitance to frame ground . . . . . 28
2.5 Representation of stator slot capacitance to frame ground . . 29
2.6 Experimental setup for DM test on a 3-phase, 5-hp induction motor . . . . . 31

2.7 Experimental setup for CM test on a 3-phase, 5-hp induction motor . . . . . 32
2.8 Experimental setup for a 3-phase, 3-hp induction motor . . . 32
2.9 Measured frequency response of a 5-hp induction motor . . 34
2.10 Measured frequency response of a 3-hp induction motor . . 34
2.11 Simulation diagram for DM test on a 5-hp induction motor . 37
2.12 Simulation diagram for CM test on a 5-hp induction motor . 37
2.13 Comparison between measured and simulated responses of impedance versus frequency in differential mode test on a 5-hp IM . . . . . 38
2.14 Comparison between measured and simulated responses of phase angle versus frequency in differential mode test on a 5-hp IM . . . . . 38
2.15 Comparison between measured and simulated responses of impedance versus frequency in common mode test on a 5-hp IM . . . . . 39
2.16 Comparison between measured and simulated responses of phase angle versus frequency in common mode test on a 5-hp IM . . . . . 39
2.17 Comparison between measured and simulated responses of impedance versus frequency in differential mode test on 3-hp IM . . . . . 39
2.18 Comparison between measured and simulated responses of phase angle versus frequency in differential mode test on a 3-hp IM . . . . . 40

2.19 Comparison between measured and simulated responses of impedance versus frequency in common mode test on a 3-hp IM . . . . . 40
2.20 Comparison between measured and simulated responses of phase angle versus frequency in common mode test on a 3-hp IM . . . . . 40

3.1 Three level decomposed discrete wavelet transform . . . . . 49
3.2 Three level decomposed stationary wavelet transform . . . . 50
3.3 Flow chart for proposed fault detection method using DWT . 52
3.4 Three-phase current signals for healthy condition of a 5-hp induction motor . . . . . 53
3.5 Three-phase current signals for 2-turn short circuit in R-phase of a 5-hp induction motor . . . . . 53
3.6 Variation in d1 coefficients for healthy condition . . . . . 53
3.7 Variation in d1 coefficients for a 2-turn short circuit in R-phase 54
3.8 Variation in fault index for healthy condition . . . . . 54
3.9 Variation in fault index for a 2-turn short circuit at 0 degree inception . . . . . 55
3.10 Variation in fault index for an inter turn fault on coil-1 . . . . 55
3.11 Three-phase current signals for a LG fault in R-phase of a 5-hp induction motor . . . . . 56
3.12 Three-phase current signals for a LL fault between R and Y phases of a 5-hp induction motor . . . . . 57
3.13 Three-phase current signals for a single phasing in R phase of a 5-hp induction motor . . . . . 57

3.14 Three-phase current signals for a 30% under voltage of a 5-hp induction motor . . . . . 57
3.15 Three-phase current signals for a 10% supply unbalance in R phase of a 5-hp induction motor . . . . . 58
3.17 Variation in d1 coefficients for a LL fault between RY phases 59
3.16 Variation in d1 coefficients for a LG fault in R-phase . . . . 59
3.18 Variation in d1 coefficients for a single phasing in R phase . 60
3.19 Variation in d1 coefficients for 30% under voltage . . . . . 60
3.21 Variation in fault index for various faults . . . . . 61
3.20 Variation in d1 coefficients for 10% supply unbalance . . . . 61
3.23 Variation in d1 coefficients for a 2-turn fault in R-phase . . . 62
3.22 Three-phase current signals for 2-turn fault in R-phase of a 5-hp induction motor . . . . . 62
3.24 Variation in fault index for a 2-turn fault at 0degree inception 63
3.25 Variation in MSE for DWT of different mother wavelets . . . 64
3.26 Variation in SNR for DWT of different mother wavelets . . . 64
3.27 Comparison of DWT and SWT . . . . . 65
3.28 Flow chart for proposed SWT and DWT based fault detection scheme . . . . . 66
3.29 Three-phase current signals for 2-turn fault in R-phase of a 3-hp induction motor under experimental case . . . . . 67
3.30 Three-phase current signals for 2-turn fault in R-phase of a 3-hp induction motor under simulation . . . . . 67
3.31 Three-phase residues for 2-turn fault in R-phase of a 3-hp induction motor based on minimax method under experimental case . . . . . 68

3.32 Three-phase residues for 2-turn fault in R-phase of a 3-hp induction motor based on proposed method under experimental case . . . . . 68
3.33 Three-phase residues for 2-turn fault in R-phase of a 3-hp induction motor based on minimax method under simulation 68
3.34 Three-phase residues for 2-turn fault in R-phase of a 3-hp induction motor based on proposed method under simulation 69
3.35 Variation in d1 coefficients for 2-turn fault in R-phase of a 3-hp induction motor based on minimax method under experimental case . . . . . 70
3.36 Variation in d1 coefficients for 2-turn fault in R-phase of a 3-hp induction motor based on proposed method under experimental case . . . . . 71
3.37 Variation in d1 coefficients for 2-turn fault in R-phase of a 3-hp induction motor based on minimax method under simulation . . . . . 71
3.38 Variation in d1 coefficients for 2-turn fault in R-phase of a 3-hp induction motor based on proposed method under simulation . . . . . 72
3.39 Experimental setup for 3-hp induction motor . . . . . 74
3.40 Experimental setup for 10-hp induction motor . . . . . 74
3.41 Simulation diagram for stator inter-turn fault in R-phase . . . 75
3.42 Simulation diagram for stator line-ground fault in R-phase . 76
3.43 Simulation diagram for stator line-line fault between R-Y phases . . . . . 76

3.44 Three-phase currents under healthy condition of a 3-hp induction motor under simulation case . . . . . 78
3.45 Three-phase residue currents under healthy condition of a 3-hp induction motor under simulation case . . . . . 78
3.46 Variation in fault index under healthy condition of a 3-hp induction motor under simulation case . . . . . 79
3.47 Three-phase currents under healthy condition with 2% supply unbalance of a 3-hp induction motor under simulation case . . . . . 79
3.48 Three-phase residue currents under healthy condition with 2% supply unbalance of a 3-hp induction motor under simulation case . . . . . 79
3.49 Variation in fault index under healthy condition with 2% supply unbalance of a 3-hp induction motor under simulation case . . . . . 80
3.50 Three-phase currents under healthy condition of a 3-hp induction motor under experimental case . . . . . 80
3.51 Three-phase residue currents under healthy condition of a 3-hp induction motor under experimental case . . . . . 80
3.53 Three-phase currents under healthy condition with 2% supply unbalance of a 3-hp induction motor under experimental case . . . . . 81
3.52 variation in fault index under healthy condition of a 3-hp induction motor under experimental case . . . . . 81

3.54 Three-phase residue currents under healthy condition with 2% supply unbalance of a 3-hp induction motor under experimental case . . . . . 81
3.56 Three-phase currents for 8-turn short circuit in R-phase of a 3-hp IM under simulation . . . . . 82
3.55 Variation in fault index under healthy condition with 2% supply unbalance of a 3-hp induction motor under experimental case . . . . . 82
3.57 Three-phase residue currents for 8-turn short circuit in R-phase of a 3-hp IM under simulation . . . . . 83
3.58 Variation in fault index for 8-turn short circuit in R-phase of a 3-hp IM under simulation . . . . . 83
3.59 Three-phase currents for for 8-turn short circuit in R-phase with 2% supply unbalance of a 3-hp IM under simulation . . 83
3.60 Three-phase residue currents for 8-turn short circuit in R-phase with 2% supply unbalance of a 3-hp IM under simulation . . . . . 84
3.61 Variation in fault index for 8-turn short circuit in R-phase with 2% supply unbalance of a 3-hp IM under simulation . . 84
3.62 Three-phase currents for 8-turn short circuit in R-phase of a 3-hp induction motor under experimental case . . . . . 85
3.63 Three-phase residue currents for 8-turn short circuit in R-phase of a 3-hp induction motor under experimental case . 85
3.64 Variation in fault index for 8-turn short circuit in R-phase of a 3-hp induction motor under experimental case . . . . . 86

3.65 Three-phase currents for 8-turn short circuit in R-phase with 2% supply unbalance of a 3-hp induction motor under experimental case . . . . . 86
3.66 Three-phase residue currents for 8-turn short circuit in R-phase with 2% supply unbalance of a 3-hp induction motor under experimental case . . . . . 86
3.67 Variation in fault index for 8-turn short circuit in R-phase with 2% supply unbalance of a 3-hp induction motor under experimental case . . . . . 87
3.68 Three-phase currents for LG fault in R-phase of a 3-hp IM under simulation . . . . . 87
3.69 Three-phase residue currents for LG fault in R-phase of a 3-hp IM under simulation . . . . . 88
3.70 Variation in fault index for LG fault in R-phase of a 3-hp IM under simulation . . . . . 88
3.71 Three-phase currents for LL fault between R and Y phases of a 3-hp IM under simulation . . . . . 88
3.72 Three-phase residue currents for LL fault between R and Y phases of a 3-hp IM under simulation . . . . . 89
3.73 Variation in fault index for LL fault between R and Y phases of a 3-hp IM under simulation . . . . . 89
3.74 Three-phase currents for LG fault in R-phase of a 3-hp IM under experimental case . . . . . 89
3.75 Three-phase residue currents for LG fault in R-phase of a 3-hp IM under experimental case . . . . . 90

3.76 Variation in fault index for LG fault in R-phase of a 3-hp IM under experimental case . . . . . 90
3.77 Three-phase currents for LL fault between R and Y phases of a 3-hp IM under experimental case . . . . . 90
3.78 Three-phase residue currents for LL fault between R and Y phases of a 3-hp IM under experimental case . . . . . 91
3.79 variation in fault index for LL fault between R and Y phases of a 3-hp IM under experimental case . . . . . 91
3.80 Three-phase currents for healthy of a 10-hp induction motor 94
3.81 Three-phase residue currents for healthy of a 10-hp induction motor . . . . . 94
3.82 Variation in fault index for healthy of a 10-hp induction motor 94
3.83 Three-phase currents for 2-turn fault in R-phase of a 10-hp induction motor . . . . . 95
3.84 Three-phase residue currents for 2-turn fault in R-phase of a 10-hp induction motor . . . . . 95
3.85 Variation in fault index for 2-turn fault in R-phase of a 10-hp induction motor . . . . . 95
3.86 Three-phase currents for single phasing in R-phase of a 10-hp induction motor . . . . . 96
3.87 Three-phase residue currents for single phasing in R-phase of a 10-hp induction motor . . . . . 96
3.88 Variation in fault index for single phasing in R-phase of a 10-hp induction motor . . . . . 96
3.89 Three-phase currents for 2% supply unbalance of 10-hp induction motor . . . . . 97

3.90 Three-phase residue currents for 2% supply unbalance of a 10-hp induction motor . . . . . 97
3.91 Variation in fault index for 2% supply unbalance of a 10-hp induction motor . . . . . 97
3.92 Three-phase currents for 7% under voltage of a 10-hp induction motor . . . . . 98
3.93 Three-phase residue currents for 7% under voltage of a 10-hp induction motor . . . . . 98
3.94 Variation in fault index for 7% under voltage of a 10-hp induction motor . . . . . 98

4.1 Proposed stator fault detector and classifier . . . . . 102
4.2 Three-phase stator currents of a 3-hp IM with 4-turn short circuit in R-phase . . . . . 103
4.3 Variation in three-phase residues of a 3-hp IM with 4-turn short circuit in R-phase . . . . . 103
4.4 Variation in fault index of a 3-hp IM with 4-turn short circuit in R-phase . . . . . 104
4.5 Variation in a2 coefficients of a 3-hp IM with 4-turn short circuit in R-phase . . . . . 104
4.6 Three-phase stator currents of a 3-hp IM with 4-turn to ground fault in R-phase . . . . . 105
4.7 Variation in three-phase residues of a 3-hp IM with 4-turn to ground fault in R-phase . . . . . 105
4.8 Variation in fault index of a 3-hp IM with 4-turn to ground fault in R-phase . . . . . 106

4.9 Variation in a2 coefficients of a 3-hp IM with 4-turn to ground fault in R-phase . . . . . 106
4.10 Three-phase stator currents of a 3-hp IM with 4-turn short circuit between R and Y phases . . . . . 106
4.11 Variation in three-phase residues of a 3-hp IM with 4-turn short circuit between R and Y phases . . . . . 107
4.12 Variation in fault index of a 3-hp IM with 4-turn short circuit between R and Y phases . . . . . 107
4.13 Variation in a2 coefficients of a 3-hp IM with 4-turn short circuit between R and Y phases . . . . . 107
4.14 Three-phase stator currents of a 10-hp IM with 3% supply unbalance . . . . . 108
4.15 Variation in three-phase residues of a 10-hp IM with 3% supply unbalance . . . . . 108
4.16 Variation in fault index of a 10-hp IM with 3% supply unbalance . . . . . 108
4.17 Variation in a2 coefficients of a 10-hp IM with 3% supply unbalance . . . . . 108
4.18 Three-phase stator currents of a 10-hp IM with 10%under voltage . . . . . 109
4.19 Variation in three-phase residues of a 10-hp IM with 10%under voltage . . . . . 109
4.20 Variation in fault index of a 10-hp IM with 10%under voltage 109
4.21 Variation in a2 coefficients of a 10-hp IM with 10%under voltage . . . . . 109
4.22 Three-phase stator currents of a 10-hp IM with single phasing 110

4.23 Variation in three-phase residues of a 10-hp IM with single phasing . . . . . 110
4.24 Variation in fault index of a 10-hp IM with single phasing . . 111
4.25 Variation in a2 coefficients of a 10-hp IM with single phasing 111
4.26 Variation in nine features for various disturbances . . . . . 112
4.27 Variation in nine features for stator faults and supply unbalance . . . . . 112
4.28 Proposed classifiers for classification of faults on a three-phase induction motor . . . . . 113
4.29 Proposed MNN-1 for disturbance classifier . . . . . 118

5.1 Three-phase currents for phase to ground fault in Y-phase of a 3-hp induction motor . . . . . 124
5.2 Three-phase currents for phase to phase fault between Y and B phases of a 3-hp induction motor . . . . . 124
5.3 Variation in fault index for phase to ground fault in Y-phase of a 3-hp induction motor . . . . . 125
5.4 Variation in fault index for phase to phase fault between Y and B phases of a 3-hp induction motor . . . . . 125
5.5 Variation in slope of detail level coefficients for phase to ground fault in Y-phase of a 3-hp induction motor . . . . . 125
5.6 Variation in slope of detail level coefficients for phase to phase fault between Y and B phases of a 3-hp induction motor 126
5.7 Variation in normalised features for YG and YB faults . . . 127
5.8 Variation in normalised features for stator phase faults . . . . 128
5.9 Proposed ANN-2 for classification of stator phase faults . . . 129

5.10 Proposed MNN-2 for classification of stator phase faults . . 131

6.1 Three-phase currents for 4-turn short circuit in R-hase . . . . 137
6.2 Three-phase residues for 4-turn short circuit in R-phase . . . 137
6.3 variation in slope of detail level coefficients for 4-turn short circuit in R-phase . . . . . 137
6.4 Variation in fourth level approximate coefficients for 4-turn short circuit in R-phase . . . . . 140
6.5 Variation in fourth level approximate coefficients for 4-turn short circuit in R-phase . . . . . 140
6.6 Variation in fourth level approximate coefficients for 4-turn short circuit in R-phase . . . . . 141
6.7 Variation in feature 4 for stator inter-turn fault in R-phase . . 142
6.8 Variation in features for various level of stator inter-turn fault in R-phase . . . . . 142
6.9 Variation in features for various level of stator inter-turn fault in Y-phase . . . . . 143
6.10 Variation in features for various level of stator inter-turn fault in B-phase . . . . . 143
6.11 Proposed MNN-3 classifier dentification of faulty phase and estimation of fault severity of stator inter-turn faults . . . . 147

# List of Tables


1.1 Distribution of induction motor faults with respect to failed component. . . . . 4

2.1 No-load test readings for a 3-phase 5-hp induction motor (IM) 33
2.2 Blocked rotor test readings for a 3-phase 5-hp induction motor (IM) . . . . . 33
2.3 No-load test readings for a 3-phase 3-hp induction motor (IM) 33
2.4 No-load test readings for a 3-phase 3-hp induction motor (IM) 34
2.5 Parameters for a 3-phase 5-hp induction motor (IM) . . . . . 35
2.6 Parameters for a 3-phase 3-hp induction motor (IM) . . . . . 35

3.1 Comparison of fault detection criteria for various practical and simulation cases of stator inter-turn faults . . . . . 92
3.2 Comparison of fault detection criteria for various practical and simulation cases other than stator inter-turn faults . . . . 93

4.1 Normalised features extracted from a2 coefficients . . . . . 111
4.2 Training and testing data for various disturbances . . . . . 115
4.3 Training performance of single multilayer ANN-1 . . . . . 115
4.4 Testing performance of single multilayer ANN-1 . . . . . 116
4.5 Testing performance of multilayer ANN-1 . . . . . 117
4.6 Performance of ANN-1 in double multilayer of 14, 20 . . . . 117

4.7 Confusion matrix for MNN-1 . . . . . 120
4.8 Performance for ANN-1 and MNN-1 in disturbance classification . . . . . 121

5.1 Self normalised features for various stator phase faults . . . 128
5.2 Training and testing data for stator phase faults classification 130
5.3 Confusion matrix for ANN-2 . . . . . 130
5.4 Confusion matrix for MNN-2 . . . . . 132
5.5 Comparison of performance between ANN-2 and MNN-2 . 133

6.1 Features extracted from slope of detail level coefficients . . . 138
6.2 Self normalised features extracted from slope of detail level coefficients . . . . . 139
6.3 Feature 4 from fourth level approximate coefficients . . . . . 141
6.4 Training and testing patterns used in ANN-3 . . . . . 145
6.5 Confusion matrix for ANN-3 . . . . . 146
6.6 Confusion matrix for MNN-3 . . . . . 148
6.7 Performance for ANN-3 and MNN-3 in stator inter-turn fault classification . . . . . 149

# List of Abbreviations

| | |
|---|---|
| **ANFIS** | Adaptive Neuro-Fuzzy Inference System |
| **ANN-1** | ANN Structure for Disturbance Classifier |
| **ANN-2** | ANN Structure for Stator Phase Fault Classifier |
| **ANN-3** | ANN based classifier for identification of faulty phase and estimation of fault severity of stator inter-turn faults |
| **ANN** | Artificial Neural Network |
| **AWT** | Analytic Wavelet Transform |
| **Bior5.5** | Biorthogonal 5.5 |
| **CBM** | Condition Based Maintenance |
| **CM** | Common Mode |
| **CWT** | Continues Wavelet Transform |
| **DM** | Differential Mode |
| **DWT** | Discrete Wavelet Transform |
| **FDIR** | Fault Detection, Isolation and Reconfiguration |
| **FFT** | Fast Fourier Transform |
| **IMs** | Induction Motors |

| | |
|---|---|
| **MCSA** | Motor Current Signature Analysis |
| **MNN-1** | MNN Structure for Disturbance Classifier |
| **MNN-2** | MNN Structure for Phase Fault Classifier |
| **MNN-3** | MNN based classifier for identification of faulty phase and estimation of fault severity of stator inter-turn faults |
| **MNN** | Modular Neural Networks |
| **MRA** | Multi-Resolution Analysis |
| **MSE** | Mean Square Error |
| **PD** | Partial Discharge |
| **PWVD** | Pseudo Winger-Ville Distribution |
| **RAT** | Relative Value of Adaptive Threshold |
| **RMFI** | Relative Value of Maximum Fault Index |
| **SNR** | Signal to Noise Ratio |
| **SPWVD** | Smoothed Pseudo Winger-Ville Distribution |
| **STFT** | Short Time Fourier Transform |
| **SWT** | Stationary Wavelet Transform |
| **WFT** | Windowed Fourier Transform |
| **WPT** | Wavelet Packet Transform |
| **WT** | Wavelet Transform |
| **WVD** | Winger-Ville Distribution |

# List of Symbols

| | |
|---|---|
| $\eta\ L_{ls}$ | Anti-resonance leakage inductance |
| $\mu Rs$ | Stator initial frame to ground damping resistance |
| $\mu\ R_{sf}$ | Anti-resonance resistance |
| $C_{sf-total}$ | Total stator to frame capacitance per phase |
| $C_{sf}$ | Stator to frame capacitance |
| $C_{sw}$ | Stator turn to turn capacitance |
| $I_f$ | Fault index |
| $L_{lr}$ | Rotor leakage inductance |
| $L_{ls}$ | Stator leakage inductance |
| $L_m$ | Magnetising inductance |
| $R_{core}$ | Core resistance |
| $R_r$ | Rotor resistance |
| $R_{sw}$ | Stator turn to turn damping resistance |
| $R_s$ | Stator resistance |

# Chapter 1

# Introduction

## 1.1 Overview

A significant issue in the operation of any equipment is the proper and reliable operation, which in economic terms is a maximum financial benefit and residing within technical constraints. Moreover, the capital investment required for equipment often necessitates high levels of accessibility to ensure a reasonable rate of return. Thus, the minimization of operational costs resulting from unexpected downtimes, unnecessary maintenance and a reduction of the system abilities has become an essential objective of any industry. Hence the detection and diagnosis of fault components in an induction motor is of great practical significance. With the proper machine monitoring and fault detection schemes, early warning signs can be obtained for preventive maintenance, enhanced safety, and improved reliability. Faults can produce plant shutdown, economic and production losses, and even human casualties. Thus early, fast and accurate detection and diagnosis of incipient faults is essential in preventing major damage to the system and allows adequate timely actions to protect the system.

AC motors play a major role in modern industrial applications. Squirrel-cage Induction Motors (IMs) are most frequently used when compared to other motors because of their low cost, ruggedness and low maintenance. Moreover, the motors undergo many abnormal conditions during their total service life. In view of above, an incorrect operation of motor always lead to various failures and finally causing production curtailments. With reference to the origin, a fault may be internal or external. These faults are caused due to electrical, mechanical, thermal and environmental stresses. Mechanical stresses are caused by overloads and abrupt load changes, which can produce bearing failures and rotor bar breakage. On the other hand, electrical stresses are usually associated with the power supply, which can produce stator faults and supply faults. Figure 1.1 shows the various industrial applications of induction motor and root causes of various stresses on three-phase induction motor. Figure 1.2 shows the detailed classification of various faults on induction motors. According to surveys reported on motor reliability in [1] and [2], bearing failures are responsible for approximately two-fifths of all faults, inter-turn short circuits in stator windings are contribute to approximately one-third of the reported faults and broken rotor bars and end ring faults contribute to around ten percent of the induction motor faults. Induction motor fault distribution is summarized in Table 1.1. In medium size induction motors bearing failures occupy the first place but in medium to large size induction motors failures are due to stator winding insulation breakdown (one of the internal types of electrical fault).

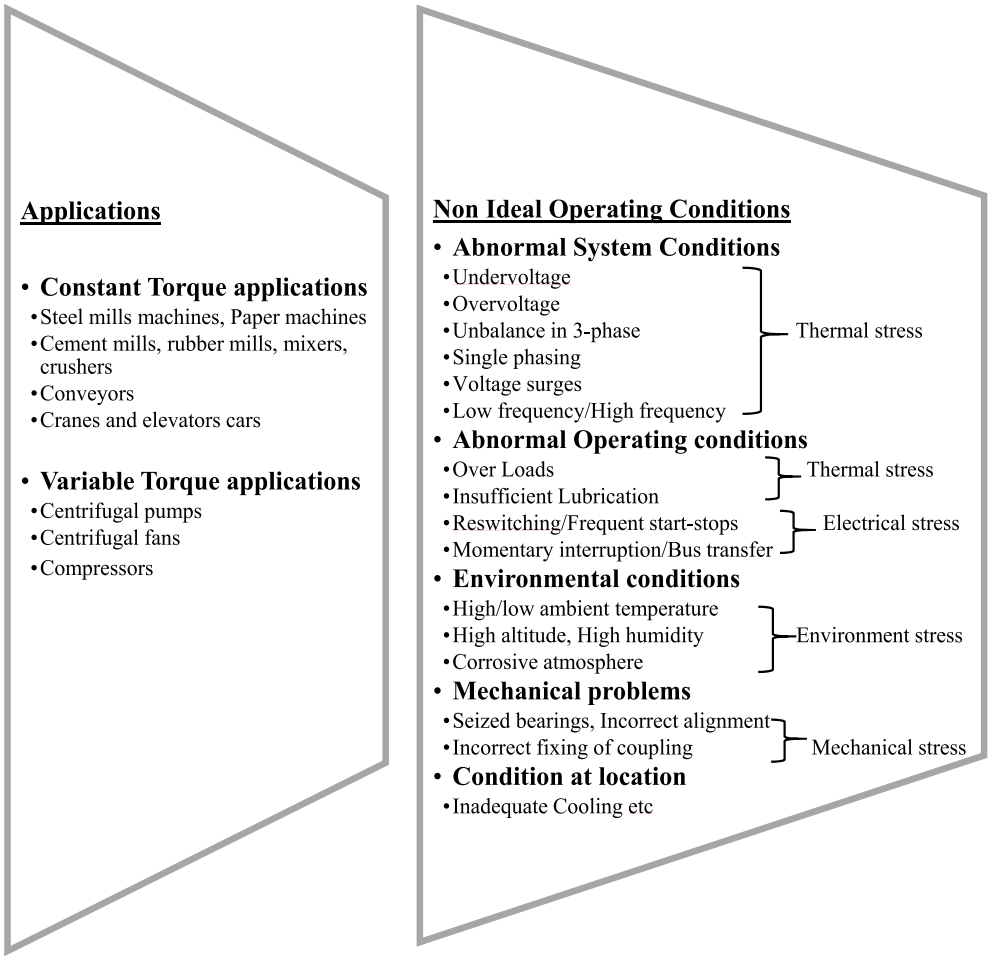


Figure 1.1: Various applications and root causes of stress on a three-phase induction motor

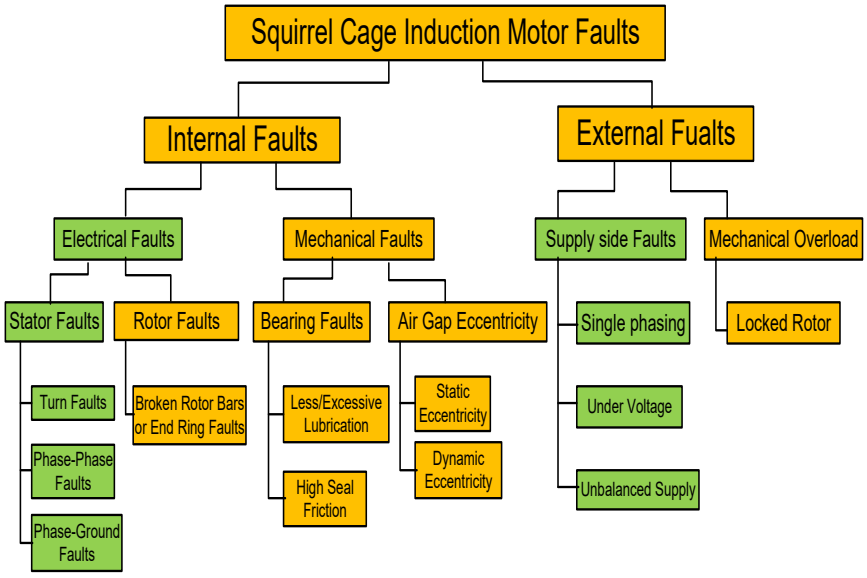


Figure 1.2: Typical failures of induction motor

Table 1.1: Distribution of induction motor faults with respect to failed component.

| % of failure | | | |
|---|---|---|---|
| **Fault related component** | **IEEE-IAS** | **EPRI** | **Allianz** |
| Bearings | 44 | 41 | 13 |
| Windings | 26 | 36 | 66 |
| Rotor | 8 | 9 | 13 |
| Other | 22 | 14 | 8 |

The organic compounds used for insulation materials in electric machines are subjected to deterioration, due to combination of thermal overloading, transient voltage stresses, mechanical stresses and environmental stresses. In spite of all possible causes, thermal stresses are the main reason for the degradation of the stator winding insulations. Thermal stress are classified into three types: aging, overloading, and cycling. Even the best insulation will fail quickly if operated above its temperature limit. As a rule of thumb, for every $10^0$C increase in temperature, useful life of insulation reduces by 50% [3]. Regardless of the causes, stator winding related failures can be divided into the following five groups: turn-to-turn, coil-to-coil, line-to-line, line-to-ground, and single or multi-phase windings open-circuit faults as presented in Figure 1.3. In particular, an undetected stator inter-turn fault may grows up and finally lead to a permanent damage of the machine. Hence, early detection of stator inter-turn faults is necessary for preventing damage to the adjacent coils and the core of the stator. Other major causes for induction motor faults are incorrect supply voltages and load changes. These are supply unbalance, single phasing, under voltage and sudden

change in electrical load.

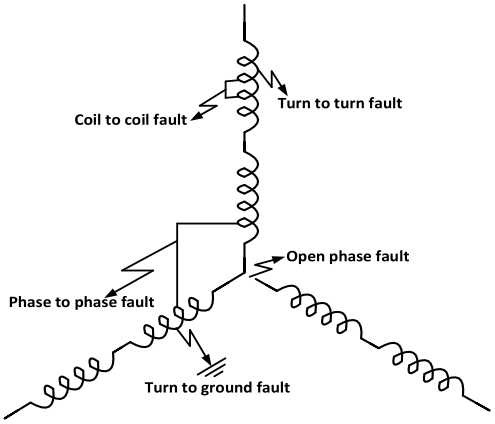


Figure 1.3: Stator winding insulation faults

In industry, basically people follows three types of maintenance procedures which include corrective maintenance, time based maintenance and condition based maintenance. Figure 1.4 illustrates the merits and demerits of the maintenance procedures. Recently, industrialists have shown much interest towards the use of prognosis techniques in Condition Based Maintenance (CBM). These techniques rely on information provided by condition monitoring and fault identification systems, which assess system conditions continuously. This requires accurate and effective fault detection methods which must be non-invasive and able to detect any type of faults in the early stages. A large amount of research has been directed towards the electrical monitoring of Motor Current Signature Analysis (MCSA), which is a non-invasive and standard for monitoring of motor faults due to its simplicity [4]. The main advantage of MCSA is to analyse the stator current in search of current harmonics directly related to new rotating flux components, which are triggered by faults in the motor-flux distribution.

## 1.2 Literature Survey on Fault Diagnosis

This section describes how significant and challenging it is to build an accurate stator fault diagnosis technique for induction machines. In addition to that an exhaustive literature survey on various condition monitoring techniques are presented which includes common modelling techniques, signal processing techniques and data based techniques. Finally, summary of various condition monitoring techniques for induction motors developed by other researchers are presented.

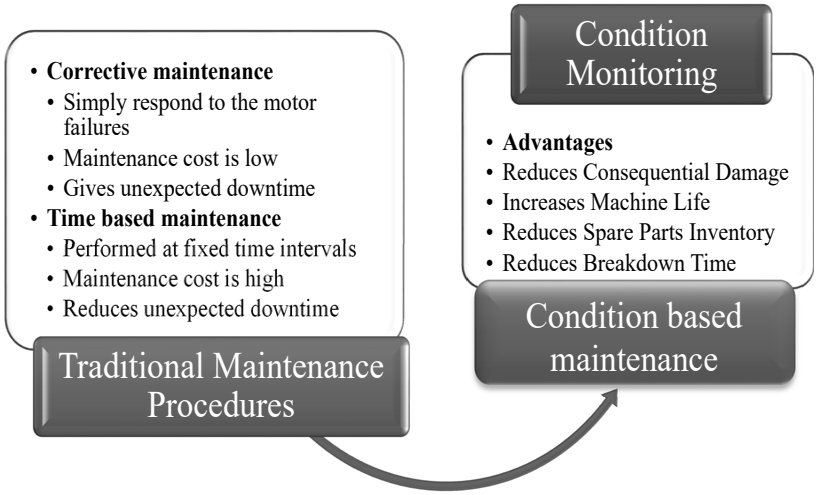


Figure 1.4: Maintenance procedures in industries and their features

Stator faults are usually associated with insulation failure. The root causes for the stator insulation failures are broadly categorised into four groups [5]. These are thermal, electrical, mechanical and environmental stresses. Normally, the deterioration of stator winding insulation usually begins with inter-turn fault which causes to produce high circulating current between adjacent coils and therefore burns the insulation in

adjacent windings. This insulation failure spreads to core very quickly and then leads to stator to core insulation failure. Hence, reliable detection techniques are essential for detecting the stator insulation failure at the earliest to avoid the catastrophic motor failures [6]. There are different types of fault detection and diagnosis methods for induction motor which have advantages and disadvantages. The main objective of the fault detection and diagnosis method is to obtain a signal sensitive to faults, but robust against model uncertainty, noise and unknown disturbances. In general, the development of a fault detection and diagnosis system involves a time consuming process to identify the symptoms to be monitored, provide the correct signals for recognition of suitable fault symptoms, and then provide the correct computational methods to process the signals. In fact, in the literature, there is still no global fault detection and diagnosis algorithm that can overcome the parametric and model uncertainty, measurement noise, load torque effects and intrinsically electrical machine mechanical unbalance for induction motor [7]. For this reason, researchers have suggested different detection and diagnosis schemes with parameter settings that are developed specifically to the system under investigation. According to the survey reports the fault diagnosis techniques are classified into two categories. These are Model based and model free methods [8].

### 1.2.1 Model Based Methods

Model-based methods have been proposed in [9] and [10]. They take advantage of the plant model, since the idea is to calculate such quantities from the models that reflect inconsistencies between nominal and faulty system operation. In the case of model-based techniques, accurate models

of the system are essentially required for achieving a good fault diagnosis [11]. More precisely, the more accurate the model, the more reliable the model-based fault diagnosis scheme will be, i.e. mathematical models among the system inputs and outputs are utilized. Most of the methods rely on the concept of analytical redundancy rather than physical redundancy. The basic idea behind the model-based fault detection and isolation approach is to take advantage of the nominal model of the system to generate residuals that contain information about the faults. Evidently, the quality of the model is of fundamental importance for both fault detection and isolation to avoid false alarms. The difference between computationally obtained quantities and measurements results is so-called residuals. Fault Detection, Isolation and Reconfiguration (FDIR) is a control methodology which ensures safe or acceptable operation of a system when a fault occurs through fault detection and isolation, as well as controller reconfiguration in response to the specific fault. Fault detection, and isolation are major part of FDIR [12]. Generally, the application of model-based methods can be divided in two parts: residual generation and decision making.

In Figure 1.5, a general framework of model-based FDIR scheme is presented [8], [12], [13], [14]. In the first step, process models in healthy and faulty operation are applied to generate residuals describing the current condition of the process. The second step is to make decisions on whether a fault has occurred (fault detection) and on the type of faults that have occurred (fault isolation) based on the residuals. Finally, the controller is reconfigured on-line in response to any faults detected. The residual generation has to be followed by residual evaluation, in order to arrive at a

detection and isolation decision.

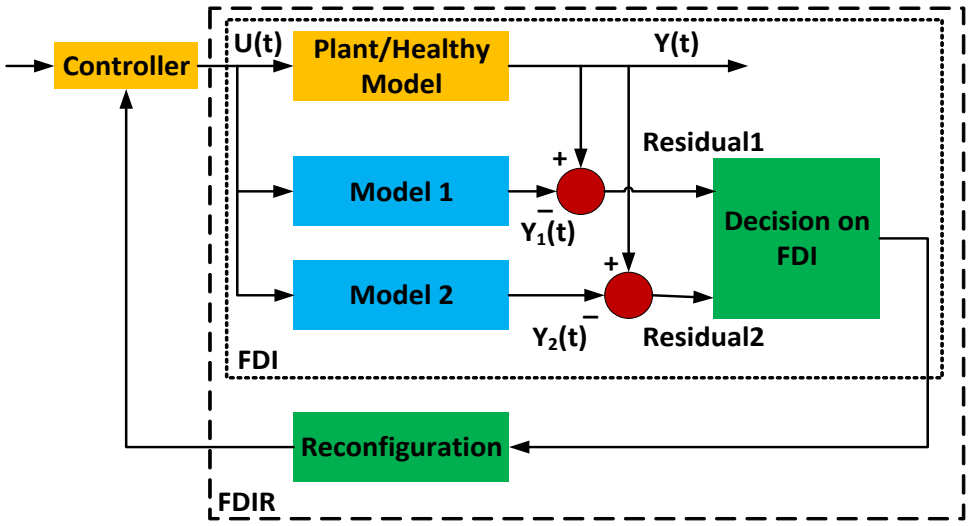


Figure 1.5: Analytical redundancy model-based fault detection, isolation, and reconfiguration

In some cases the residuals never become zero because of the presence of noise and model errors, even if there is no fault. Therefore the detection decision requires testing the residuals against thresholds, obtained empirically, or by theoretical considerations in which the condition is decided based on the residuals [12]. To overcome this problem, robust residual generation can be addressed by using observer-based methods [15], the parity relation methods [11], the parameter estimation methods [16] and Kalman filter-based method [17].

The model-based method can be divided into three classes [13], [16], [18] based on their analysis: data based model, analytical model, and knowledge-based model. Analytical models are based on the known physical interactions in the diagnosed plant. It can be applied using observers [19], parameter estimation [18], or parity equations [16]. Knowledge-based models rely on human-like knowledge of the process and its faults [13], whereas Data-based models are applied when the process model is not known in the analytical form and expert

knowledge of the process performance under faults is not available. However, for complex and uncertain systems, the derivation of high-fidelity mathematical models from physical principles can become very complicated, time consuming, and even sometimes unfeasible (for instance, some systems cannot be represented accurately enough by a lumped parameter system). Generally obtaining accurate model parameter values may become a very tedious job, or even practically impossible, due to proprietary issues regularly imposed by system integrators [18].

### 1.2.2 Model-Free Methods

Model-free methods can be carried out by monitoring and processing the signals. These methods use suitable sensor signals such as voltage, current, vibration, temperature, etc., at the initial stage. The second stage extracts the useful information by using one or more of the signal processing techniques e.g. Fourier techniques, wavelet, etc [8]. The third stage, considered the heart of the condition monitoring, is the stage where the fault is detected and identified according to the extracted data from the previous stage. The advantages of the model-free approaches are that they are able to avoid parameter mismatches between theoretical model and actual motor [13].

#### 1.2.2.1 Signal Monitoring Methods

In any machine, a key factor for detection of fault is proper signal conditioning and monitoring. They are mainly five types of monitoring techniques such as temperature monitoring, chemical monitoring, vibration monitoring, electrical monitoring and Partial Discharge (PD) monitoring.

Numerous fault detection and identification techniques that have been reported for the past two decades are based on electrical monitoring which includes currents, voltages and power. Out of all electrical monitoring techniques, motor current signature analysis is well known and recognised technique because it is more practical and no additional sensors are required [20]. Other techniques include vibration analysis, torque profile analysis, acoustic noise measurement, magnetic field analysis and temperature analysis [5]. These techniques require sophisticated and expensive sensors, extra electrical and mechanical installations and frequent maintenance. Moreover, the use of a physical sensor in induction motor fault identification system results in lower system reliability compared to other fault monitoring systems that do not involve extra instrumentation. This is due to the susceptibility of the sensor to fail is added to the inherent susceptibility of the induction motor to fail. The remaining monitoring techniques, such as chemical and PD Motor Current Signature Analysis analysis are presented in [21], [7]. In these two techniques, PD is only applicable for above 4 kV rating of the motors. Other monitoring technique is not useful for stator incipient fault cases. PD and chemical analysis techniques are not applicable for low and medium range induction motors due to their higher cost and other limitations.

#### 1.2.2.2 Signal Analysing Methods

Generally, the signal analysing methods can be carried out either in frequency domain or time domain or time-frequency domain.

**1.2.2.2.1 Time Domain Analysis:** In time domain analysis, the fault detection algorithms are developed based on the signal features of root mean square, shape factor or crest factor. The same inferred can be drawn from other methods based on statistical measures such as mean, standard deviation and Kurtosis. In that the last one is based on higher order moments [22]. Generally, the three-phase stator currents of an induction motor is in a periodic nature which is dominated by fundamental component. Whenever fault occur, the fault related frequency components present in the stator current is less compared with fundamental frequency. Thus, fault detection makes difficult using time domain analysis. The more reliable fault techniques in time domain is addressed by using the notch-filtered stator current [23]. However, it is hard to relate the origin of the fault from the features because the obtained features for different kinds of faults could be similar. Hence, fault classification needs the post-processing step [24].

**1.2.2.2.2 Frequency Domain Analysis:** The frequency domain analysis is widely applied for diagnosis of electrical faults in induction machines such as broken bar faults, rotor faults and stator faults since their corresponding fault characteristic frequencies are well defined [19], [25]. The mechanical faults such as bearing, eccentricity and load unbalance faults can also be detected using stator current frequency spectrum [19]. In several research works, the feature extraction in the frequency domain is not restricted to the monitoring of fault-related frequencies magnitudes in the stator current spectrum. It has been shown that the spectrum statistical information such as the frequency centre, the root mean square frequency and the root

variance frequency are also efficient for electrical and mechanical faults diagnosis in induction machines [24], [22], [26]. The performance of frequency domain analysis is mainly influenced by two factors which are frequency resolution and spectrum leakages. Detection of fault using frequency component of electrical signatures are commonly load and slip dependent.

**1.2.2.2.3 Time-Frequency Domain Analysis:** The frequency domain analysis cannot give a reliable solution in harsh industrial environment since the fault frequency components are generally load and slip dependent. A straightforward solution for that is to analyse the signal in time-frequency domain. The Windowed Fourier Transform (WFT) or Short Time Fourier Transform (STFT) is a well-known method to diagnosis the mechanical and electrical faults in an induction motor. The WFT gives equivalent time and frequency resolutions in the overall time-frequency plane. But, diagnosis of fault under non-stationary condition is a challenging problem which requires advanced time-frequency analysis techniques. Quadratic time-frequency analysis techniques are efficient alternatives to the WFT due to their independence from the type or the size for the window function. In essence, these methods compute energy distributions of the signal over both time and frequency planes. Particularly, the mechanical faults in electrical machines have been detected using time-frequency domain analysis of Wigner-Ville Distribution (WVD) and its variants, the pseudo-WVD (PWVD) and the smoothed pseudo-WVD (SPWVD). it WVD gives a better frequency resolution rather than WFT under similar conditions. But, it has a limitation due to inner interference terms. This

effect diminishes the ability to estimate the fault severity. To avoid this practical drawback, the PWVD uses a time window function like Hanning, Hamming, Blackman, Kaiser, Bartlett, and Gaussian in order to smooth the time-frequency distribution in the frequency plane at the cost of decreasing the frequency resolution. The SPWVD attempts to reduce the magnitude of inner interference terms by smoothing in both time and frequency planes. This reduces more efficiently the effect of inner interference terms at the cost of decreasing both time and frequency resolutions. In [27], authors have applied the SPWVD for rotor faults detection in brushless DC motors (BLDCM) in continuous time-varying conditions. For instance, the WVD has been used to track frequency components related to both eccentricity and broken rotor bar faults in the stator current of an induction machine at start-up [28], [29]. Climente-Alarcon and et. al have published two interesting contributions on this subject [30], [31]. In [30], the load torque oscillations have been associated with the stator current phase modulation in three-phase induction machines. Authors state that this technique has been considered as a general one for mechanical faults detections such as load unbalance, shaft misalignment, gearbox and rolling-bearing defects. In [31], authors have used the WVD as a mean to distinguish between magnitude and phase modulation effects of eccentricity and load torque oscillations.

Diagnosis of electrical machine faults using Wavelet Transform (WT) is another well-known method in time-frequency domain because of its multi resolution property [32]. Mathematically, mother WT is based on two function scale dilatation and translation. These two facts lead to give good resolutions in both time and frequency [33]. This means that when the

scale is small the resolution is coarse in the time domain and fine in the frequency domain and vice-versa when the scale is large [34]. There are several Wavelet functions such as Daubechies, Biorthogonal and Coiflet wavelet for real and Morelet wavelet for complex [35]. The fundamental idea is to replace the frequency shifting operation which occurs in the WFT by a time scaling operation. This makes the WT a time-scale representation rather than a time-frequency one. The time-scale representation of the squared-modulus of Continues Wavelet transform (CWT) is called the scalogram. A particular case of the CWT is called analytic or cross wavelet transform (AWT). The AWT separates the phase and the magnitude information of a signal which allows for analysing the time evolution of frequency tones.

### 1.2.3 Classification Methods

Recently, significant efforts have been made on the use of artificial intelligence tools to develop condition monitoring and fault diagnostic techniques for electric machines. Artificial intelligence techniques are considered significant in condition monitoring and fault diagnosis of electrical machines, reviewed in [36]. Neural network and fuzzy logic techniques have their own limitations as discussed in [37] and thus a specific combination of these two techniques, known as Adaptive Neuro-Fuzzy Inference System (ANFIS), have developed as a better alternative solution [38]. The ANFIS technique offers the best training feature of neural network and heuristic interpretation of the process results similar to fuzzy logic theory, thus providing a powerful tool that can be employed in conjunction with the condition monitoring and fault

diagnostic applications. The use of ANFIS is growing towards in this niche application area and a significant amount of literature is available [39], [40] and [41]. Bearing failures and inter-turn insulation failure of main winding of a single-phase induction motor is considered in [42]. Stator current, rotor speed, temperature of the winding, bearing temperature and motor noise are considered as input to the ANFIS. However, additional noise sensors are not very reliable and the data collected from such sensors is not very accurate. Classification of more faults with single parameter is more complicated than multiple parameters. Modular Neural Networks (MNN) have remarkable ability to derive meaning from complicated or imprecise data and is used to extract patterns and detect trends that are too complex. Such an approach has noticeable advantages of simple and reduced architecture and better learning capability [43], [44].

## 1.3 Summary of Various Monitoring Techniques

Monitoring parameters and analysing techniques have been used to identify the faults during last 2 decades are illustrated in figure1.6. This figure shows that the most commonly used monitoring parameter in fault diagnosis is MCSA because of its non-invasive nature. In that one of the more frequently used technique for fault diagnosis in the area of induction motors is Fast Fourier Transform (FFT), which is suitable for steady state analysis only [45]. Due to this reason the usage of time-frequency domain analysis has been enlarged in recent times towards fault diagnosis community. STFT overcomes the certain limitations of FFT but not all due to a sort of compromise between time and frequency based view of signal

representation, which has limited precision due to fixed size of window. Wavelet transform overcome this limitation. Wavelet analysis allows the use of long time intervals for low-frequency information, and shorter regions for high-frequency information [46] that means it gives multi-resolution. Thus, it is a powerful tool for condition monitoring and fault diagnosis [47]. A well-known technique to detect inter-turn short circuits in time domain analysis is negative sequence components of stator currents, which is presented in [48]. The asymmetries produced by a faulty motor with shorted turns in the stator winding are the basis for fault diagnosis, such asymmetries will generate a negative sequence current and is used to detect the fault. However, some effects can yield misclassification due to unbalanced power supply voltage, certain types of load, and measurement errors. These effects can also produce negative sequence currents even in healthy motors. Even though such effects were considered in [48], but still fails to detect faults for induction motors with inherently unbalanced windings as explained in [49]. The other frequency analysis technique can also be well associated for MCSA are Parks vector approach. Detection of faults using dq0 components [50] and the envelope of the stator currents [51] are just an alternative representation of the negative sequence current component. Methods using other signatures, such as slot harmonics [45], pendulous oscillation phenomenon [52] and observer-based method [53] are proposed in the literature. Fault detection using induced voltage at motor terminals when the power supply is turning off is proposed in [54], but this method cannot provide continuous monitoring and protection. Using high resolution spectral analysis of stator current spectrum through experiment, the voltage unbalance and open

phase external fault condition are identified. In [55], two approaches have developed based on Discrete Wavelet Transform (DWT) for induction motor fault detection. In that, the first fault detection criteria is the comparison between threshold determined experientially during healthy condition of motor and sixth level DWT coefficients of fault currents obtained by using selected mother wavelet of $db3$. The second approach was based on comparison of modulus maxima of the DWT coefficients. The DWT of the shifted (down sampled) signal, in general, is different from the shifted version of the DWT of the original signal. This is because DWT is not a shift-invariant transform. Such a drawback can cause problems in fault detection and classification. Wavelet packet transform based protection system developed in [56] coefficients of the Wavelet Packet Transform (WPT) line currents compared experimentally decided threshold for detecting and diagnosing various disturbance occurring in induction motor. Single phasing, phase to earth and short circuit faults. WPT is similar to DWT, but in WPT, the high-pass and low-pass filters are applied to both the detail and approximation coefficients at each level. Hence, at the $n^{th}$ level, WPT gives 2n coefficients while DWT gives only two. The draw back of DWT can be over come by using Stationary Wavelet Transform (SWT) and CWT.

## 1.4 Motivation

In harsh industrial environments the noise level and its variation should be considered precisely for fault diagnosis because the fault signature due to stator inter-turn short circuit is much lower than the noise level. Hence, it requires a good technique with a capability to suppress the noise without

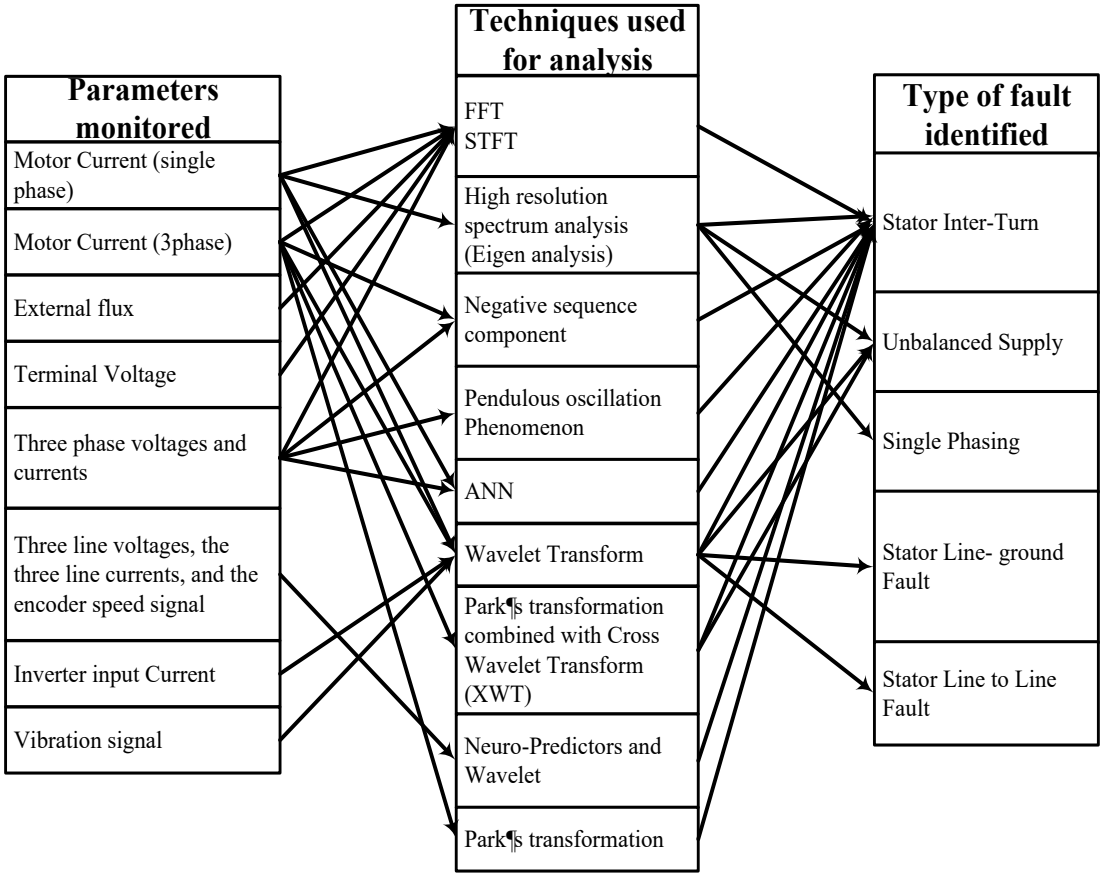


Figure 1.6: Mapping between monitoring parameters and analysing techniques to detect the faults

corrupting the fault signature. Most of the existing techniques require some sort of domain expertise to identify whether the three-phase induction motor is operating in normal or abnormal condition.

In actual practice, the captured currents are influenced by many factors, which include supply unbalance, static eccentricity, load level variations and noise. These conditions may lead to errors in fault detection. Hence, an accurate inter-turn fault diagnosis technique must be required to detect the inception of a fault and its location. To detect the inception of a fault than it requires time-frequency localisation. Wavelet transform is a one the best technique for analysing the signal in both time and frequency domain, they have capability to reconstruct the signal from the decomposed signal. However the discrete wavelet transform (DWT) is not suitable for signal

noise reduction applications due to the lack of invariant translation property. But this effect can be overcome by using stationary wavelet transform (SWT) that has been discussed in [57] and [58]. Especially, only little contributions have been presented based on SWT in the area of motor condition monitoring. From the perspective of long-term research on the diagnosis of electrical machines, it appears that recent focus has been on the use of signal processing and AI in order to improve the performance of traditional model-based methods. However, the lack of evaluation techniques for classifying various faults such as supply side faults and stator internal faults on induction motors are significant.

Specifically, this thesis addresses electrically detectable faults that occur in the stator windings and supply side faults, namely inter-turn, line-line, line to ground short circuits in stator windings, single phasing, under voltage, supply unbalances and sudden electrical load changes. The methods developed in this thesis detect motor faults without the necessity of invasive tests or process shut downs. Moreover, the presented methods monitor the operating condition of induction motor continuously, so that human inspection is not required to detect motor faults.

## 1.5 Contributions

According to exhaustive literature survey, effective fault detection is very essential for induction motors. The exhaustive literature survey on induction motor condition monitoring is inferred that majority of the cases the monitoring parameter is a current and analysing method is a time-frequency which is best for non-stationary signals. However, to

improve the sensitivity of the fault detection and identification, it is required to integrate the various analysing methods. Till now there is no such algorithm for detecting multiple faults with minimum number of non-invasive monitoring parameters and classifying the various faults with minimum features. Hence, the following objectives are outlined in this thesis to fulfil the gap in the literature survey.

- To develop an accurate machine model which is valid for wide range of frequencies.
- Monitoring measurements should be non-invasive and minimum.
- Integrating the analysing techniques (Wavelet and ANN).
- To diagnosis all possible and frequently occurring faults on induction motor such as supply unbalance, single phasing, under voltage, switching of sudden electrical loads, stator inter-turn (same phase) faults, stator turn-ground faults and stator turn-turn (different phases) faults.
- Detection procedure should be made with variable threshold as the fault component is not constant, and depends on the inception of fault, supply and load conditions.

To achieve the above objectives, in this thesis two robust fault diagnosis schemes are developed by integrating the wavelet with artificial neural network and wavelet with modular neural network, which can improve system's reliability and effectiveness towards detection, classification and evaluation of the severity level of stator inter-turn short circuit. Figure 1.7 illustrates the road map for research work presented in this thesis.

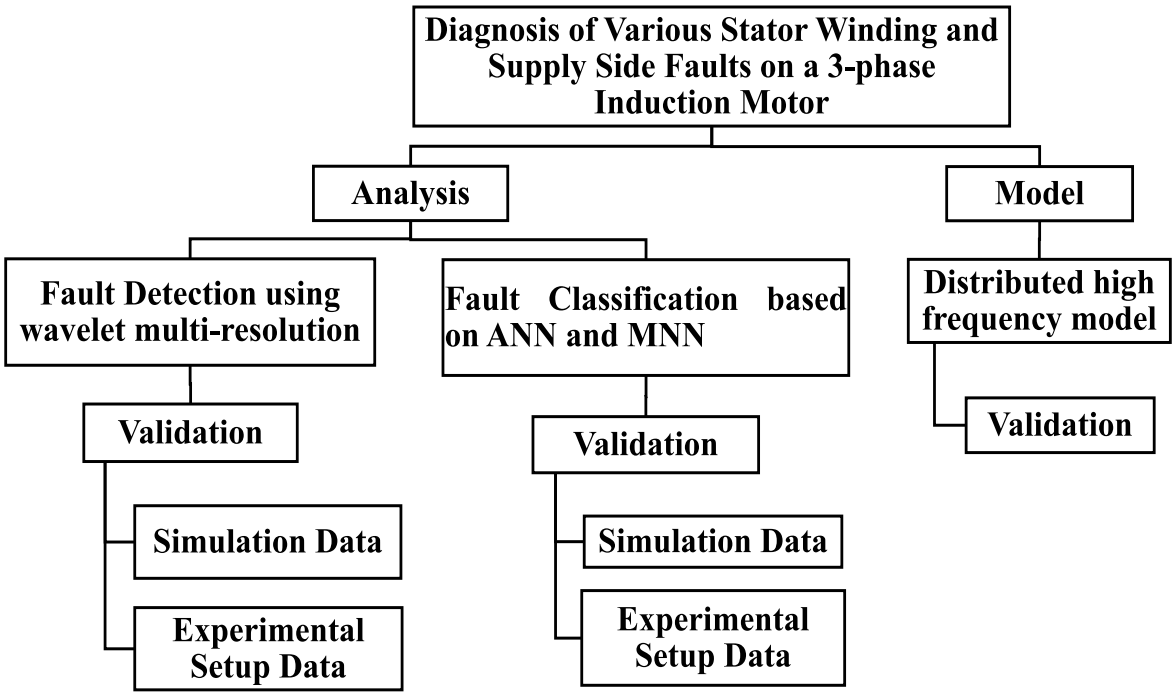


Figure 1.7: Road map for research work

## 1.6 Organization of the Thesis

This thesis is organized as follows:

Chapter 2 describes the development of a low-high frequency distributed model for an induction motor. The low and high frequency parameters are derived by conducting various tests which includes no-load, rotor blocked, differential and common mode test. This chapter also demonstrated the validation of the considered models of 3-hp and 5-hp motors by comparing frequency responses obtained from the experimental setup and simulation.

Chapter 3 deals the fault detection algorithms for three-phase induction motor based on discrete wavelet transform and stationary wavelet transform. The proposed algorithms are tested with various faults, which are modelled and simulated in MATLAB/Simulink environment. The proposed algorithms are also verified by using data obtained from

experimental setup provided for a 3-hp and 10-hp three-phase induction motors.

Chapter 4 describes the classification algorithms for various disturbances and stator winding insulation faults on a three-phase induction motor based on Feed Forward Neural Network (FNN) and Modular Neural Network (MNN). The proposed disturbance classifiers are trained and tested by using data obtained from the simulation studies for a 3-hp 3-phase induction motor. Experimental setup was arranged for the analysis of a 3-hp and 10-hp three-phase induction motors.

Chapter 5 presents the classification of stator phase faults along with faulty phase on a three-phase induction motor based on Feed Forward Neural Network (FNN) and Modular Neural Network (MNN). The proposed algorithms are verified by using data obtained from the simulation studies for a 3-hp 3-phase induction motor and experimental setup are provided for a 3-hp and 10-hp three-phase induction motors.

Chapter 6 discusses the identification of faulty phase and severity level of stator inter-turn faults on a three-phase induction motor. The defined features are not effected by the supply unbalances and load conditions.

Chapter 7 summarizes the conclusions of the work and recommendations for future work.

# Chapter 2

# Modelling of Stator Winding in 3-Phase Induction Motor for Fault Diagnosis-Validation

## 2.1 Introduction

Modelling of machines operating under fault conditions is essential in predicting the behaviour of the machine. The analysis of stator winding faults especially turn-to-turn short-circuit can be made by different models. With the advent of more powerful computers and sophisticated electric machine models, there is a possibility of transient analysis of the motor.

## 2.2 Modelling of 3-phase Induction Motor

Conducting experiments repeatedly on a real machine to study the behaviour of faults is not economical as it can lead to the destruction of the machine. However, many parametric studies can be carried out if an accurate and simple model is available to study the behaviour of the motor operating under fault condition. In this thesis, a low-to-high frequency

model is considered to analyse the stator faults. Motor behaviour under low frequencies is described by IEEE standard 112 [59] and per phase low-frequency T-equivalent circuit is shown in figure 2.1. In medium to high frequency ranges, a distributed parameter model is best for analysing the motor behaviour. Compared to low frequency model, the distributed high frequency model requires extra elements such as stator to frame capacitance ($C_{sf}$), anti-resonance resistance ($\mu\ R_{sf}$), anti-resonance leakage inductance ($\eta\ L_{ls}$), stator turn to turn capacitance ($C_{sw}$) and stator turn to turn damping resistance ($R_{sw}$). Each coil of the Stator winding is represented by a distributed $\Pi$ model as shown in figure 2.2. Figure 2.3 shows the distributed model of a 3-phase induction motor. The additional parameters of the distributed model are calculated from Differential Mode (DM) and Common Mode (CM) test which has been discussed in [60]. Fast switching means shorter voltage rise time, which can lead to the reflected wave phenomenon as well as high-frequency leakage currents through the systems stray capacitors. Reflected waves cause voltage spikes at the motor terminals and the high frequency leakage currents cause electromagnetic interference (EMI). These two phenomena are commonly modelled as two decoupled single-line circuits, namely, DM and CM.

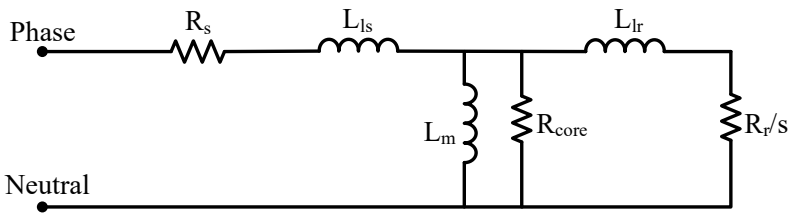


Figure 2.1: Lumped parameter model

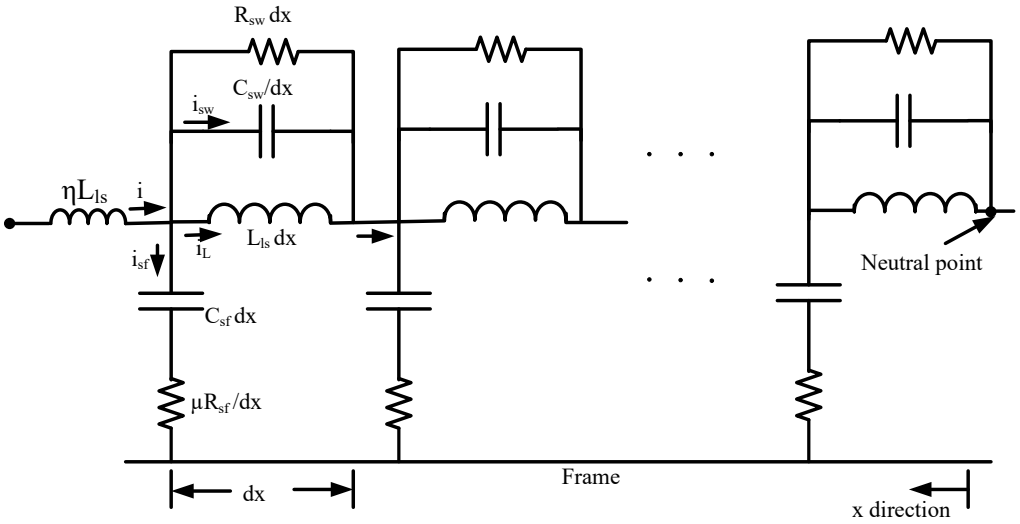


Figure 2.2: Distributed parameter model

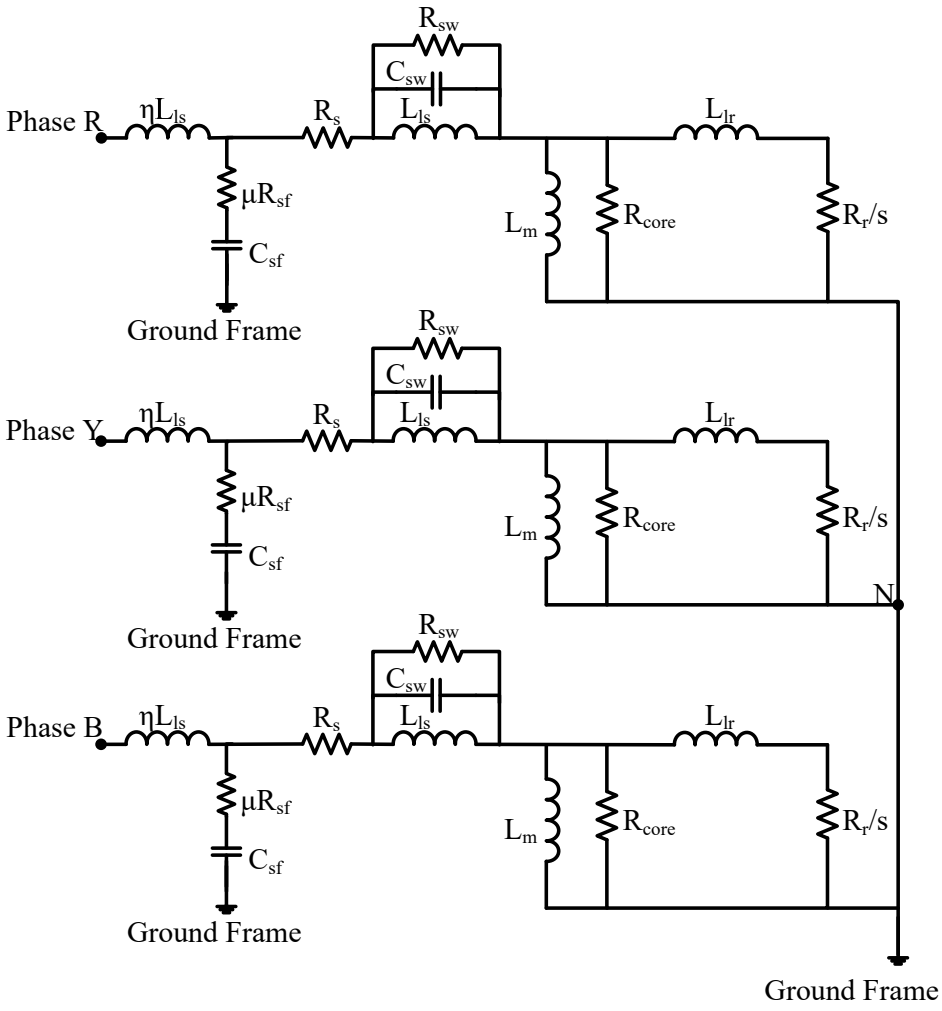


Figure 2.3: 3-phase induction motor distributed model

## 2.3 Distributed Model Parameters

### 2.3.1 Stator First Turn Leakage Inductance ($\eta\ L_{ls}$):

This is one of the critical parameters in defining the DM motor high frequency impedance to reflected wave, predicting the antiresonance point of Figure 2.2 and setting correct EMI leakage current to ground in the CM circuit. The $\eta\ L_{ls}$ parameter is used to account for the fact that only a fraction of total stator leakage inductance is attributed to the high frequency ($\sim$ 5 MHz) anti-resonance point, specifically the first few turns (typically 4) in the first slot of the entry winding. Thus, mathematically it is expressed as in equation 2.1. Winding data is available from machine geometry. If the value of $L_{ls}$ is too high, then this inductance isolates the rest of the winding from the cable and a wave shaped reflected wave appears DM simulation is a wave-shape which exhibits of an ideal open circuit. If $\eta\ L_{ls}$ is high, then this inductance also isolates the $C_{sf} - slot$ term and current-to-ground peak and ring wave shape will not be correct in the CM simulation.

$$\eta L_{ls} \sim (\frac{4turns}{totalturnsperphase})^2 L_{ls} \tag{2.1}$$

### 2.3.2 Total Stator to Frame Capacitance per Phase ($C_{sf-total}$):

A physical representation of ($C_{sf-total}$) total stator winding capacitance to frame ground is shown in figure 2.4. At high frequencies especially more than resonance frequency, the behaviour of DM and CM motor can be described by the parameter of stator slot winding-to-frame capacitance ($C_{sf}$). At low frequencies, the parameter $C_{sf-total}$ plays a major role in matching CM transfer function. $C_{sf-total}$ is calculated from machine

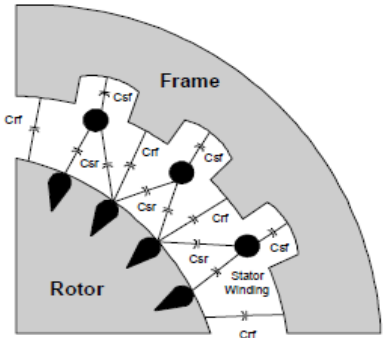


Figure 2.4: Physical representation of stator winding capacitance to frame ground

geometry by analysing each slot capacitance to ground and multiplying it by the number of stator slots. Each stator slot can be considered approximately as a rectangular shaped conductor with stack stator length $L$, slot average width $w$ and slot average depth $d$; see figure 2.5. The capacitance value between the conductor in each slot and the motor frame can be obtained as follows

$$C_{sf-slot} = \frac{\varepsilon_0 L_{slot} L_{Stack}}{\frac{K_t \delta_1}{\varepsilon_{r1}} + \frac{\delta_2}{\varepsilon_{r2}} + \frac{K_t \delta_3}{\varepsilon_{r3}}} \tag{2.2}$$

where, $L_{slot}$ is the stator slot circumference which can be calculated approximately using the expression as $L_{slot} \cong 2d_{slot} + 1.5w_{slot}$ , $\delta_1$, $\delta_2$ and $\delta_3$ are the thickness of slot wall, wire insulation and air gap, with a relative permittivity of $\varepsilon_{r1}$, $\varepsilon_{r2}$ and $\varepsilon_{r3}$ respectively. Effective $C_{sf-total}$ and $C_{sf-slot}$ may change in 2:1 ration with liner air gaps, making calculations less precise. For a motor with $N_{slot}$ stator slots, the total stator winding to frame capacitance can be obtained as follows:

$$C_{sf-total} = N_{slot} C_{sf} \tag{2.3}$$

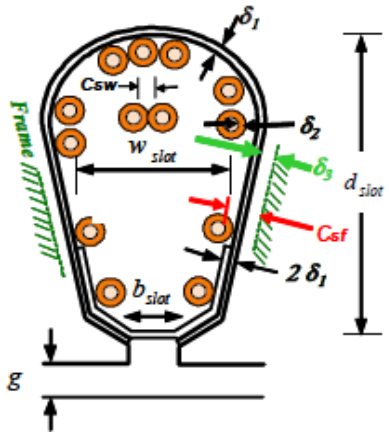


Figure 2.5: Representation of stator slot capacitance to frame ground

### 2.3.3 Stator Turn to Turn Winding Capacitance ($C_{sw}$):

This parameter can be determined in a two ways. In the first method parameter can be obtained as a function of $C_{sf-effective}$. The mathematical representation $C_{sw}$ is given in equation 2.4. The second method is to solve equation 2.5 for $C_{sw}$ and assuming $f_{r1}$ is known.

$$C_{sw} = \frac{{f_{r2}}^2}{f_{r2}} C_{sf-effective} \tag{2.4}$$

$$f_{r1} and f_{r2} = \frac{1}{2\Pi} \sqrt{(\beta \pm \sqrt{(\beta^2 - 4\alpha)})/(2\alpha)} \tag{2.5}$$

where $\alpha = L_{ls}\, L_{lr}\, C_{sw}\, C_{sf}$ , $\beta = (L_{ls} + L_{lr})C_{sf} + L_{ls}\, C_{sf}$ and $f_{r1} < f_{r2}$.

### 2.3.4 Stator Turn to Turn Damping Resistance in Winding ($R_{sw}$):

This parameter accounts for skin and proximity effect of the wire and high frequency core loss. Quite simply, at first resonance peak of the DM

impedance measured is equal to the 3/2 times the damping resistance ($R_{sw}$) for a parallel resonant circuit. It has been found that $R_{core}$ resistor does not have a great impact on the damping resistor required.

### 2.3.5 Stator Initial Frame to Ground Damping Resistance ($\mu Rs$):

This component is the ac resistance of the fractional part of total stator $R_s$ due to the $\eta\ L_l s$ segmentation described. The $\mu Rs$ is proportional ($\frac{4turns}{total\_turns\_per\_phase}$) and multiplying factor of 10 to 20 is used for ac skin and proximity effects. In addition, it also encompasses the resistivity of the steel laminations from the slots to where the motor ground wire in the junction box is connected. The term $\mu\ R_s$ affects peak CM current as well as damping of oscillations in the CM current to ground.

## 2.4 Experimental Setup for DM and CM Test

In general, distributed parameters are determined by measuring the frequency response from DM test setup and CM test setup. A three-phase, 3-hp, 415 V, 4 pole 50 Hz induction motor with 36 slots, 6 coils per phase and 72 turns per coil and a three-phase, 5 HP, 440 V, 4 pole 50 Hz induction motor with 36 slots, 6 coils per phase and 54 turns per coil is considered for the present study. Initially, the low frequency parameters are estimated by conducting no-load and rotor blocked tests. Later, differential mode and common mode tests are conducted to estimate the high frequency parameters of a 5-hp Induction Motor (IM). Differential mode test was performed by connecting LCR meter between phase A and tied leads of phase B and phase C. This test procedure is recommended [60] for


Figure 2.6: Experimental setup for DM test on a 3-phase, 5-hp induction motor

an ungrounded motor frame with LCR meter in Z-$\theta$ mode. Common mode test was performed with ground frame as one probe and phase A, phase B and phase C motor leads tied together to form the second probe to LCR meter in Z-$\theta$ mode. LCR meter was manufactured by Agilent, whose model number is 16089A and having a frequency range of 20Hz to 1MHz is used for taking measurements. Figure 2.6 shows the experimental setup for DM test on a three-phase 5-hp IM. Similarly, Figure 2.7 shows the experimental setup of a three-phase 5-hp IM in CM test. Similar tests are conducted on another 3-hp induction motor. The experimental procedure for a 3-phase 3-hp induction motor is shown in figure 2.8.

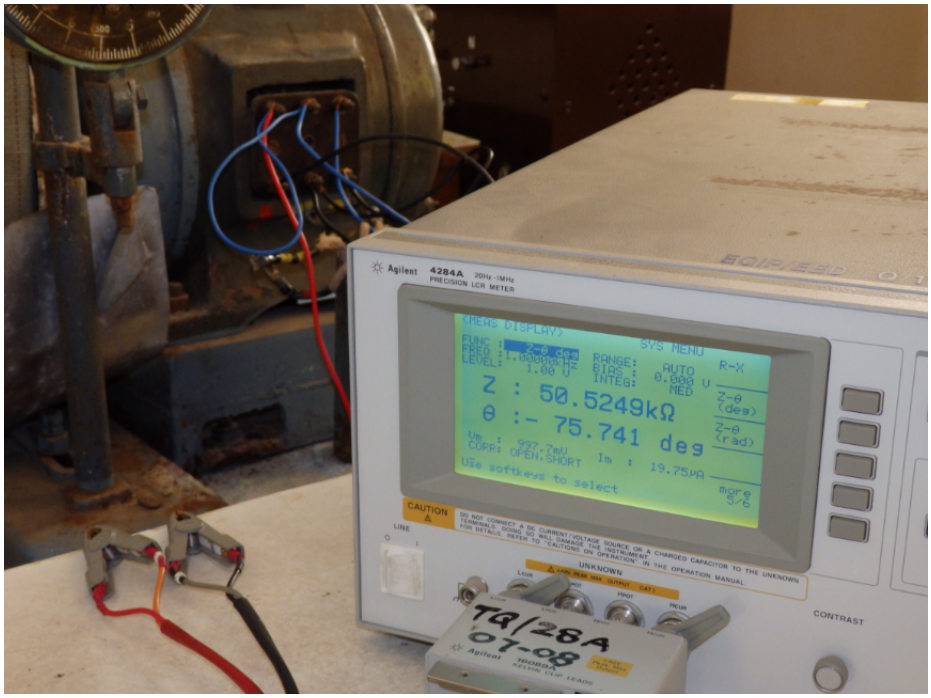


Figure 2.7: Experimental setup for CM test on a 3-phase, 5-hp induction motor


Figure 2.8: Experimental setup for a 3-phase, 3-hp induction motor

## 2.5 Estimation of Parameters

The low frequency parameters are estimated by conducting no-load and blocked rotor tests. Readings obtained from no-load and blocked rotor tests for a 3-phase, 5-hp induction motor are tabulated in Table 2.1 and Table 2.2 respectively. Similarly, readings for a 3-hp induction motor are tabulated in Table 2.3 and Table 2.4 respectively. The distributed parameters are estimated by using the first and second resonance frequencies of impedance which are obtained from the frequency response of a motor during DM and CM test. Figure 2.9 shows the frequency response of a 5-hp induction motor during DM and CM test. Similarly, Figures 2.10 shows the frequency responses of a 3-hp induction motor in DM and CM test.

Table 2.1: No-load test readings for a 3-phase 5-hp induction motor (IM)

| **Voltage**($Volts$) | **Current**($Amps$) | **Power**($Watts$) | **Power**($Watts$) |
|---|---|---|---|
| 400 | 0.98 | 240 | -150 |

Table 2.2: Blocked rotor test readings for a 3-phase 5-hp induction motor (IM)

| **Voltage**($Volts$) | **Current**($Amps$) | **Power**($Watts$) | **Power**($Watts$) |
|---|---|---|---|
| 225 | 7.0 | 1440 | 30 |

Table 2.3: No-load test readings for a 3-phase 3-hp induction motor (IM)

| **Voltage**($Volts$) | **Current**($Amps$) | **Power**($Watts$) | **Power**($Watts$) |
|---|---|---|---|
| 415 | 0.8 | 208 | -136 |

Table 2.4: No-load test readings for a 3-phase 3-hp induction motor (IM)

| **Voltage**(*Volts*) | **Current**(*Amps*) | **Power**(*Watts*) | **Power**(*Watts*) |
|---|---|---|---|
| 236 | 4.8 | 1050 | 100 |

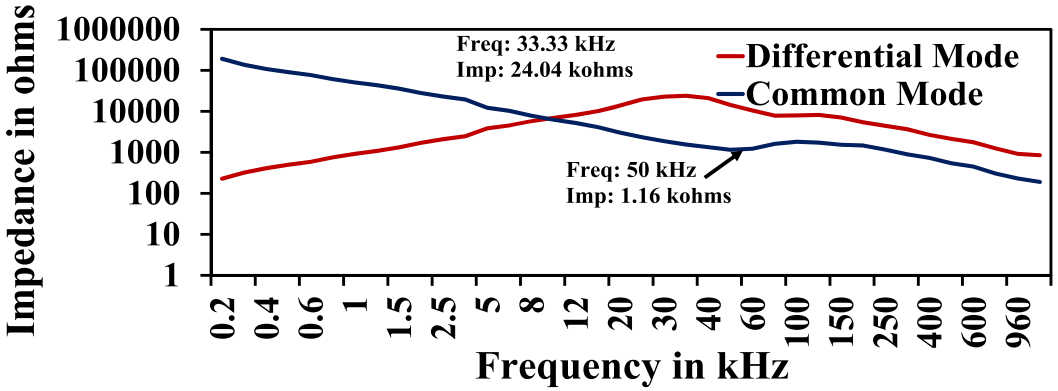


Figure 2.9: Measured frequency response of a 5-hp induction motor

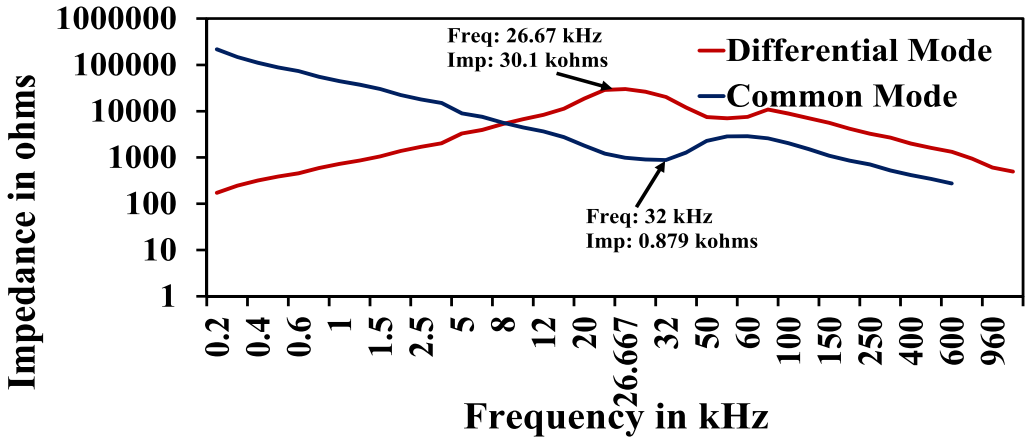


Figure 2.10: Measured frequency response of a 3-hp induction motor

Table 2.5: Parameters for a 3-phase 5-hp induction motor (IM)

| **Motor Parameters** | **5-hp IM** | **Parameters are obtained from** |
|---|---|---|
| Stator resistance ($R_s$) | 5.2 Ω | |
| Stator leakage inductance ($L_{ls}$) | 37.335 mH | |
| Rotor resistance ($R_r$) | 4.8 Ω | No load |
| Rotor leakage inductance ($L_{lr}$) | 16.587 mH | and Blocked rotor test |
| Magnetising Inductance ($L_m$) | 757.68 mH | |
| Core Resistance ($R_{core}$) | 1778.9 Ω | |
| Stator to frame capacitance ($C_{sf}$) | 0.562 nF | |
| Anti-resonance resistance ($\mu\ R_s$) | 39.2 Ω | Differential mode |
| Anti-resonance leakage inductance ($\eta\ L_{ls}$) | 18 $\mu$H | and Common mode test |
| Stator turn to turn capacitance ($C_{sw}$) | 0.603 nF | |
| Stator turn to turn damping resistance ($R_{sw}$) | 14700 Ω | |

Table 2.6: Parameters for a 3-phase 3-hp induction motor (IM)

| **Motor Parameters** | **3-hp IM** | **Parameters are obtained from** |
|---|---|---|
| Stator resistance ($R_s$) | 9.1 Ω | |
| Stator leakage inductance ($L_{ls}$) | 41.38 mH | |
| Rotor resistance ($R_r$) | 8.08 Ω | No load |
| Rotor leakage inductance ($L_{lr}$) | 31.83 mH | and Blocked rotor test |
| Magnetising Inductance ($L_m$) | 904.44 mH | |
| Core Resistance ($R_{core}$) | 2842.8 Ω | |
| Stator to frame capacitance ($C_{sf}$) | 0.253 nF | |
| Anti-resonance resistance ($\mu\ R_s$) | 2.667 Ω | Differential mode |
| Anti-resonance leakage inductance ($\eta\ L_{ls}$) | 3.547 $\mu$H | and Common mode test |
| Stator turn to turn capacitance ($C_{sw}$) | 0.853 nF | |
| Stator turn to turn damping resistance ($R_{sw}$) | 17356 Ω | |

The distributed parameters are estimated by substituting the values of low frequency parameters, measured frequency responses, total number of slots and total number of turns in equations 2.1 to 2.5. Tables 2.5 and 2.6 represent the low to high frequency parameters of a 5-hp induction motor and 3-hp induction motor respectively.

## 2.6 Model Validation

The low and high frequency parameters obtained using procedures mentioned in Section 2.5 are used to simulate the models of 3-hp and 5-hp induction motors in MATLAB/Simulink environment. Both differential and common mode tests are carried out in MATLAB/simulink environment and frequency responses are plotted. The MATLAB/simulink models for DM and CM tests on a 5-hp induction motor are shown in Figures 2.11 and 2.12 respectively. Figures 2.13 and 2.14 demonstrate the comparison between measured and simulated frequency responses in a DM test on a 5-hp induction motor. Similarly, figures 2.15 and 2.16 represent the comparison between measured and simulated frequency responses in CM test on a 5-hp IM. These figures demonstrate that the frequency response observed in simulation closely matches with frequency response measured on practical machine. Comparison between measured and simulated frequency responses in DM test on a 3-hp induction motor are shown in figures 2.17 and 2.18 respectively. Similarly, figures 2.19 and 2.20 show the comparison between measured and simulated frequency responses in CM test on a 3-hp induction motor. The second resonance impedance wave

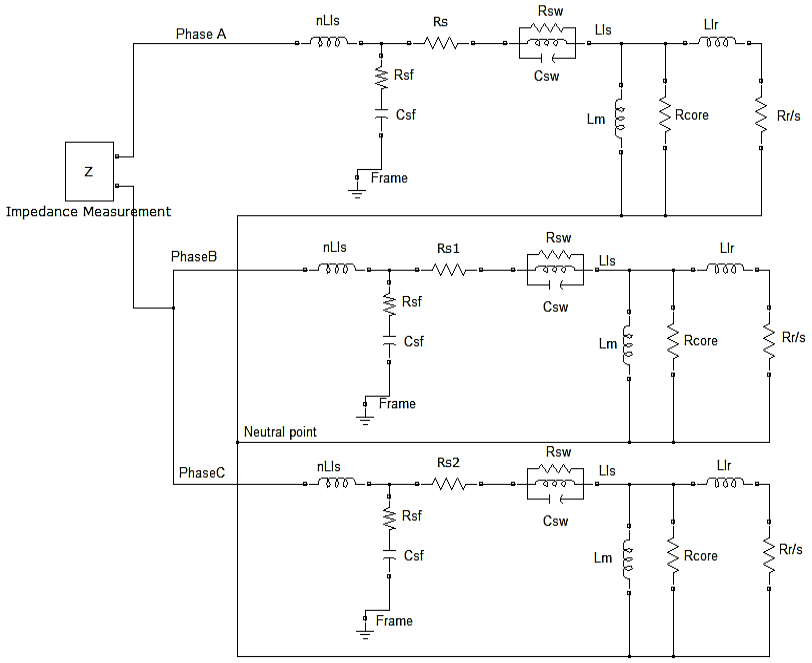


Figure 2.11: Simulation diagram for DM test on a 5-hp induction motor

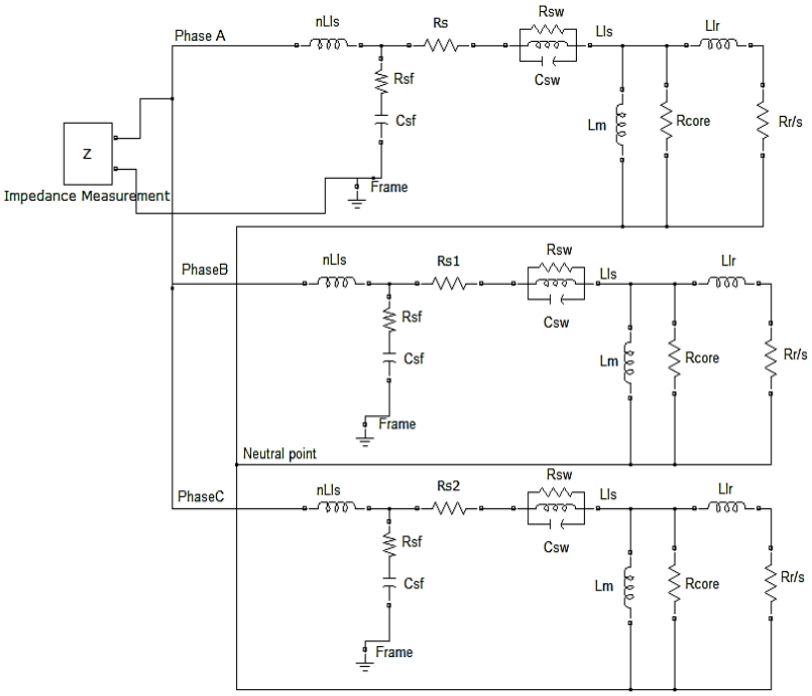


Figure 2.12: Simulation diagram for CM test on a 5-hp induction motor

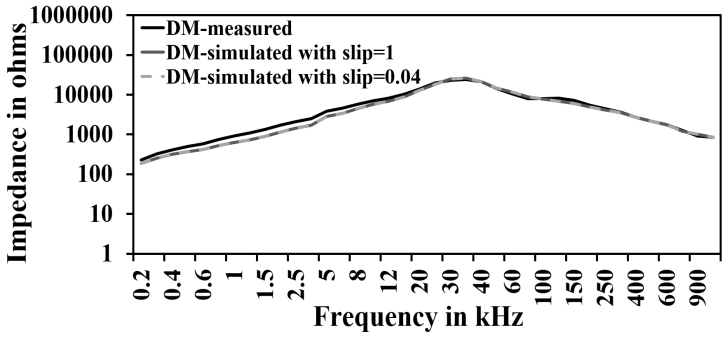


Figure 2.13: Comparison between measured and simulated responses of impedance versus frequency in differential mode test on a 5-hp IM

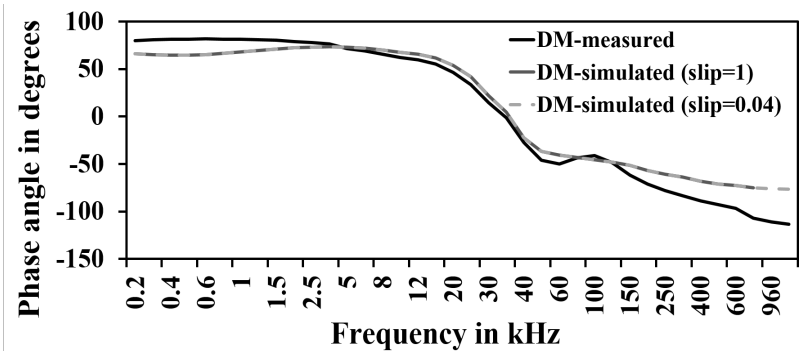


Figure 2.14: Comparison between measured and simulated responses of phase angle versus frequency in differential mode test on a 5-hp IM

shape is similar, however, the frequency value in case of simulation is different from measured value because of the coil level parameter distribution. Even then, results from the graphs show that the measured and simulated responses are close to each other. Hence, the model is valid for transient studies.

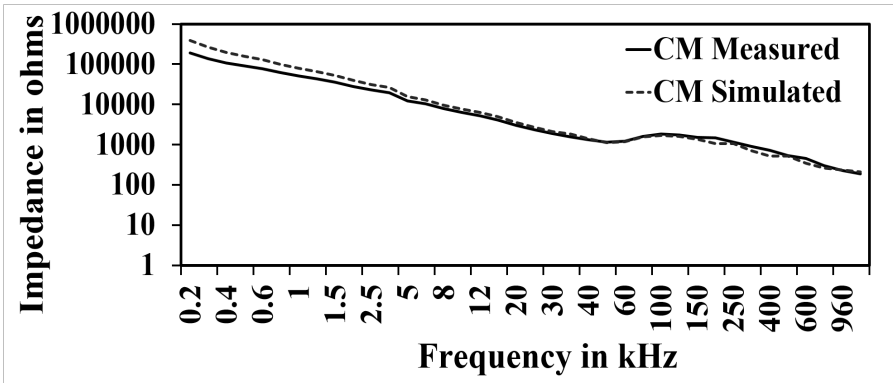


Figure 2.15: Comparison between measured and simulated responses of impedance versus frequency in common mode test on a 5-hp IM

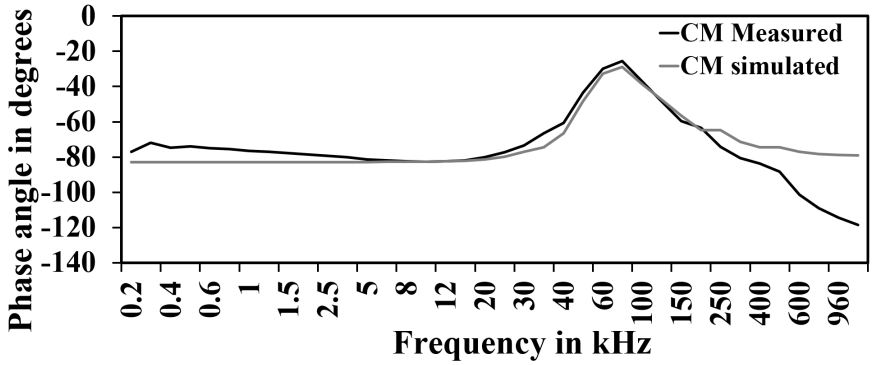


Figure 2.16: Comparison between measured and simulated responses of phase angle versus frequency in common mode test on a 5-hp IM

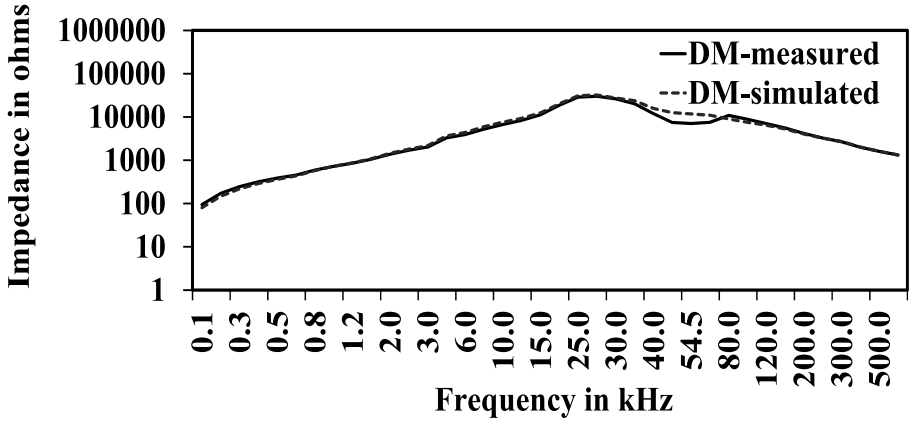


Figure 2.17: Comparison between measured and simulated responses of impedance versus frequency in differential mode test on 3-hp IM

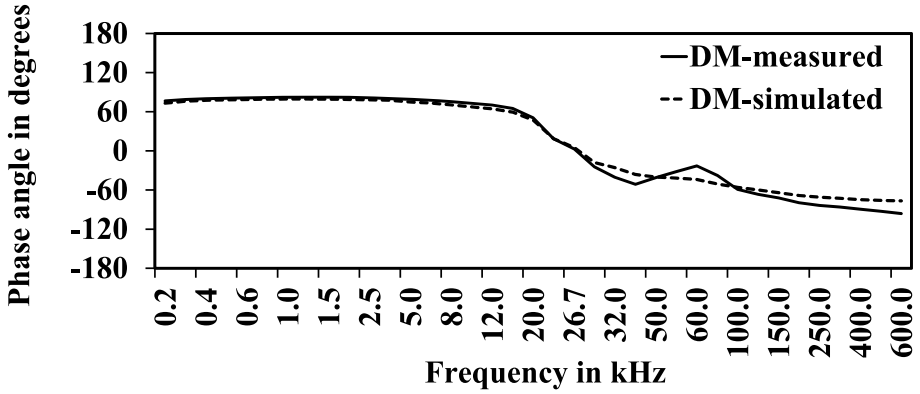


Figure 2.18: Comparison between measured and simulated responses of phase angle versus frequency in differential mode test on a 3-hp IM

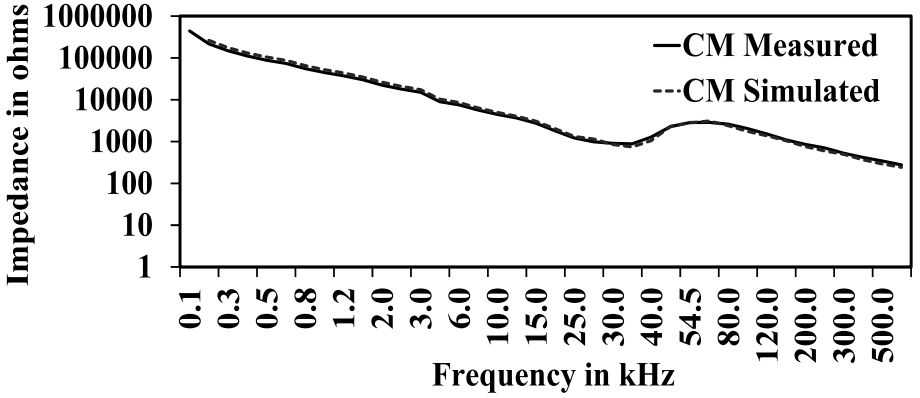


Figure 2.19: Comparison between measured and simulated responses of impedance versus frequency in common mode test on a 3-hp IM

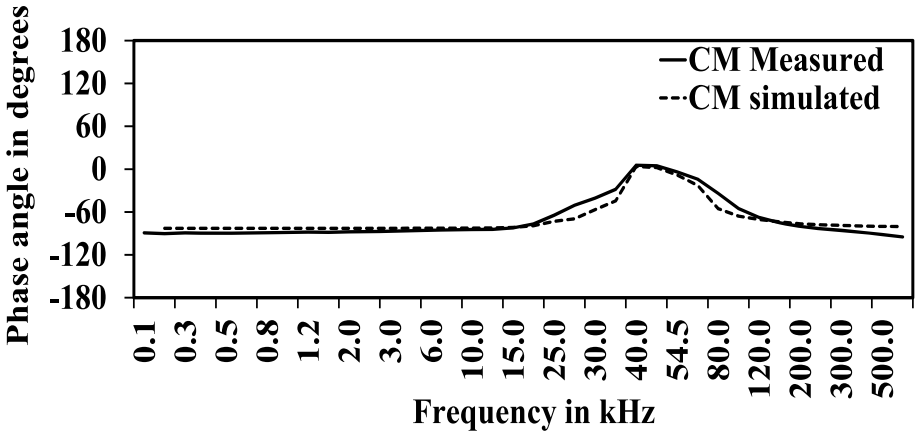


Figure 2.20: Comparison between measured and simulated responses of phase angle versus frequency in common mode test on a 3-hp IM

## 2.7 Conclusions

In this chapter, model parameters are estimated from physical tests conducted on induction motor. Applicability of the model is validated by comparing the frequency responses obtained from simulation and experimental setup. Considering the fact that actual parameters are distributed, the responses obtained through simulation, matches well with experimental observations. Hence, the model is validated and it can be used for transient analysis.

# Chapter 3

# Fault Detection Schemes

## 3.1 Introduction

The objective of this chapter is to propose condition monitoring techniques of three phase induction motor using wavelet transform for detection of various faults. The proposed DWT and combination of SWT and DWT algorithms are tested with various faults in three phase induction motor and are simulated in MATLAB/Simulink platform. Both the methods are effective in detecting the faults without having any noise. In case of noise, the combined scheme of SWT and DWT algorithm performance is well as compared to DWT.

## 3.2 Various Stator and Supply Side Faults in a 3-Phase Induction Motor

Electric motors are critical components of many industrial processes and are frequently integrated with commercially available equipment and industrial processes. Squirrel cage induction motors are more prevalent in use than other motors due to their low cost, ruggedness, low maintenance

and operation with an easily available power supply. Although induction motors are reliable electric machines, they are susceptible to internal and external faults. Different internal motor faults includes inter-turn short circuits, ground faults, mechanical failure where as external motor faults includes: a) mechanical overloads, which define prolonged starting or locked rotor and stalling; b) abnormal supply conditions such as loss of supply voltage, unbalanced supply voltage, phase sequence reversal of supply voltage, over voltage, under voltage, and under frequency; c) faults in starting supply / circuit, which include interruptions in phases or blowing of fuse / single phasing, and short circuit in supply cable. These faults are expected to happen at any stage of motor life time [61], [62], [63]. Correct diagnosis and early detection of faults result in fast unscheduled maintenance and short shut down time for the machine under consideration. It not only reduces maintenance costs but also increases productivity. Statistical analysis proved that the stator winding faults constitute the largest portion of the electrical faults [64], [65].

### 3.2.1 Stator Faults

The stator winding of an induction machine is subject to stresses induced by a variety of factors which include thermal overload, mechanical vibrations and voltage spikes caused by adjustable-speed drives. The stator winding short circuit fault in electric motors usually start as an undetected insulation failure between two adjacent turns and it develops into a short circuit isolating a few number of turns [66]. Though it starts as an incipient inter-turn short circuit, undetected small insulation failures can deteriorate and accumulate rapidly and finally lead to a loss of a phase winding, phase

to phase or phase to ground fault. Failure of insulation between phases and phase to ground can cause a large ground current which would result in irreversible damage to the core of the machine. The incipient winding faults in a single stator coil may have relatively little effect on motor performance but may affect overall motor reliability, availability and longevity. Typical protection for stator insulation failure in an industrial environment includes the use of ground fault relays and negative-sequence or phase current balance relays. Negative-sequence relays would cause nuisance trips with unbalanced line voltages. Ground fault relays would not be effective for early fault detection. Hence, the stator incipient fault diagnosis is essential to avoid the catastrophic failures and production curtailments.

### 3.2.2 Unbalanced Supply

Voltage unbalance of a 3-phase system is expressed as a percentage value and is often defined as the maximum deviation from the average of the 3-ph voltages divided by the average of the 3-ph voltages [63]. Many times the supply to an induction motor is unbalanced due to the presence of unbalanced loads on the system or due to some line disturbances. When the voltages are unbalanced, a much higher current is induced in the rotor because it has much lower impedance to the negative sequence voltage component. The percentage increase in temperature of the winding is approximately two times the square of the voltage unbalance. These higher temperatures soon result in degradation of the motor insulation and reduce motor life. This additional rotor heat can exist for a considerable time period and since the rotor and shaft are a continuous metallic structure, the

heat transfer to the shaft ends can leads to the bearing failure.

### 3.2.3 Single-Phasing

Single phasing can occur as a result of a fuse blowing or a protection device opening on any one phase of the motor. Other possibilities include feeder or step down transformer fuses blowing [62]. The loss of one phase or leg of a 3-phase line causes serious problems for induction motor. If single phasing occurs when the motor is rotating, the torque produced by the remaining two positive rotating fields continues to rotate the motor and develop the torque demanded by the load. The negatively rotating field i.e. the field associated with the lost phase produces currents in the inductive loads resulting in voltages at the faulted leg of the 3-phase supply. These voltages may be nearly equal to the phase voltage that was lost. Three-phase motor may continue to run, but they are not capable of starting on single-phasing. Even though the motor will continue to operate in this condition, the motor will heat up quickly and hence, it is essential that the motor be removed from service. Though the overload devices on the energized phases isolate the motor, the motor is not isolated from the lost phase; subsequent attempt to restart the motor on that single-phasing supply will cause the motor to draw locked rotor current. The effects of single phasing are similar to the unbalanced voltages, since the single phasing represents the worst case of an unbalanced voltage condition. An additional effect is the remaining phase windings experience excessive overheating, thereby creating a greater potential for stator winding failure.

### 3.2.4 Under Voltage

Under voltage protection for induction motor is provided for both sustained and transitory under voltages. With three phase motors, the under voltages are assumed to be the balanced type. An example of sustained under voltage is bus voltage that remains approximately 10% below nominal rating. The reduction in supply voltage for constant torque load lowers the motor speed because it is directly proportional to the square of the voltage drop. Thus the operating slip would increase and rotor power factor would be reduced. Hence the current supply to the motor is increased drastically. This suggests that low voltage is serious enough to warrant protection in certain cases.

## 3.3 Wavelet Transform

A wavelet is a wave-like oscillation with an amplitude that starts out at zero, increases and then decreases back to zero. Unlike the sines used in Fourier transform for decomposition of a signal, wavelets are generally much more concentrated in time [67]. Wavelet Transform was introduced at the beginning of the 1980s and has attracted much interest in the fields of speech and image processing since then [35]. Its potential applications to power industry have been discussed in the recent literature [68], [69], [70]. A brief introduction to the WT and its Multi-Resolution Analysis (MRA) is given here. They usually provide an analysis of the signal which is localized in both time and frequency whereas Fourier transform is localized only in frequency. Jean Morlet in 1982, introduced the idea of the wavelet transform and provided a new mathematical tool for seismic wave analysis. Morlet first considered wavelets as a family of functions

constructed from translations and dilations of a single function called the "mother wavelet" $\Psi(t)$. They are defined by

$$\Psi_{a,b}(t) = \frac{1}{\sqrt{a}}\Psi(\frac{t-b}{a}) \tag{3.1}$$

where a, b $\epsilon$ R , a≠0. The parameter 'a' is the scaling parameter or scale and it measures the degree of compression. The parameter 'b' is the translation parameter which determines the time location of the wavelet. If $||a|| < 1$ the wavelet is the compressed version (smaller support in time- domain) of the mother wavelet and corresponds mainly to higher frequencies. On the other hand, when $||a|| > 1$, then $\Psi_{a,b}(t)$ has a larger time-width than $\Psi(t)$ and corresponds to lower frequencies. Thus, wavelets have time-widths adapted to their frequencies. This is the main reason for the success of the Morlet wavelets in signal processing and time-frequency signal analysis. The Continuous Wavelet Transform is defined as the sum over all time of the signal multiplied by scaled, shifted versions of the wavelet function:

$$CWT(a,b) = \int f(t)\Psi_{a,b}(t)dt \tag{3.2}$$

In practice, the transform which is used is the discrete wavelet transform which transforms discrete (digital) signals to discrete coefficients in the wavelet domain. This transform is essentially a sampled version of CWT. Instead of working with a, b $\epsilon$ R, the values of CWT(a,b) are calculated over a discrete grid: a = $2^j$ ; b = $k^{2^j}$ ; j, k $\epsilon$ Z where this type of discretization is called dyadic dilation and dyadic position.

### 3.3.1 Discrete Wavelet Transform (DWT)

Wavelet calculations are based on two fundamental equations: the scaling function $\varphi(t)$ and the wavelet function $\psi(t)$.

$$\varphi(t) = \sqrt{2} \sum h(n)\varphi(2t - n) \tag{3.3}$$

$$\psi(t) = \sqrt{2} \sum g(n)\varphi(2t - n) \tag{3.4}$$

where $g(n) = (-1)^n h(1 - n)$. These functions are two-scale difference equations based on a chosen scaling function (mother wavelet), with properties that satisfy the following conditions.

$$\sum_{n=1}^{N} h(n) = \sqrt{2} \tag{3.5}$$

$$\begin{aligned} \sum_{n=1}^{N} h(n)h(2n + l) &= 1 \; if \; l = 0 \\ &= 0 \; if \; l \neq 0 \end{aligned} \tag{3.6}$$

The discrete sequences $h(n)$ and $g(n)$ represent discrete filters that solve each equation, where $g(n) = (-1)^n h(N - n + 1)$. The scaling and wavelet functions are the prototype of a class of orthonormal basis functions of the form

$$\varphi_{m,n}(t) = 2^{\frac{m}{2}} \varphi(2^m t - 1); \;\; m, n \in Z \tag{3.7}$$

$$\psi_{m,n}(t) = 2^{\frac{m}{2}} \psi(2^m t - 1); \;\; m, n \in Z \tag{3.8}$$

Where, the parameter 'm' controls the dilation or compression of the function in time scale and amplitude. The parameter 'n' controls the translation of the function in time and Z is the set of integers. The DWT is implemented by sending a signal successively through a low pass and high

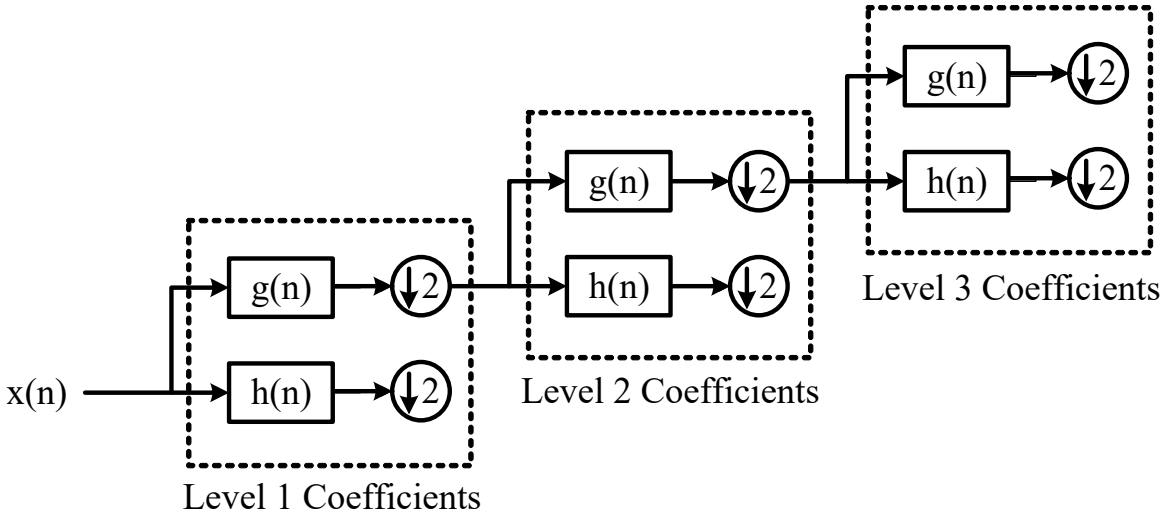


Figure 3.1: Three level decomposed discrete wavelet transform

pass filters to produce the approximation and detailed coefficients respectively. This can be described as follows.

$$a_1(n) = g(n) * x(n) = \sum g(k)x(2n-k) \tag{3.9}$$

$$d_1(n) = h(n) * x(n) = \sum h(k)x(2n-k) \tag{3.10}$$

where $a_1(n)$ and $d_1(n)$ are the approximation and detailed coefficients at first level of decomposition. The lengths of $a_1(n)$ and $d_1(n)$ is N/2 where N is the length of the signal x(n). A 3-level multi-resolution DWT decomposition has been illustrated in Fig.3.1.

### 3.3.2 Stationary Wavelet Transform (SWT)

A threshold is used in wavelet domain to smooth out or to eliminate some coefficients of wavelet transform of the measured signal. The noise content of the signal is reduced effectively under the non-stationary environment, but the results obtained from it are not optimal mainly because of the loss of the invariant translation property [71]. To overcome this deficiency of DWT, SWT can be used. The SWT is similar to the DWT where the high-pass and

low-pass filters are applied to the input signal at each level, in which the downsampling stage at each scale is replaced by an upsample of the filter before the convolution, as illustrated in Fig.3.2.

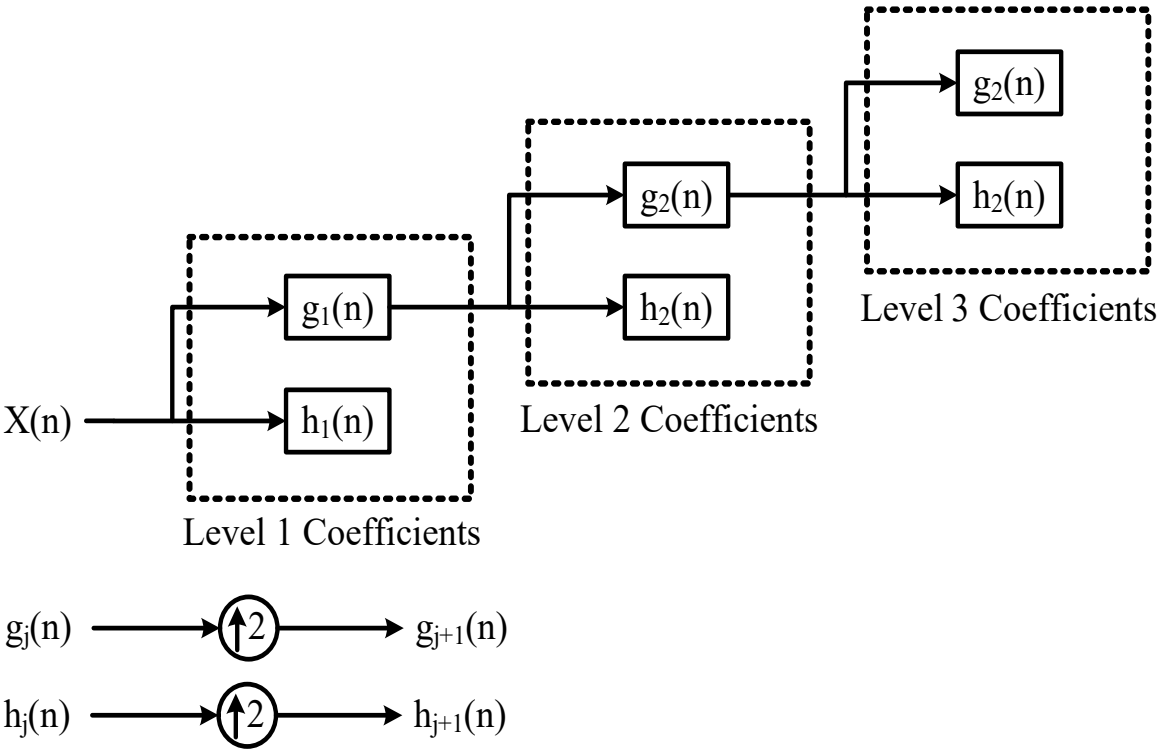


Figure 3.2: Three level decomposed stationary wavelet transform

Suppose we are given a signal $x(n)$ of length N where N $=2^J$ for some integer J. Let h(n) and g(n) be the impulse responses of the low-pass filter and the high-pass filter. The impulse responses are chosen such that the outputs of the filters are orthogonal to each other. At the first level of SWT, the input signal $x(n)$ is convolved with $g_1(n)$ to obtain the approximation coefficients $h_1(n)$ and with $g_1(n)$ to obtain the detailed coefficients $d_1(n)$, i.e

$$a_1(n) = g_1(n) * x(n) = \sum g_1(n-k)x(k) \tag{3.11}$$

$$d_1(n) = h_1(n) * x(n) = \sum h_1(n-k)x(k) \tag{3.12}$$

$a_1(n)$ and $d_1(n)$ are of length N instead of N/2 as in the DWT case because no sub-sampling is performed,. At the next level of the SWT, $a_1(n)$ is used

to generate $a_2(n)$ and $d_2(n)$ with modified filter $h_2(n)$ and $g_2(n)$, which are obtained by up sampling $h_1(n)$ and $g_1(n)$, respectively.

$$a_2(n) = h_2(n) * x(n) = \sum h_2(n-k)a_1(k) \tag{3.13}$$

$$d_2(n) = g_2(n) * x(n) = \sum g_2(n-k)a_1(k) \tag{3.14}$$

This process is continued recursively. The output of the SWT is then the detail coefficients $d_1(n)$, $d_2(n)$,....,$d_{J0}(n)$ and the approximation coefficients $a_{J_0}(n)$ where $J_0 < J$. Compare with the traditional WT, the SWT has several advantages. First, each sub-band has the same size, so it is easier to get the relationship among the sub-bands. Second, the resolution can be retained since the original data is not decimated. Also at the same time the wavelet coefficients contain many redundant information which helps to distinguish the noise from feature.

## 3.4 Proposed Fault Detection Scheme using DWT

A 3-phase, 5-hp, 415 V, 4 pole Induction Motor with 36 slots, 6 coils per phase and 54 turns per coil is considered for the present study. In this thesis diagnosis of various faults such as single phasing, under voltage, unbalanced supply, stator inter-turn fault, stator line to ground fault, stator line to line fault and sudden electrical load change are discussed. To identify the best mother wavelet, various types of wavelets have been tested using MRA of three-phase currents. Biorthogonal 5.5 (Bior5.5) is found to be the most suitable mother wavelet for the proposed scheme. The three-phase currents of the motor are sampled at 6 kHz and decomposed with Bior5.5 to obtain detailed level coefficients over a moving window of a chosen sample length.

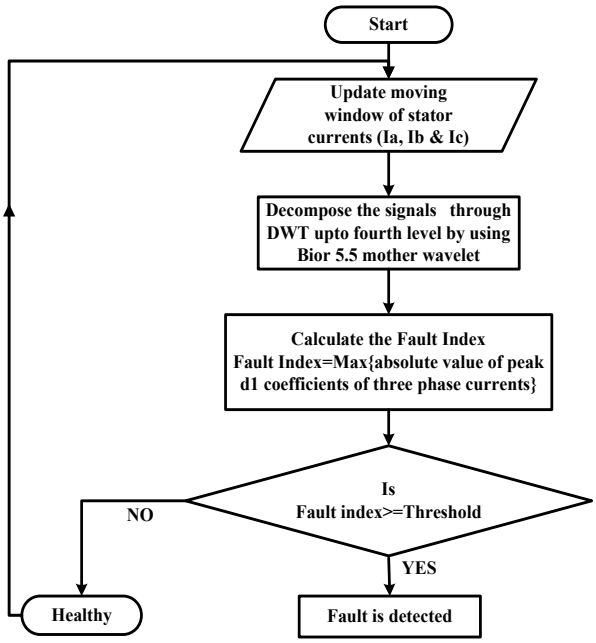


Figure 3.3: Flow chart for proposed fault detection method using DWT

The absolute value of peak d1 coefficients are obtained for all the phase currents. The maximum value of these absolute peak values is defined as fault index ($I_f$) and this is compared with fixed threshold value to detect the fault. Figure 3.3 illustrates the proposed detection algorithm using DWT.

### 3.4.1 Validation of Proposed Fault Detection Scheme using DWT

Initially, the proposed algorithm is tested with various faults data obtained from the simulated models which are created in MATLAB/Simulink environment. The variations in captured three-phase currents of normal and stator inter-turn fault are shown in figures 3.4 and 3.5 respectively. By looking these waveform, nothing is detected as a short circuit between the turns in a stator winding causes a small degree of unbalance in stator current. These unbalances cannot be seen directly from the three-phase stator currents if the level of turn short circuit is too small i.e. 1 or 2 turns.

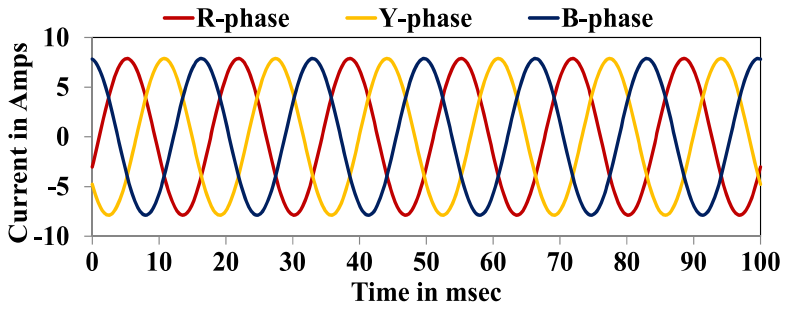


Figure 3.4: Three-phase current signals for healthy condition of a 5-hp induction motor

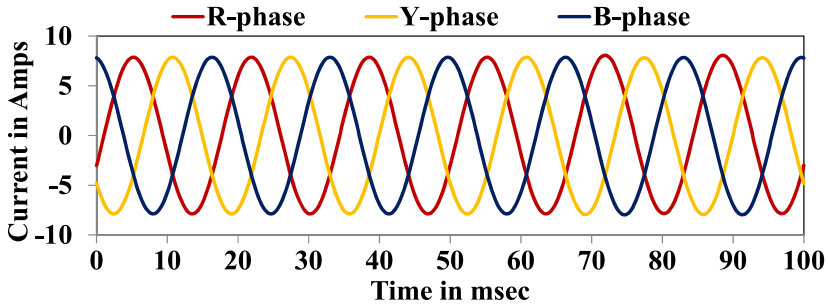


Figure 3.5: Three-phase current signals for 2-turn short circuit in R-phase of a 5-hp induction motor

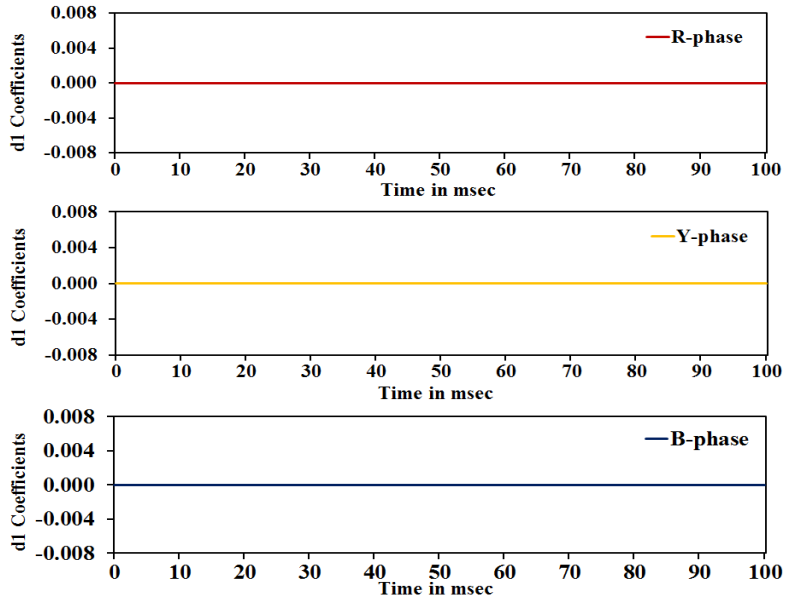


Figure 3.6: Variation in d1 coefficients for healthy condition

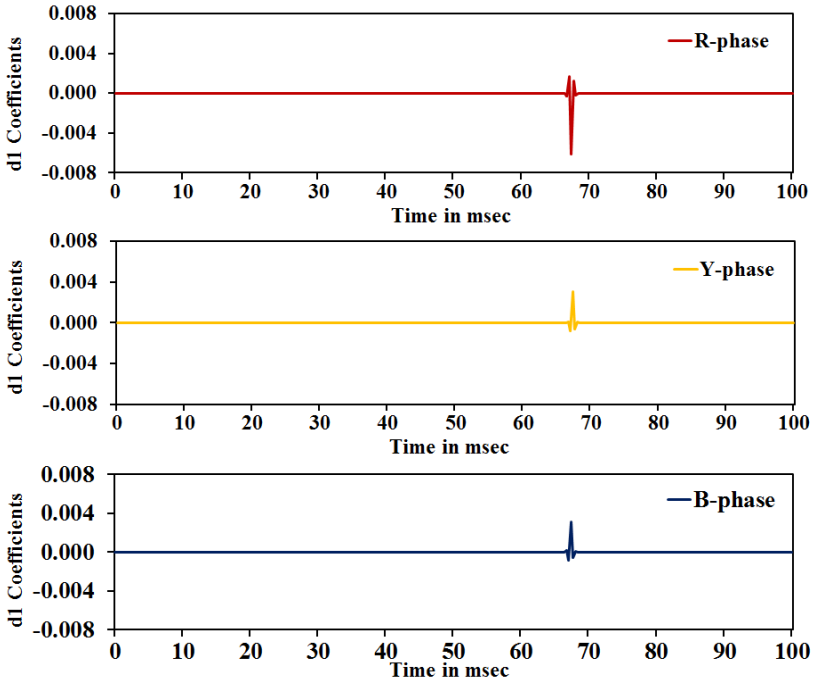


Figure 3.7: Variation in d1 coefficients for a 2-turn short circuit in R-phase

Thus, frequency domain analysis is needed for analysing the signal but this can not give the fault instant. Hence, a time-frequency domain analysis of Bior5.5 mother wavelet is used to analyse the three-phase current signals. The corresponding variation in detail level coefficients are demonstrated in figures 3.6 and 3.7. From these figures, it is cleared that the high frequency component is exist in case of fault only.

The maximum absolute peak values of three-phase detail level

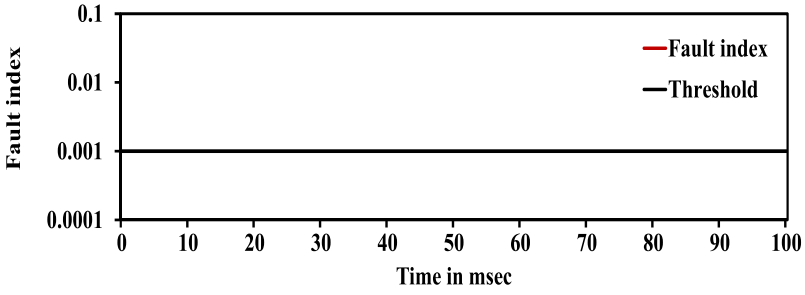


Figure 3.8: Variation in fault index for healthy condition

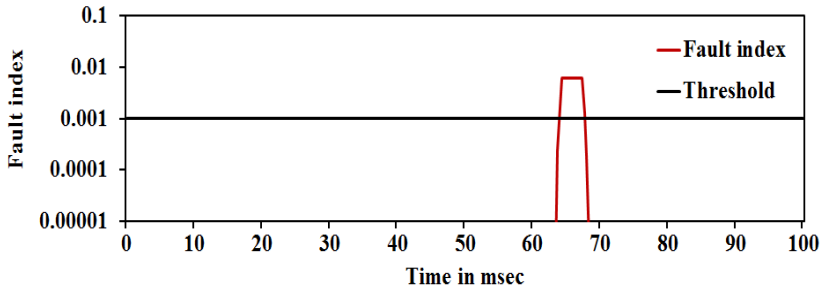


Figure 3.9: Variation in fault index for a 2-turn short circuit at 0 degree inception

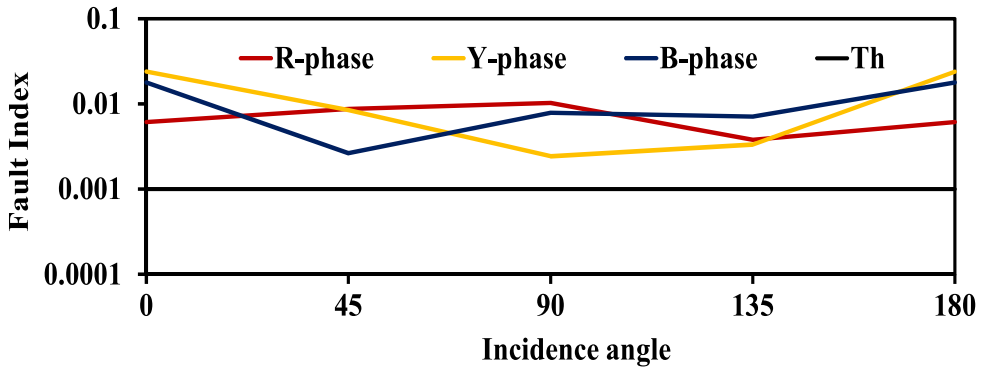


Figure 3.10: Variation in fault index for an inter turn fault on coil-1

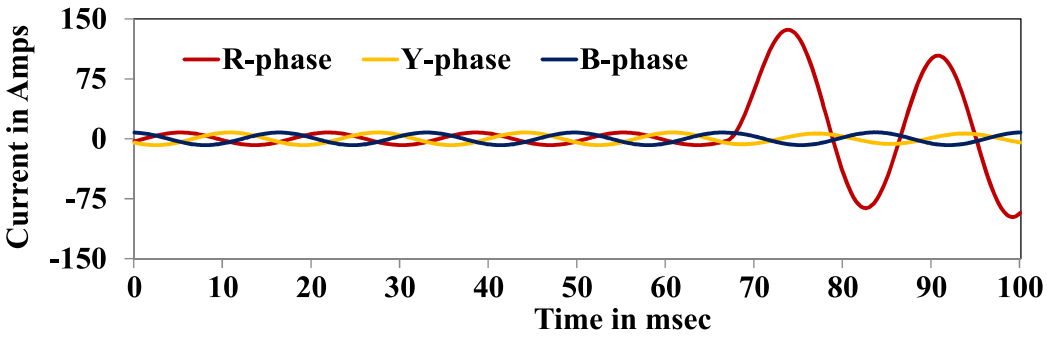


Figure 3.11: Three-phase current signals for a LG fault in R-phase of a 5-hp induction motor

coefficients is set as a fault index which is compared with fixed threshold to detect the fault and its instant. Figures 3.8 and 3.9 demonstrate the variations in fault index w.r.t the defined threshold of healthy and 2-turn fault cases. These results predicted that the fault index crosses the threshold when the fault occurs. But the fault index depends on fault incidence angles. Hence, to check the reliability of the proposed algorithm, vary the fault instant from $0 - 180^0$ insteps of $45^0$. Figure 3.10 shows the variation in fault indices w.r.t incidence angle for stator inter-turn fault in R-phase of coil-1. The results demonstrate that the fault index is above the threshold if machine is under fault condition other wise it is below the threshold.

The variations in three-phase currents of other considered cases of stator line to ground fault, stator line-line fault, single phasing, under voltage and supply unbalance are shown in figures 3.11, 3.12, 3.13, 3.14 and 3.15 respectively. The figures 3.11 to 3.15 are demonstrates that the current drawn by the machine increases when the fault occurs. Figures 3.16, 3.17, 3.18, 3.19 and 3.20 illustrate the variation in d1 coefficients for various cases such as stator line to ground fault, stator line-line fault, single

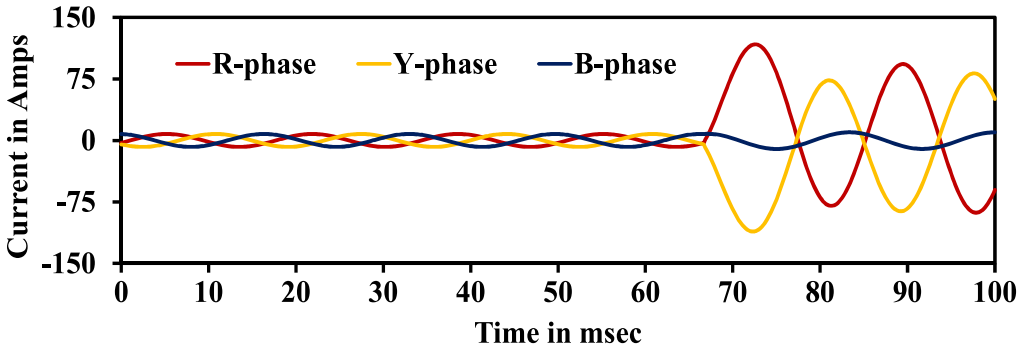


Figure 3.12: Three-phase current signals for a LL fault between R and Y phases of a 5-hp induction motor

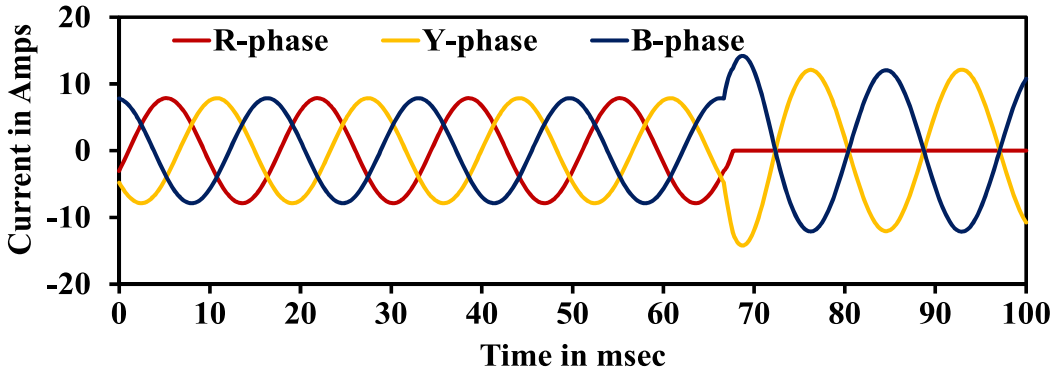


Figure 3.13: Three-phase current signals for a single phasing in R phase of a 5-hp induction motor

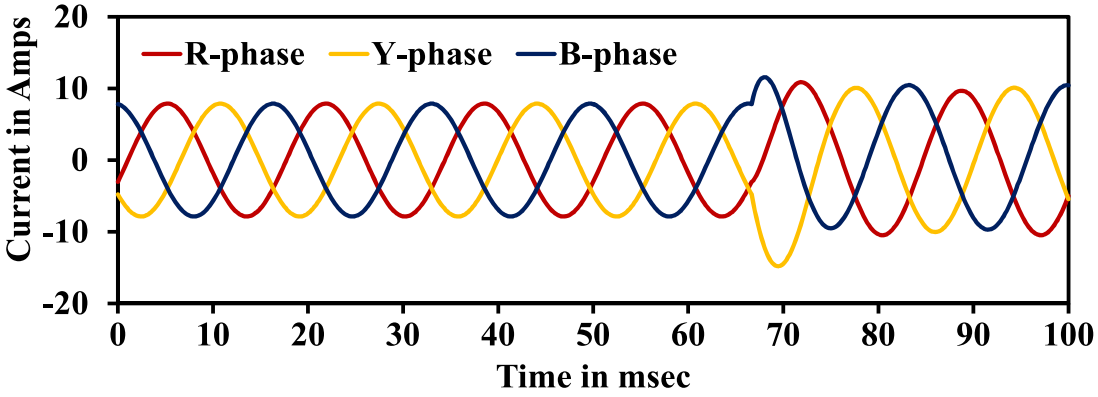


Figure 3.14: Three-phase current signals for a 30% under voltage of a 5-hp induction motor

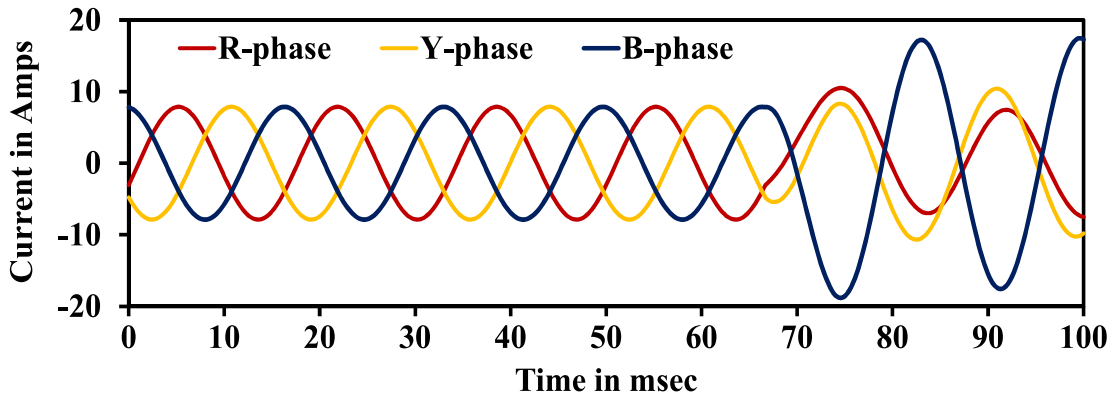


Figure 3.15: Three-phase current signals for a 10% supply unbalance in R phase of a 5-hp induction motor

phasing, under voltage and supply unbalance respectively. From these figures, it is cleared that the magnitude of high frequency component is more in fault effected phase. Figure 3.21 shows the variation of fault indices w.r.t incidence angles of the considered cases. From this figure, it is proved that the fault index is above the threshold for any type of fault happened on a 3-phase Induction motor. Hence, the proposed method is effective in detecting the fault and its instant.

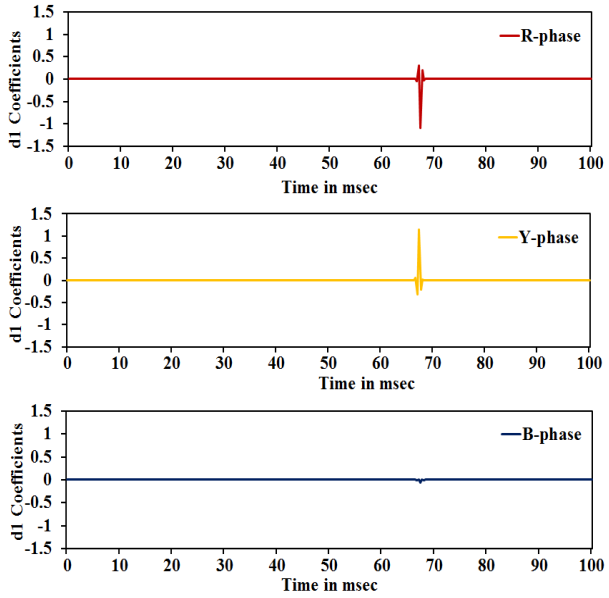


Figure 3.17: Variation in d1 coefficients for a LL fault between RY phases

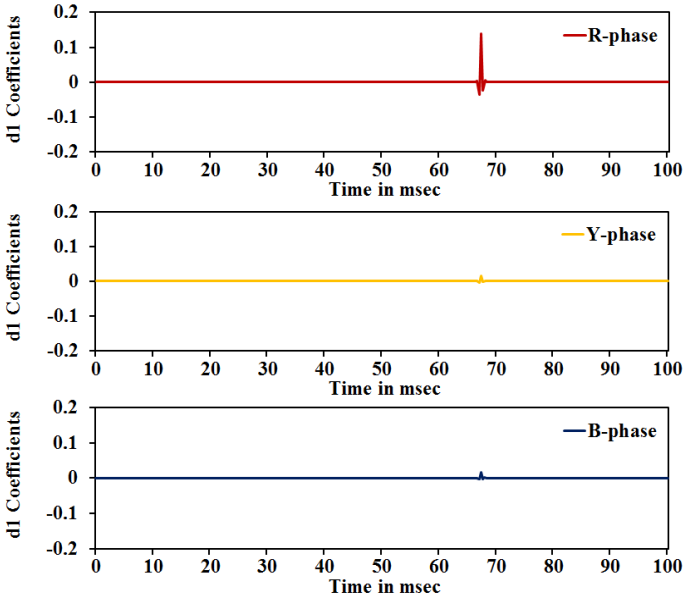


Figure 3.16: Variation in d1 coefficients for a LG fault in R-phase

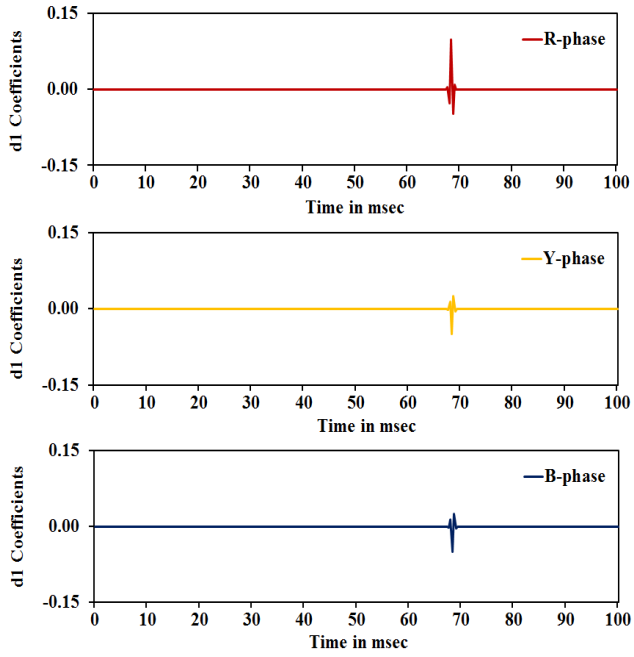


Figure 3.18: Variation in d1 coefficients for a single phasing in R phase

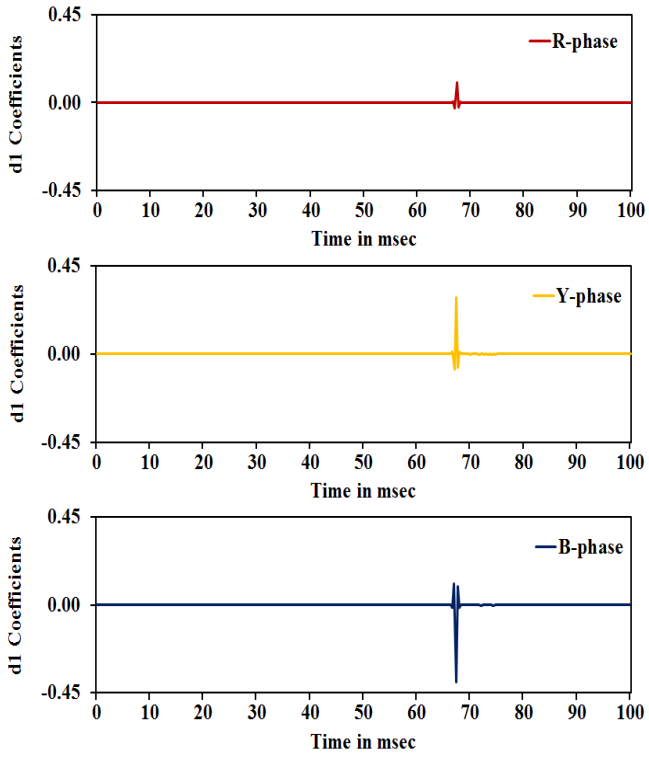


Figure 3.19: Variation in d1 coefficients for 30% under voltage

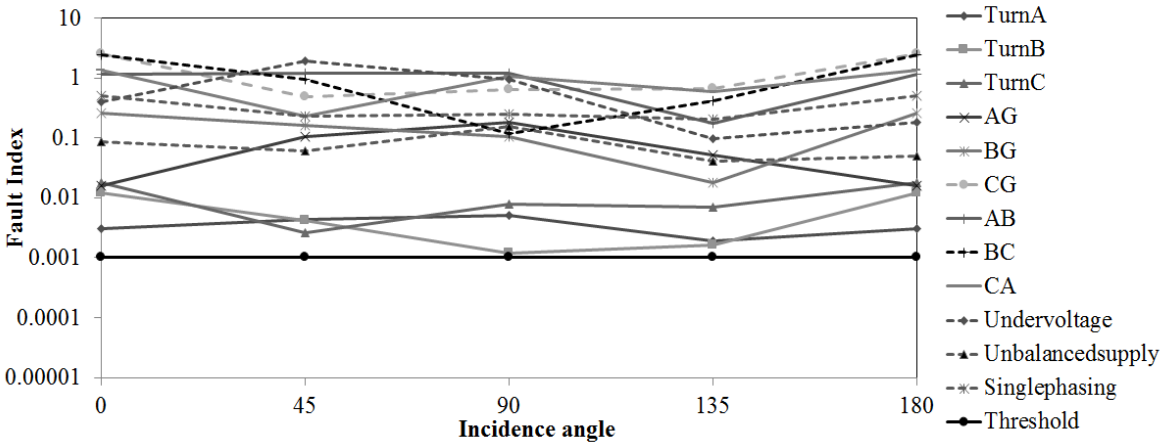


Figure 3.21: Variation in fault index for various faults

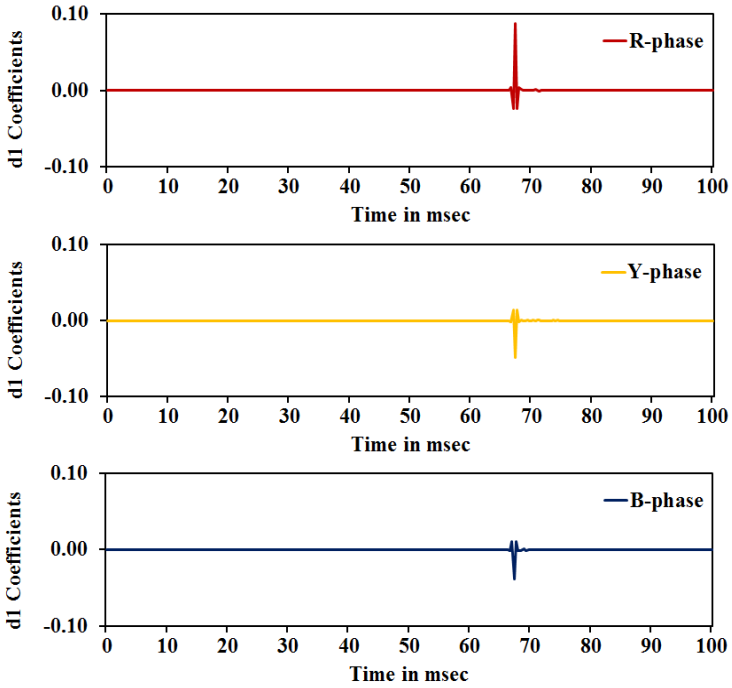


Figure 3.20: Variation in d1 coefficients for 10% supply unbalance

To check the reliability and practicality of the proposed detection algorithm, a 10 dB of Gaussian noise is added to each phase. Figures 3.22 and 3.23 demonstrate the three-phase currents and detail level coefficients for a 2-turn fault in R-phase of a 5-hp induction motor under noise condition. The variations in fault indices are shown in figure 3.24. The

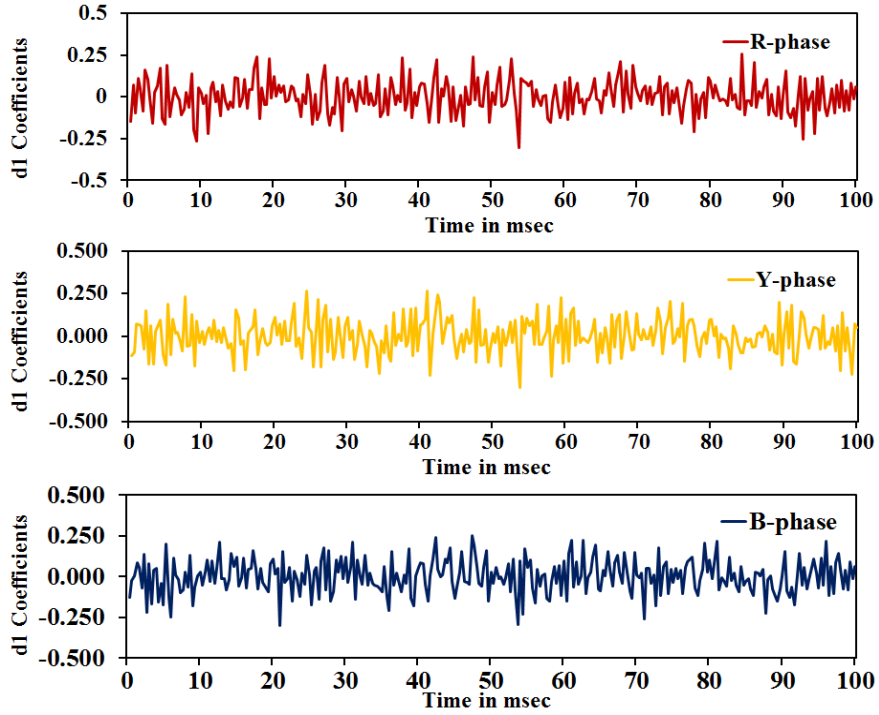


Figure 3.23: Variation in d1 coefficients for a 2-turn fault in R-phase

variation of fault indices in figure 3.24 are above threshold through out window but fault is created at an instant of 66.67 msec. Hence, the proposed fault detection algorithm is fail to work under noisy environment.

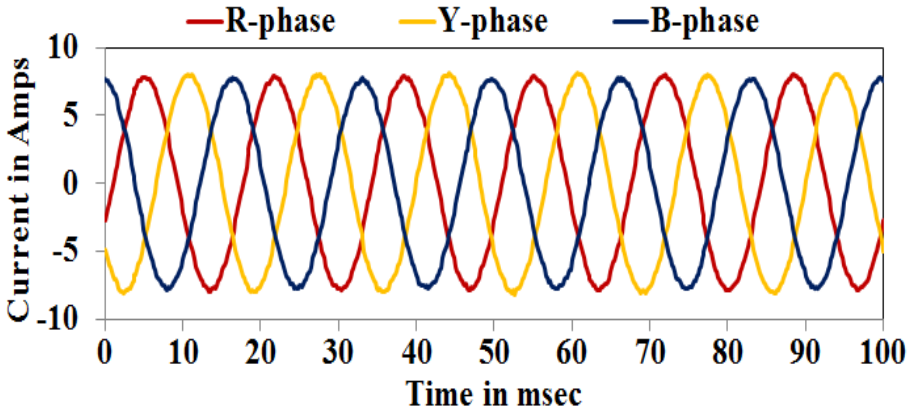


Figure 3.22: Three-phase current signals for 2-turn fault in R-phase of a 5-hp induction motor

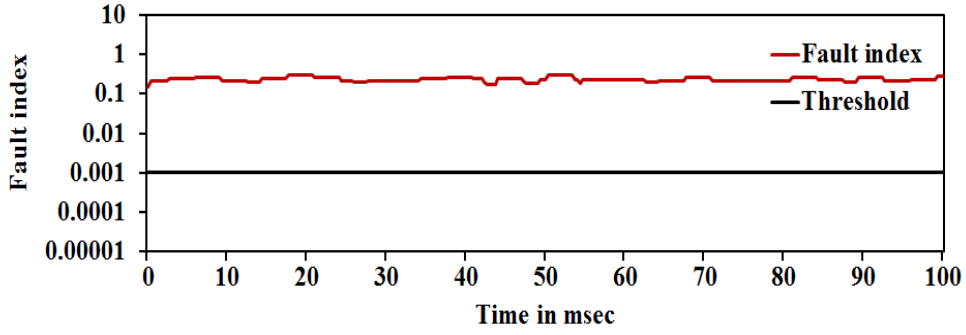


Figure 3.24: Variation in fault index for a 2-turn fault at 0degree inception

## 3.5 Proposed Fault Detection Scheme using SWT and DWT

In signal processing based techniques the fault detection takes place based on a threshold logic, which is used to distinguish the fault condition from normal condition. The fault signature in stator inter-turn short circuit is much smaller due to noise level and supply unbalance conditions, thus the fault detection using fixed threshold in both the cases are error prone. Hence, an adaptive threshold based fault detection algorithm is essential for fault diagnosis in a 3-phase induction motor. In wavelet de-noising techniques, the threshold selection is very important. Donoho and Johnstone [72] have introduced various threshold schemes and discussed both hard and soft thresholds in a general context. Among these threshold selection rule, universal threshold (fixed threshold) selection rule is the most widely used rule. However, in practical applications the variance of the noise signal changes time to time. Thus, the threshold should be selected based on an interval or level. Hence, a level-based threshold has been selected for the proposed algorithm. The selection of mother wavelet

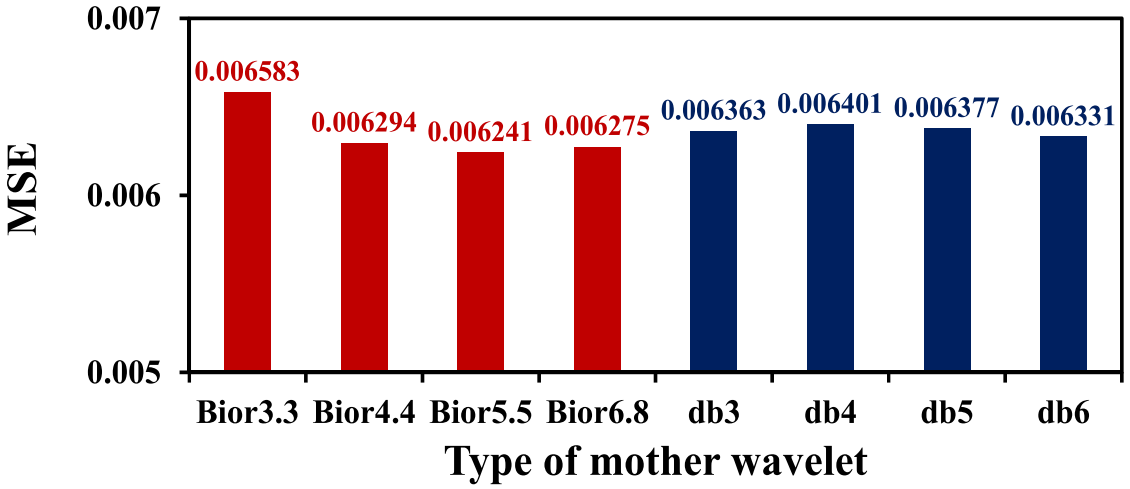


Figure 3.25: Variation in MSE for DWT of different mother wavelets

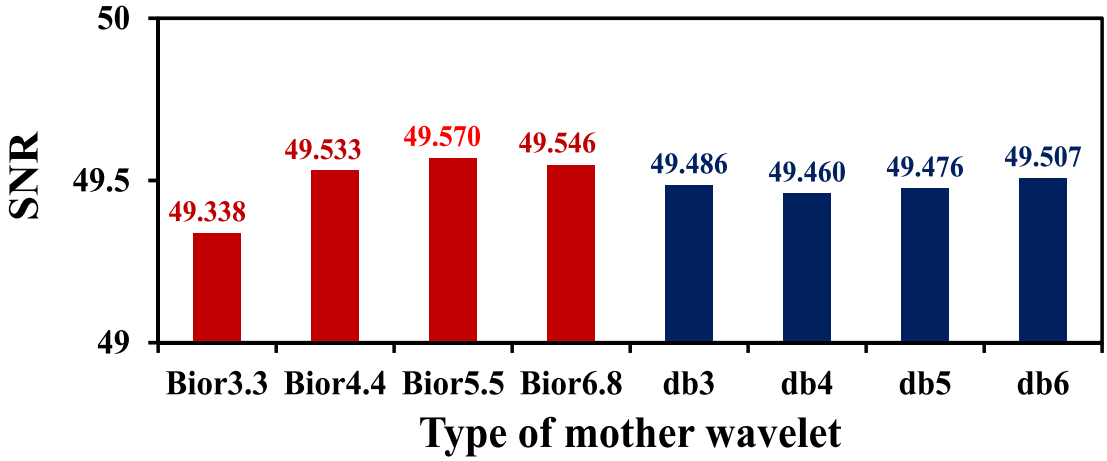


Figure 3.26: Variation in SNR for DWT of different mother wavelets

mainly depends on the type of application. In the proposed technique, Bior5.5 wavelet has been used as the wavelet basis function for fault detection and identification. Initially, the captured signal is reconstructed by using DWT with different mother wavelet. The performance of signal denoising based on wavelet has been addressed in [73], [74]. Figures 3.25 and 3.26 represent the variation in Mean Square Error (MSE) values and Signal to Noise Ratio (SNR) values. From the results, it is observed that

the best performance by using biorthogonal family of mother wavelet. Later, the performance of signal denoising is checked with SWT and DWT for different wavelets of biorthogonal family and calculating MSE and SNR between the reference signal and reconstructed signal of stator current in phase R. Figure 3.27 shows the MSE and SNR of SWT and DWT for different wavelets of bi-orthogonal family. Results are clearly demonstrated that SWT is far better than DWT in the application of noise elimination or signal reconstruction and also highlighted that Bior5.5 mother wavelet have less MSE compared to others.

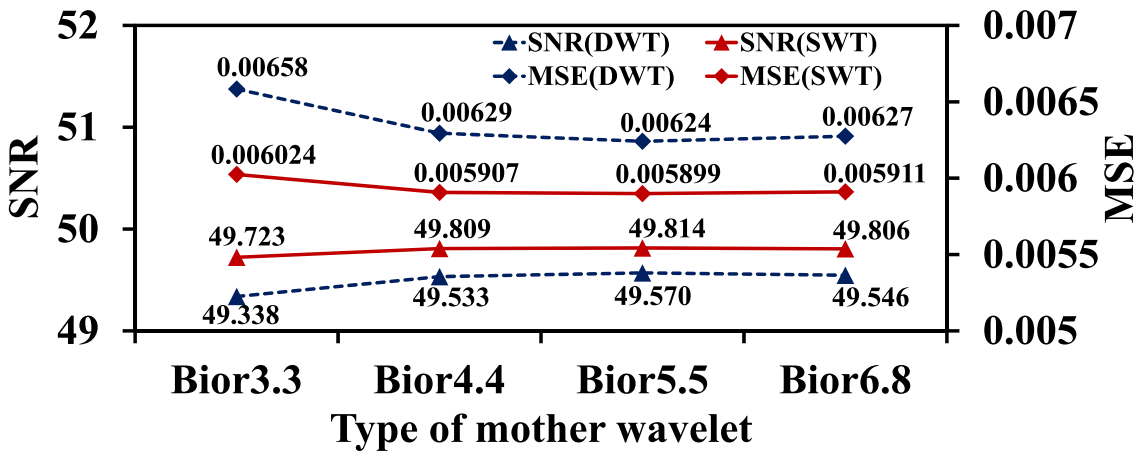


Figure 3.27: Comparison of DWT and SWT

Figure 3.28 shows the flowchart for the proposed fault detection technique using SWT and DWT. In this scheme, the level based threshold reconstruction is used to eliminate the effects due to supply unbalance and machine unbalance. The reconstructed three phase current signals are obtained by using stationary wavelet denoising technique with level based threshold. The three-phase currents of the motor are decomposed with SWT of Bior5.5 to obtain approximate and detail level coefficients up to $6^{th}$ level. The thresholds of d1 coefficients to d4 coefficients are made

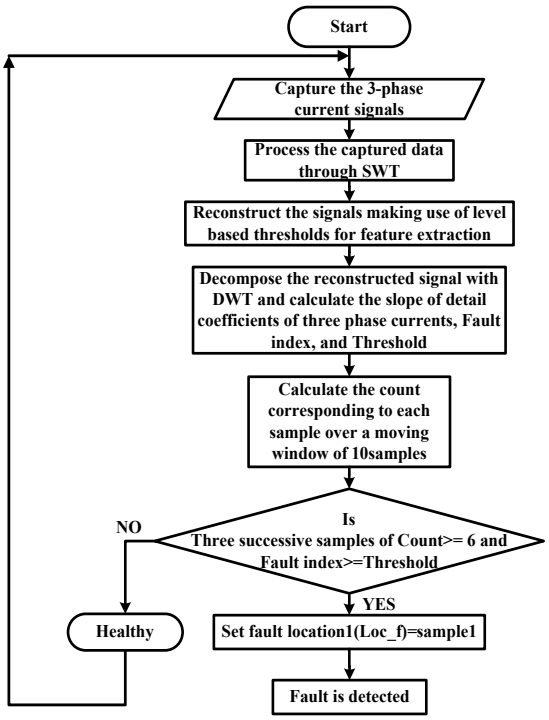


Figure 3.28: Flow chart for proposed SWT and DWT based fault detection scheme

maximum while threshold value of d5 coefficients is set to a high value as this band of frequency components is sensitive to the supply unbalances. The threshold value of d6 is calculated based on its peak value in the $1^{st}$ cycle and multiplied with a distortion factor which is calculated from RMS value of the current signal during start-up (preferably in the $1^{st}$ cycle). The threshold value of d6 coefficient may enhance the fault signature because the pre-fault value is subtracted from the captured signal. Therefore, the reconstructed signals are called as fault residues. This type of reconstruction is essential especially if fault feature is very close to the noise level.

A short circuit between the turns in a stator winding causes an unbalance in stator currents. These unbalances cannot be seen directly from the three-phase stator currents if the level of turn short circuit is too

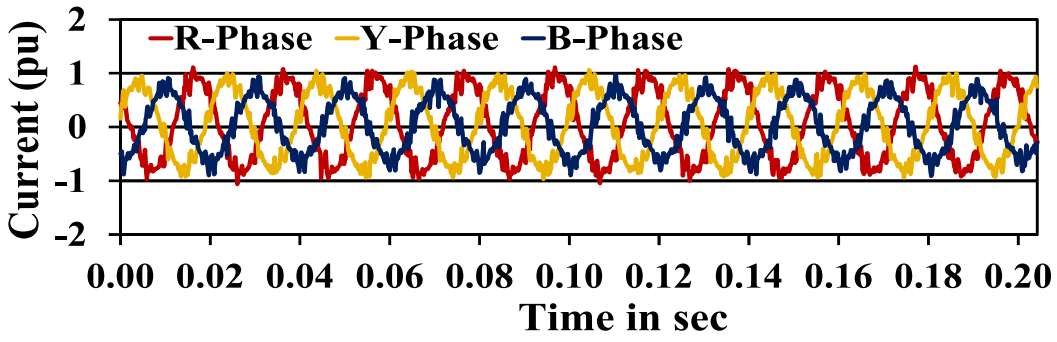


Figure 3.29: Three-phase current signals for 2-turn fault in R-phase of a 3-hp induction motor under experimental case

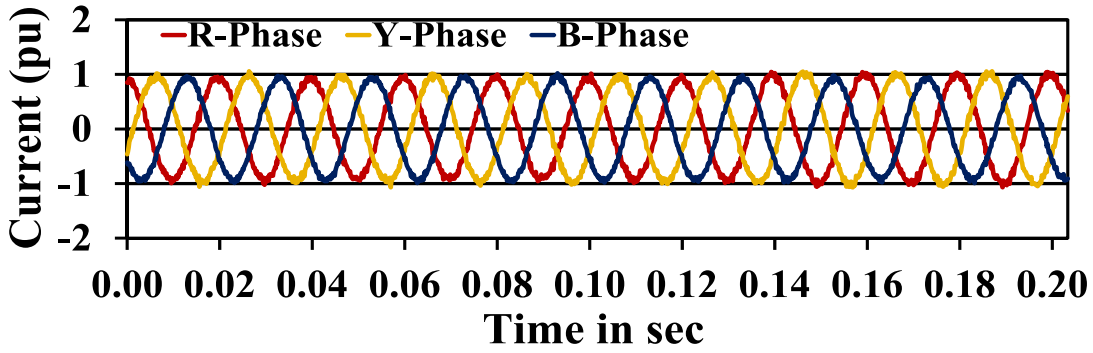


Figure 3.30: Three-phase current signals for 2-turn fault in R-phase of a 3-hp induction motor under simulation

small i.e. 1 or 2 turns. Figures 3.29 and 3.30 illustrate the three-phase stator currents for 2-turn short circuit in R-phase of a 3-hp induction motor under experimental and simulation cases respectively. From these figures, the unbalance due to stator inter-turn short circuit is not predictable by visual observation due to the noise and supply or machine unbalances. Hence, an efficient pre-processing method is required for extracting the fault residues and instant of fault even though the motor is operated under noisy environment. In this regard, time-frequency domain analysis of SWT is considered and carried out in MATLAB/Simulink environment for predicting the fault residues. Figures 3.31 and 3.32 show the three-phase

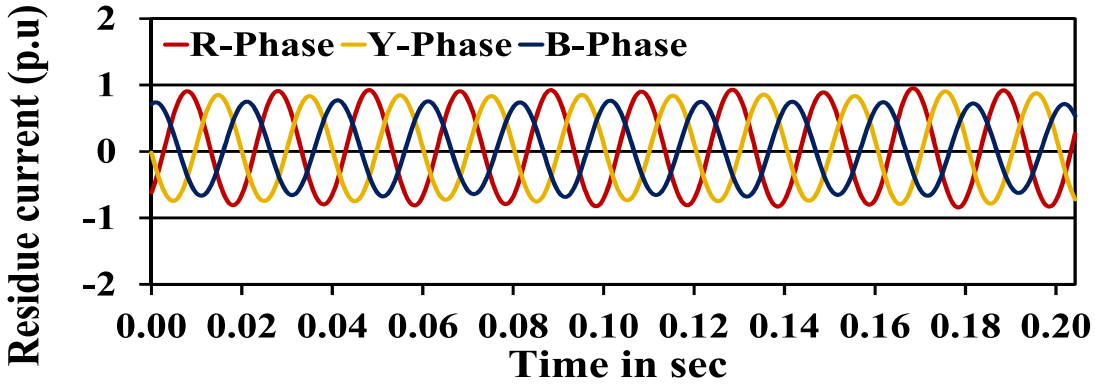


Figure 3.31: Three-phase residues for 2-turn fault in R-phase of a 3-hp induction motor based on minimax method under experimental case

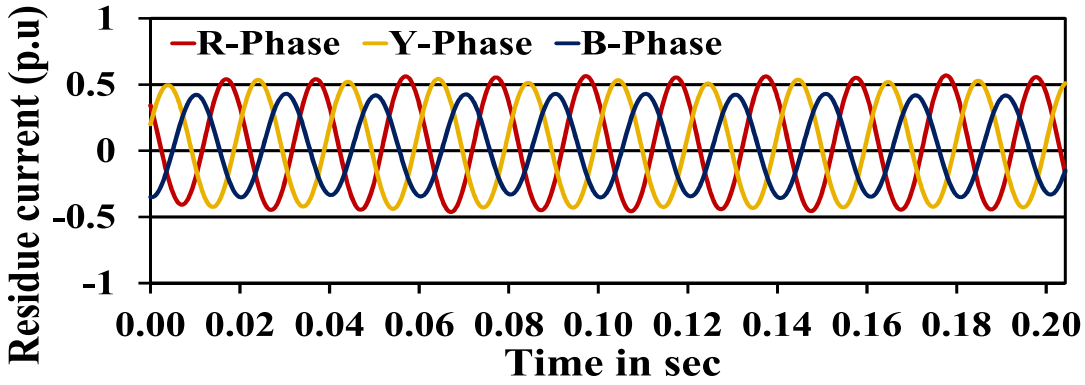


Figure 3.32: Three-phase residues for 2-turn fault in R-phase of a 3-hp induction motor based on proposed method under experimental case

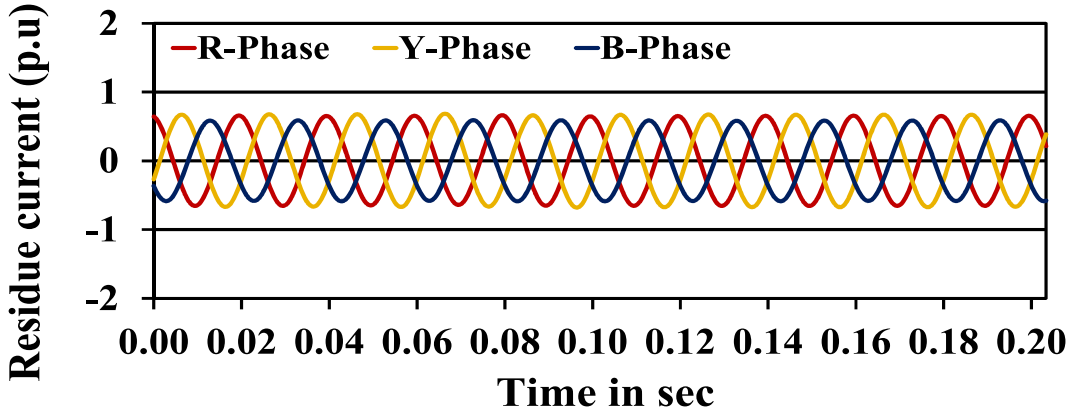


Figure 3.33: Three-phase residues for 2-turn fault in R-phase of a 3-hp induction motor based on minimax method under simulation

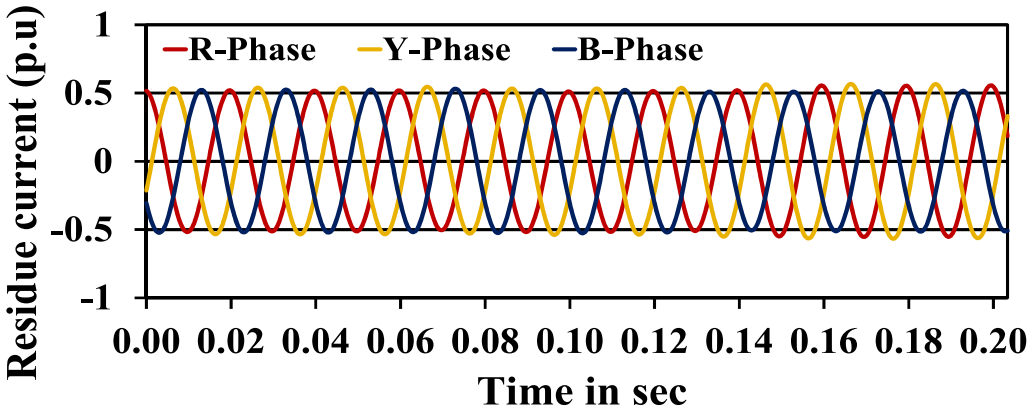


Figure 3.34: Three-phase residues for 2-turn fault in R-phase of a 3-hp induction motor based on proposed method under simulation

residues based on minimax method and proposed threshold based method (mentioned in above section) for 2-turn short circuit in R-phase under experimental case. Similarly, Figures 3.33 and 3.34 show the simulation cases of three-phase residues based on minimax method and proposed method respectively. From the waveforms, the identification of the fault instant is not possible. Hence, once again the reconstructed signals are decomposed by using DWT of Bior5.5 mother wavelet. To extract the fault features, the three-phase residues are decomposed up to $4^{th}$ level. Figures 3.35 and 3.36 demonstrate the experimental cases of detail coefficients of residues based on minimax method and proposed method respectively. Similarly, Figures 3.37 and 3.38 show the simulation cases of detail coefficients of residues based on minimax method and proposed method. The variation in detail level coefficients in Figures 3.36 and 3.38 have clearly demonstrated that the proposed wave reconstruction and decomposition is superior than the existing method to extract the fault features and its instant. The variation in three-phase detail level coefficients exists throughout the interval if decomposed signal is reconstructed with

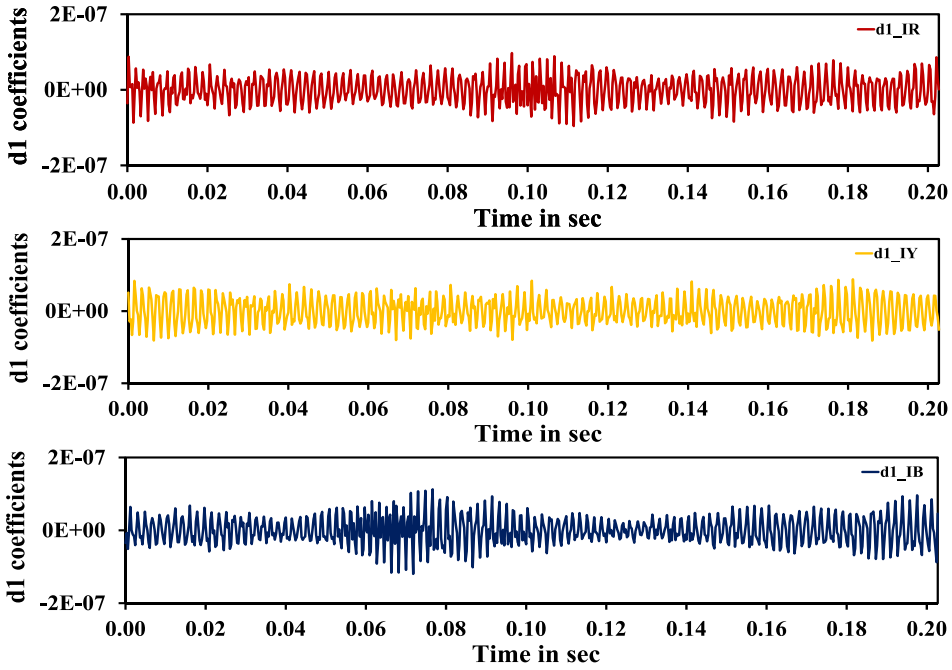


Figure 3.35: Variation in d1 coefficients for 2-turn fault in R-phase of a 3-hp induction motor based on minimax method under experimental case

minimax method. Hence, fault feature extraction and instant of fault identification are not possible by using minimax method.

In this, the instant of fault disturbance is estimated accurately by calculating the ratio between the difference in sample values of the $d1$ coefficients of three phase residues over a moving window of 3 samples and difference in sample intervals. In discrete signal the ratio between the difference in sample values and difference in sample intervals is called as a slope. The slopes of each phase $d1$ coefficients are calculated for identifying the variation levels due to disturbances. A fault is detected by comparing the fault index with adaptive threshold. The fault index $I_f$ and Adaptive Threshold $Th$ are calculated using the following equations.

$$\begin{aligned} I_f(n) &= |slope\_d1I_R(n)| + |slope\_d1I_Y(n)| \\ &\quad + |slope\_d1I_B(n)| \end{aligned} \tag{3.15}$$

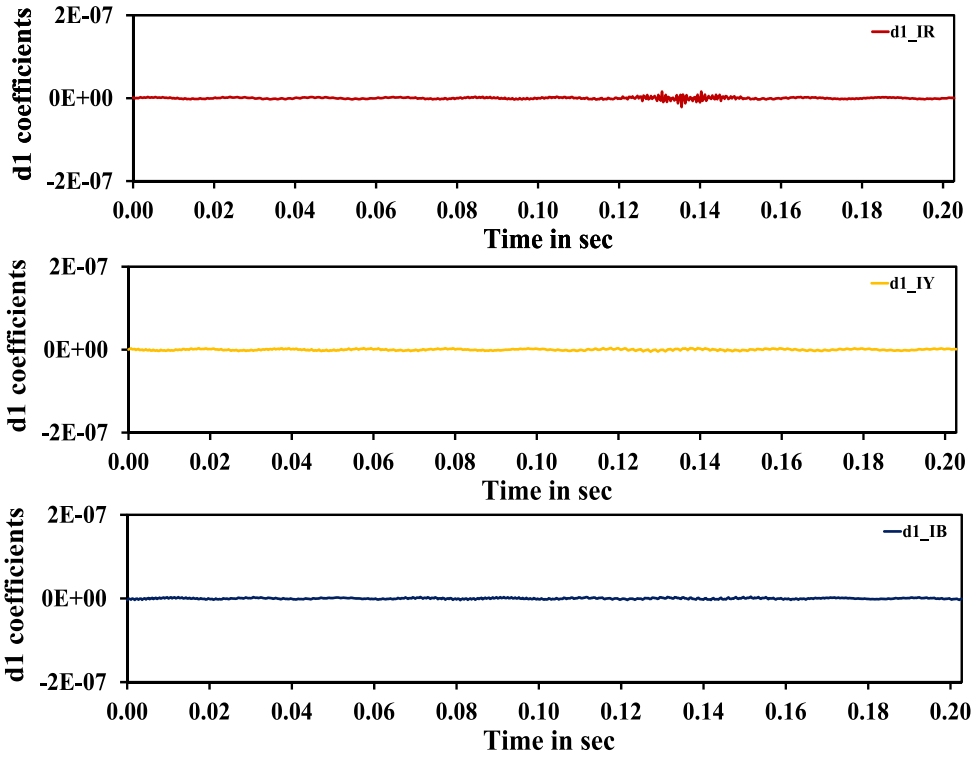


Figure 3.36: Variation in d1 coefficients for 2-turn fault in R-phase of a 3-hp induction motor based on proposed method under experimental case

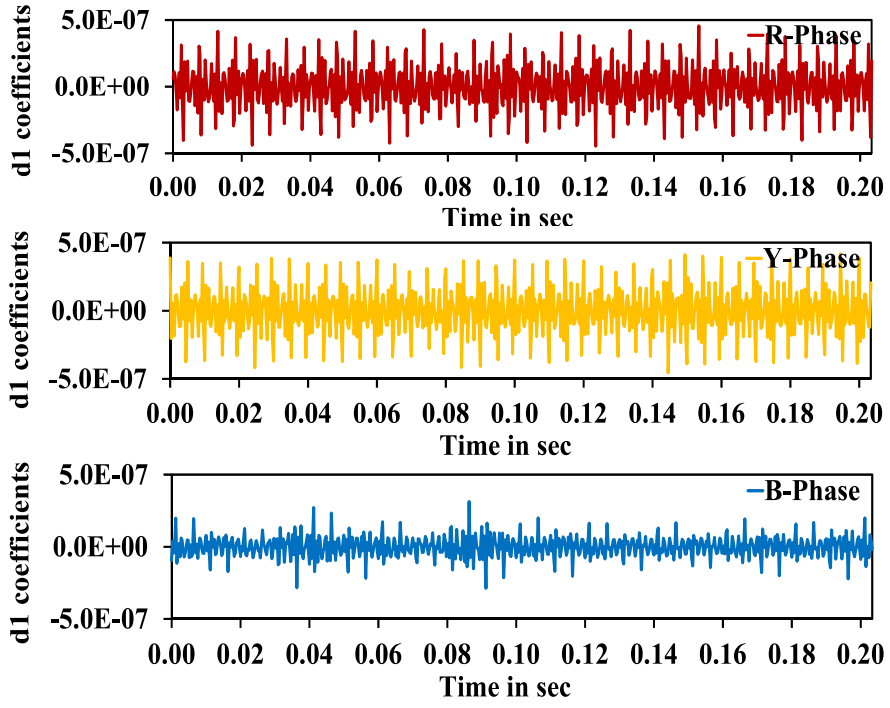


Figure 3.37: Variation in d1 coefficients for 2-turn fault in R-phase of a 3-hp induction motor based on minimax method under simulation

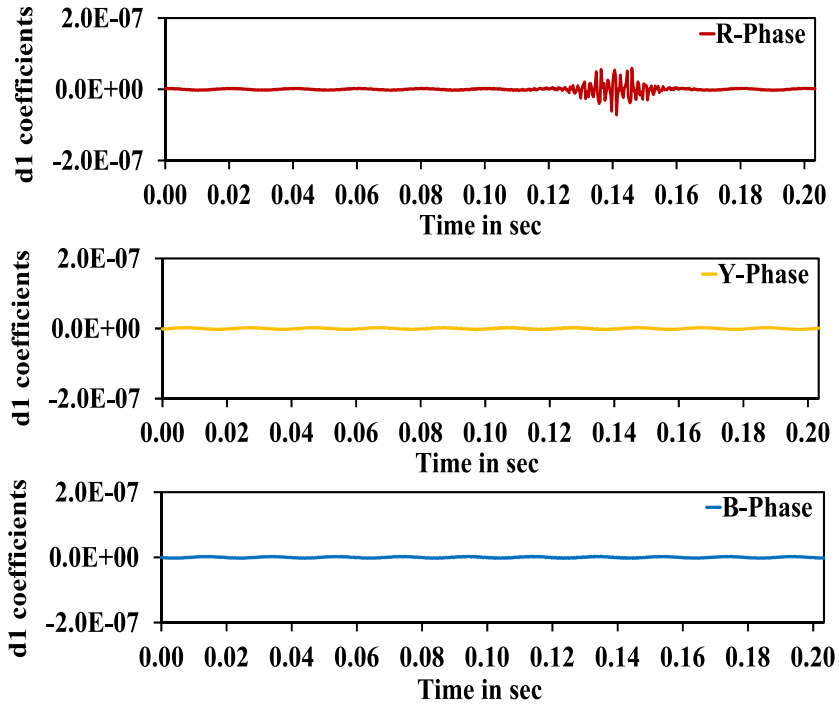


Figure 3.38: Variation in d1 coefficients for 2-turn fault in R-phase of a 3-hp induction motor based on proposed method under simulation

where $n = 1 : N_1$; $N_1$ is the total number of samples in captured window (1 Sec); $slope\_d1I_R$, $slope\_d1I_Y$, and $slope\_d1I_B$ are the slopes of $d1$ coefficients of residue currents in R, Y and B phases respectively.

$$Th = max(Fault\ index\ in\ 1^{st}\ cycle) * K * max(Current\ in\ 1^{st}\ cycle) * factor \tag{3.16}$$

where K is the rise factor and

$$factor = \begin{cases} 2 \text{ if Ratio} \leq 3 \\ \dfrac{\text{Significand value of max}(I_f) \text{ in a captured window}}{\text{Largest integer less than the significand value}} \\ \text{if Ratio} > 3 \end{cases}$$

$$where\ Ratio = \frac{Maximum\ I_f\ in\ a\ captured\ window}{Maximum\ I_f\ in\ 1^{st}\ cycle}$$

### 3.5.1 Validation of Proposed Detection Scheme

#### 3.5.1.1 Experimental Setup

An experimental setup was prepared with a 3-phase, 3-hp, 4 pole, 50 Hz, 415 V induction motor with 36 slots, 6 coils per phase and 72 turns per coil. In order to create the inter-turn short circuit, two tapping points were taken out per phase from the neutral of the stator winding. Each tapping is having a resistance of 0.8 ohms. The stator inter-turn faults are created experimentally by connecting a suitable resistance between tapping point and ungrounded neutral [6]-[7]. If the fault is a turn-turn or turn to ground then suitable resistance is connected between tapping point of one phase to another or phase to ground. Another rating of 10-hp induction motor is also considered for creating various stator faults for a level of 2 turns to 8 turns in steps of 2 turns without connecting any resistance between tapping point and neutral of the stator winding because in this case tapping points are directly taken to the level of 2 turns. Totally 6 types of disturbances are created in these machines. Figures 3.39 and 3.40 show the experimental setup for creating various disturbances on a 3-hp and 10-hp induction motors respectively. In the proposed method, three-phase stator currents were captured in 1 Sec with a sampling frequency of 6.6 kHz by using UNIPOWER DIP 8000 network analyzer. To acquire the signals the network analyzer is connected to a personal computer.

#### 3.5.1.2 Simulation Models for Stator Faults

To create the stator faults, a 3-hp induction motor with a star connected stator winding is considered and various abnormalities are simulated in

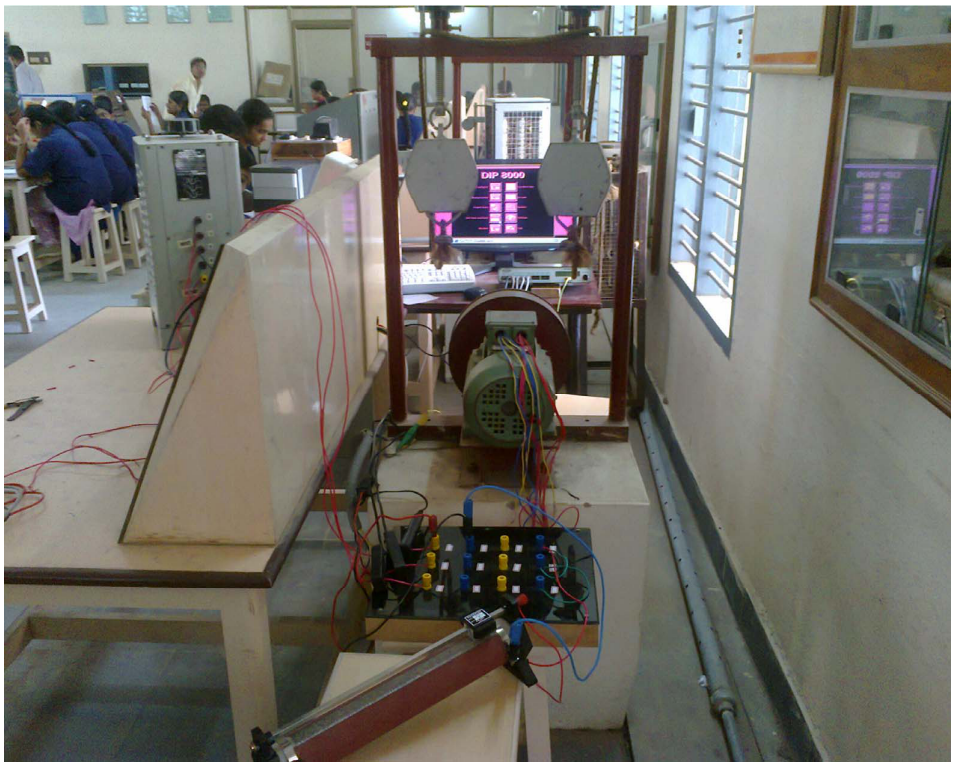


Figure 3.39: Experimental setup for 3-hp induction motor

Figure 3.40: Experimental setup for 10-hp induction motor

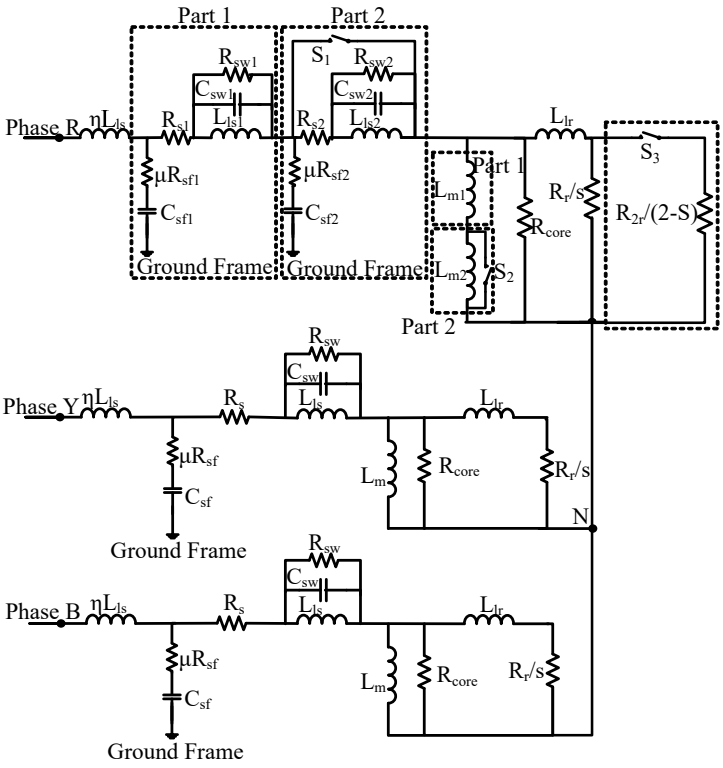


Figure 3.41: Simulation diagram for stator inter-turn fault in R-phase

MATLAB/Simulink environment. The stator winding corresponding to the phase in which the fault is created is divided into two parts. An additional branch is connected in parallel to the rotor resistance to simulate the disturbance component due to stator inter-turn fault. The fault is created by closing three switches as shown in Figure 3.41 and it illustrates the stator inter-turn fault in R-phase of a 3-phase induction motor. In this figure Part 1 refers to a healthy portion of the winding and Part 2 refers the shortened turns of the winding. The resistance, inductance, and insulation capacitance are divided in proportion to the number of short-circuited turns. The various percentages of turn level short circuits in different phases have been simulated in the MATLAB/Simulink environment. In case of stator turn-turn faults, the switches S1 and S2 are connected between phases and if it is a stator turn to ground fault the switches S1 and

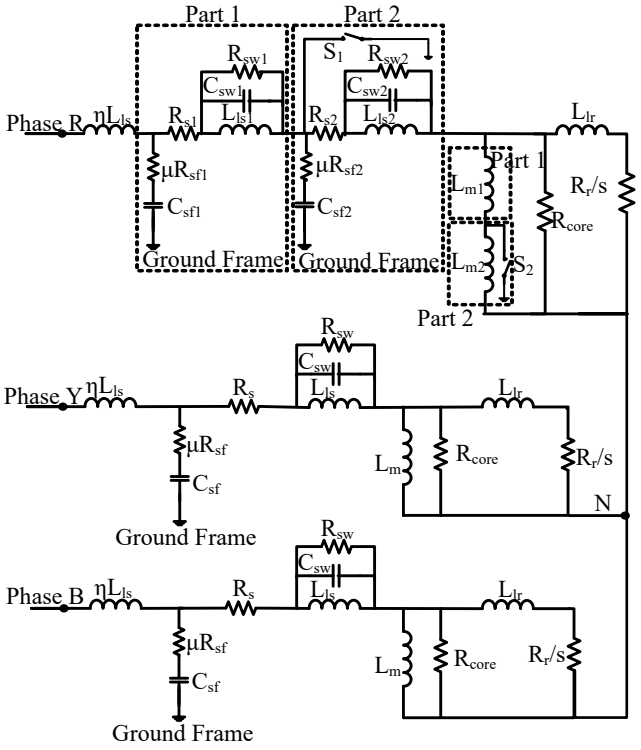


Figure 3.42: Simulation diagram for stator line-ground fault in R-phase

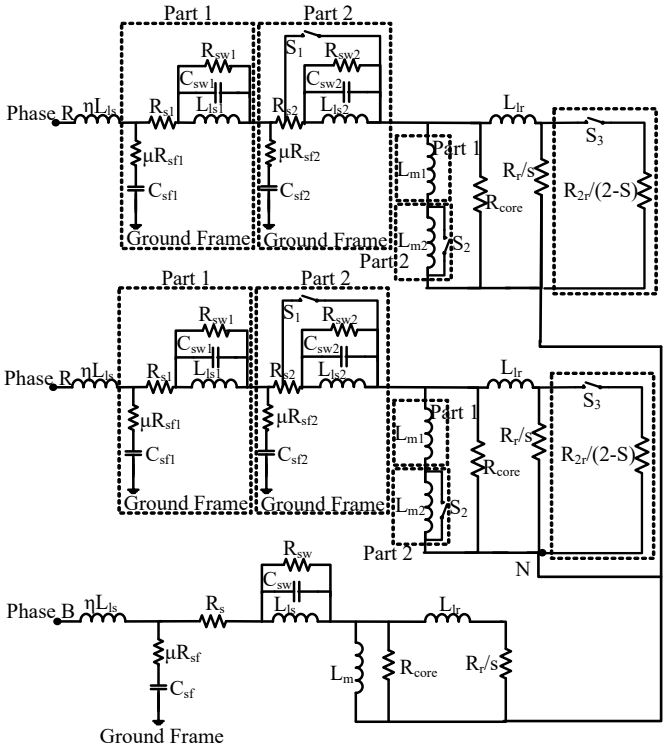


Figure 3.43: Simulation diagram for stator line-line fault between R-Y phases

S2 are connected between phase and ground. To bring the simulation model more close to practical scenarios Gaussian noise is injected in each phase. The noise level to be injected is calculated from the captured three-phase stator currents in the experimental setup. Totally 9 types of stator faults are considered for simulation such as stator inter-turn fault in R phase, Y phase, B phase, stator phase-phase fault between RY phases, YB phases, BR phases and stator phase-ground fault in R phase, Y phase, B phase. Figures 3.42 and 3.43 show the circuit diagram for stator phase-phase fault and stator phase-ground fault respectively.

To validate the proposed detection criteria, a 3-hp induction motor is considered and various abnormalities are simulated in MATLAB/Simulink environment. The same abnormalities are created on a 3-hp induction motor using experimental setup also. Especially, stator inter-turn are created under certain loaded conditions such as 0%, 50% and 100%. Stator inter-turn faults are also created experimentally on no-load condition with minor supply unbalances like 1%, 2%, and 3%. In case of simulation that is extended up to 5% due to numerous data required for classification.

#### 3.5.1.3 Experimental and Simulation Results for a 3-hp Induction Motor

The variation in captured three-phase currents, three-phase residues and fault indices along with its count values for healthy case under simulation are shown in figures 3.44, 3.45 and 3.46. Similarly, figures 3.47, 3.48 and 3.49 represent the variation in three-phase currents, three-phase residues and fault indices along with its count values for healthy with 2% supply unbalance case under simulation. Figures 3.50, 3.51 and 3.52 show the variation in three-phase currents, three-phase residues and fault indices

along with its count values for healthy case under experimental setup. Similarly, figures3.53, 3.54 and 3.55 represent the variation in three-phase currents, three-phase residues and fault indices along with its count values for healthy with 2% supply unbalance case under experimental setup. The results illustrated that all the cases of fault indices are below the adaptive threshold because the motor is operated under healthy condition.

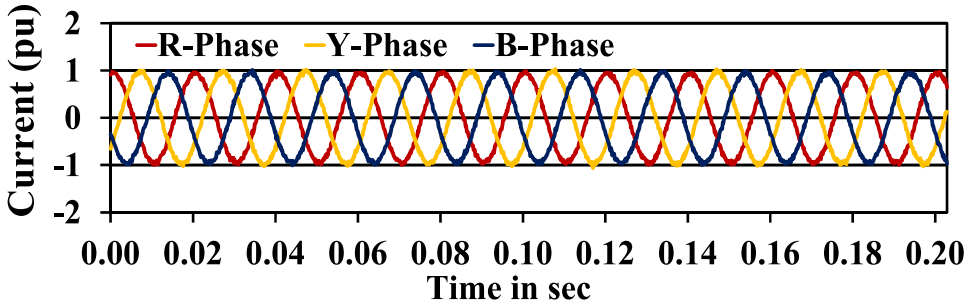


Figure 3.44: Three-phase currents under healthy condition of a 3-hp induction motor under simulation case

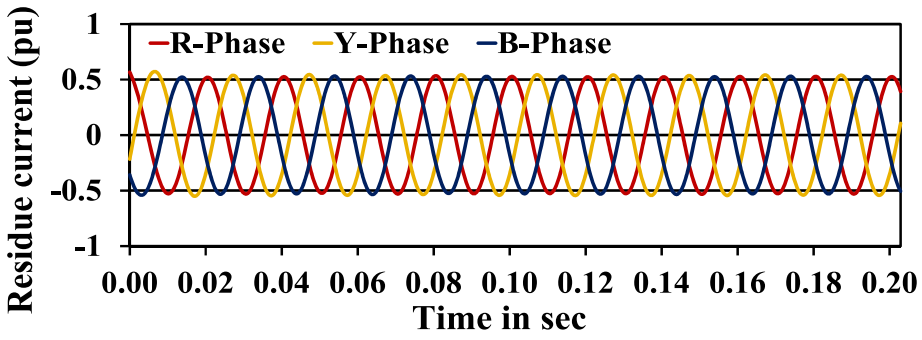


Figure 3.45: Three-phase residue currents under healthy condition of a 3-hp induction motor under simulation case

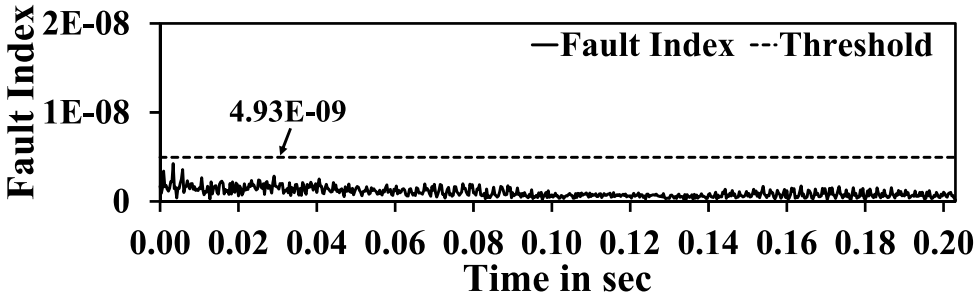


Figure 3.46: Variation in fault index under healthy condition of a 3-hp induction motor under simulation case

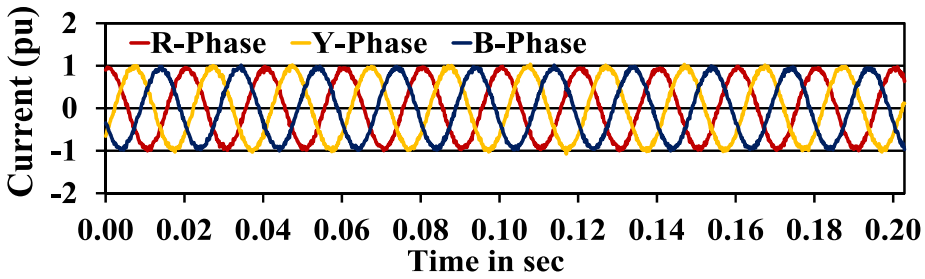


Figure 3.47: Three-phase currents under healthy condition with 2% supply unbalance of a 3-hp induction motor under simulation case

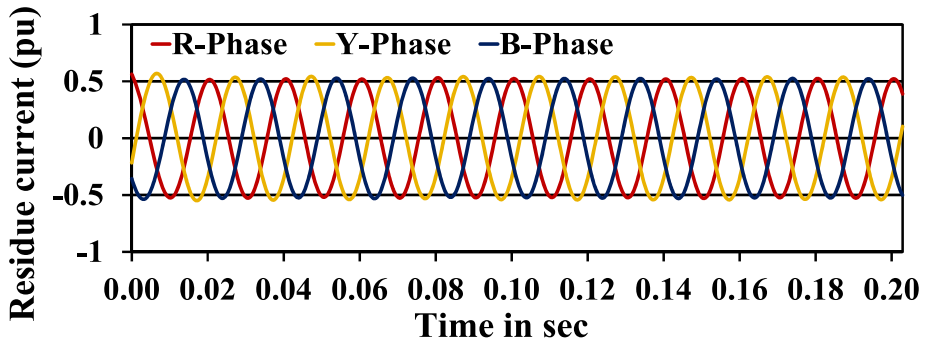


Figure 3.48: Three-phase residue currents under healthy condition with 2% supply unbalance of a 3-hp induction motor under simulation case

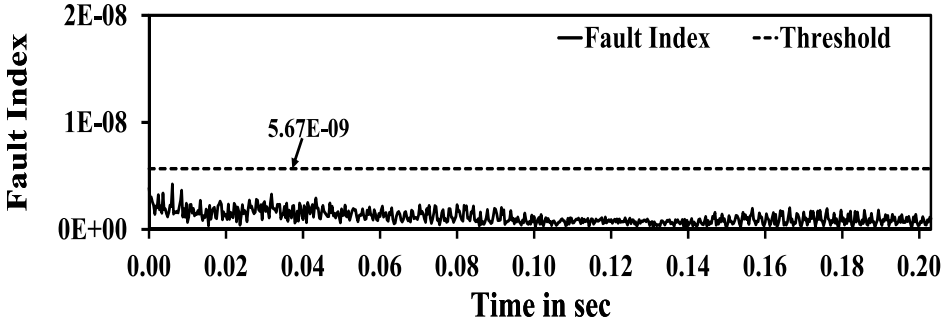


Figure 3.49: Variation in fault index under healthy condition with 2% supply unbalance of a 3-hp induction motor under simulation case

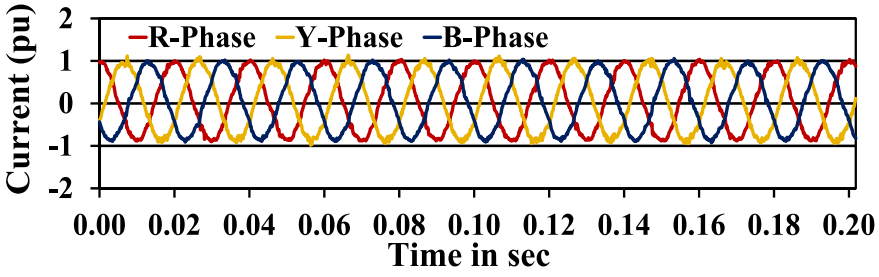


Figure 3.50: Three-phase currents under healthy condition of a 3-hp induction motor under experimental case

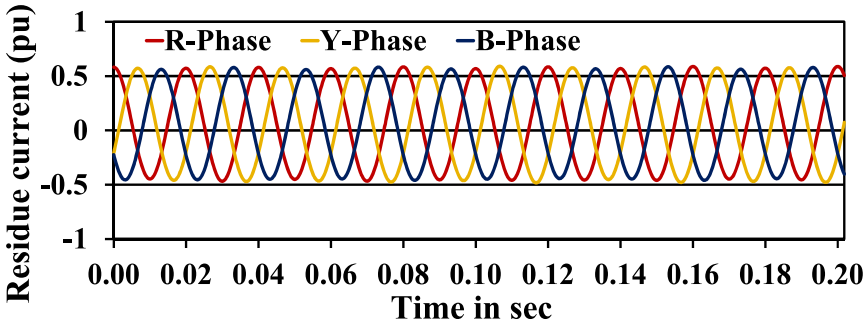


Figure 3.51: Three-phase residue currents under healthy condition of a 3-hp induction motor under experimental case

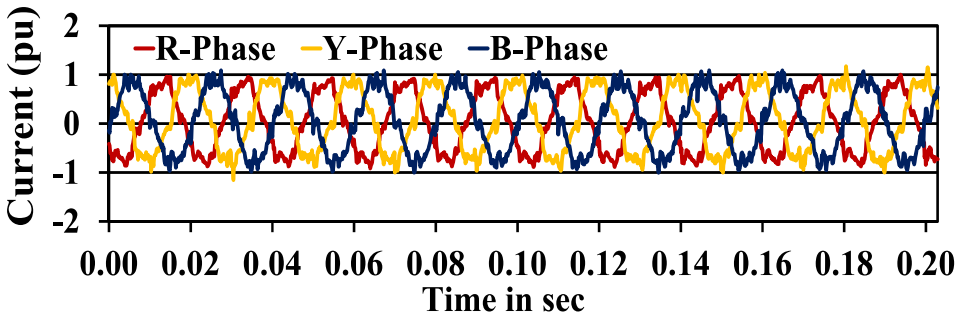


Figure 3.53: Three-phase currents under healthy condition with 2% supply unbalance of a 3-hp induction motor under experimental case

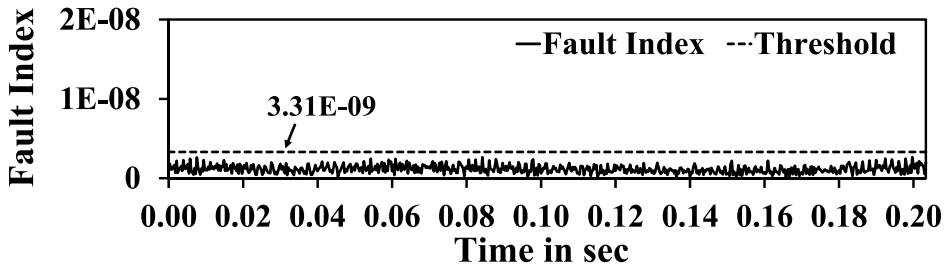


Figure 3.52: variation in fault index under healthy condition of a 3-hp induction motor under experimental case

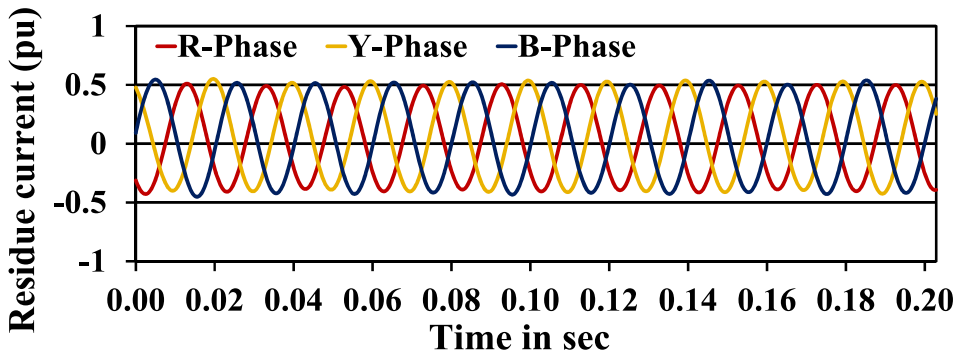


Figure 3.54: Three-phase residue currents under healthy condition with 2% supply unbalance of a 3-hp induction motor under experimental case

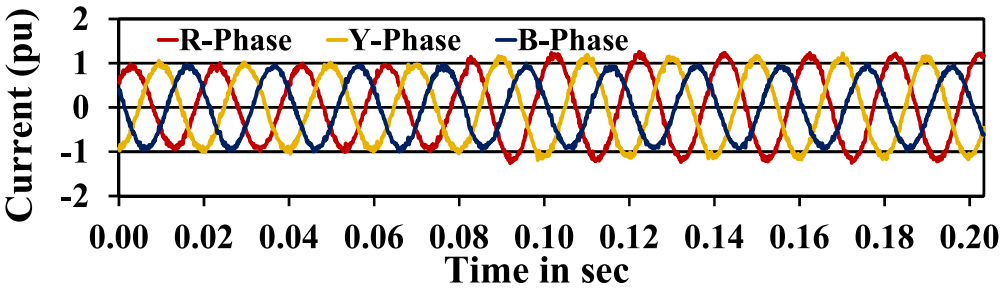


Figure 3.56: Three-phase currents for 8-turn short circuit in R-phase of a 3-hp IM under simulation

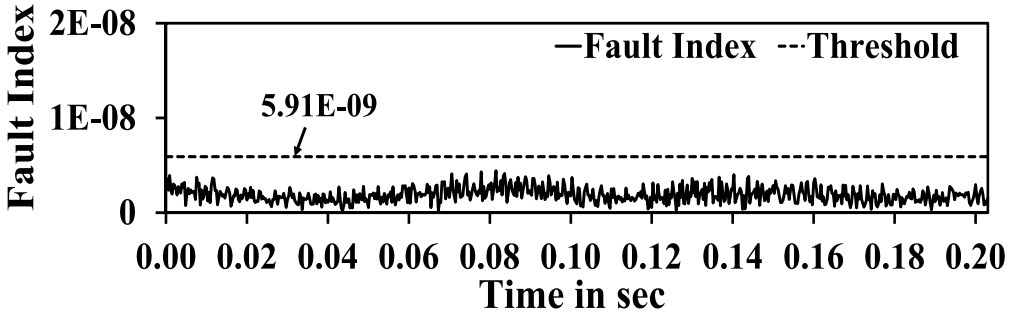


Figure 3.55: Variation in fault index under healthy condition with 2% supply unbalance of a 3-hp induction motor under experimental case

The variation in three-phase currents, three-phase residues and fault indices along with its count values of 8-turn short circuit case under simulation are shown in figures 3.56, 3.57 and 3.58. Similarly, figures 3.59, 3.60 and 3.61 show the 8-turn short circuit with 2% supply unbalance case under simulation. Figures 3.68, 3.69 and 3.70show the variations in three-phase currents, three-phase residues and fault indices along with its count values of 8-turn short circuit case under experimental setup. Similarly, figures 3.71, 3.72 and 3.73 illustrate the variations in three-phase currents, three-phase residues and fault indices along with its count values of 8-turn fault with 2% supply unbalance cases under experimental setup. Both the results of simulation and experimental case values of fault indices

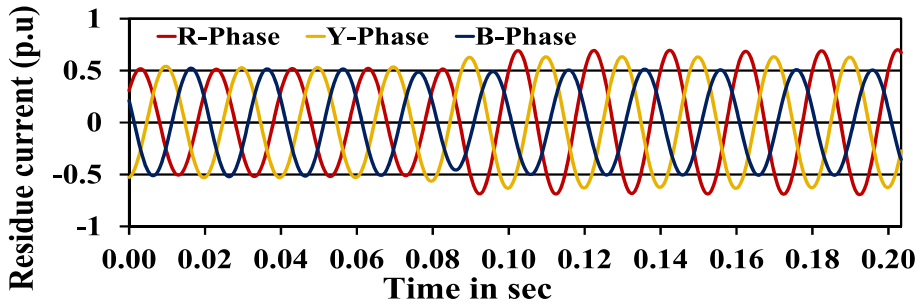


Figure 3.57: Three-phase residue currents for 8-turn short circuit in R-phase of a 3-hp IM under simulation

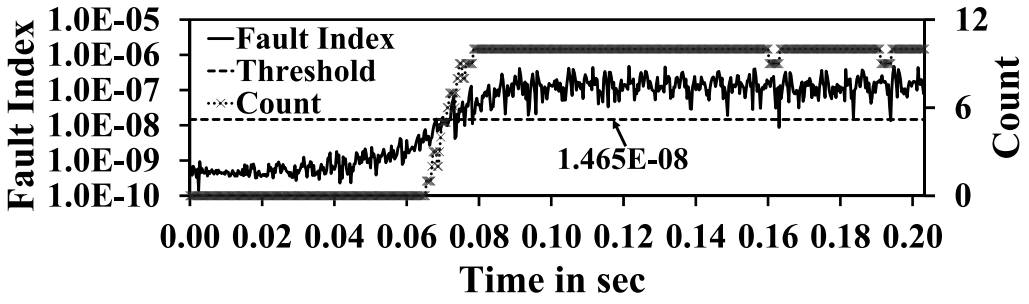


Figure 3.58: Variation in fault index for 8-turn short circuit in R-phase of a 3-hp IM under simulation

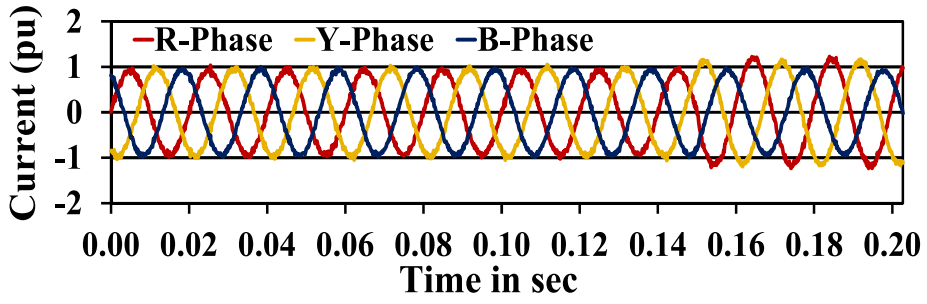


Figure 3.59: Three-phase currents for for 8-turn short circuit in R-phase with 2% supply unbalance of a 3-hp IM under simulation

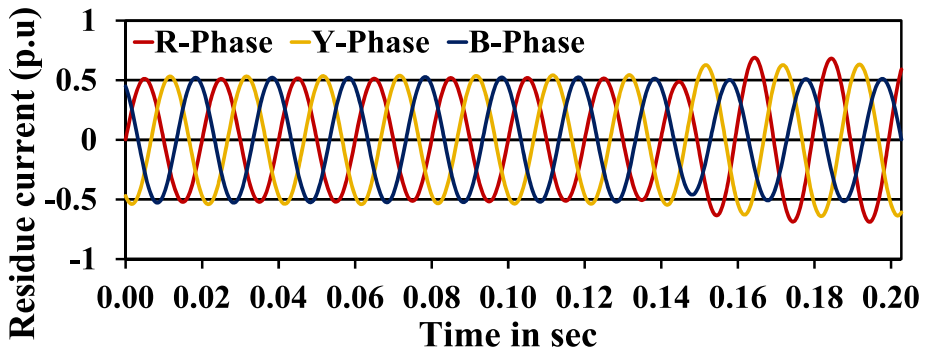


Figure 3.60: Three-phase residue currents for 8-turn short circuit in R-phase with 2% supply unbalance of a 3-hp IM under simulation

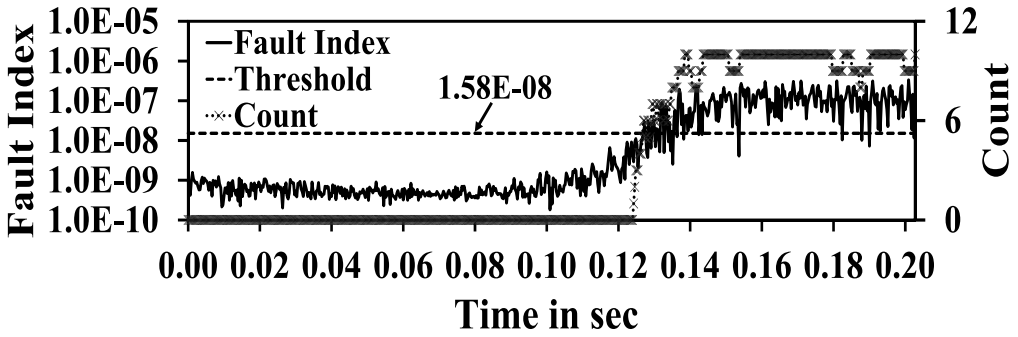


Figure 3.61: Variation in fault index for 8-turn short circuit in R-phase with 2% supply unbalance of a 3-hp IM under simulation

of 8-turn short circuit 8-turn short circuit with 2% supply unbalance crosses the adaptive threshold and count values are also more than 6. Hence, faults are detected even under the presence of supply unbalances also. Similarly, the proposed method is verified with 6-turn, 4-turn and 2-turn of both experimental and simulation cases. The verification of proposed method is extended with supply unbalances and load conditions.

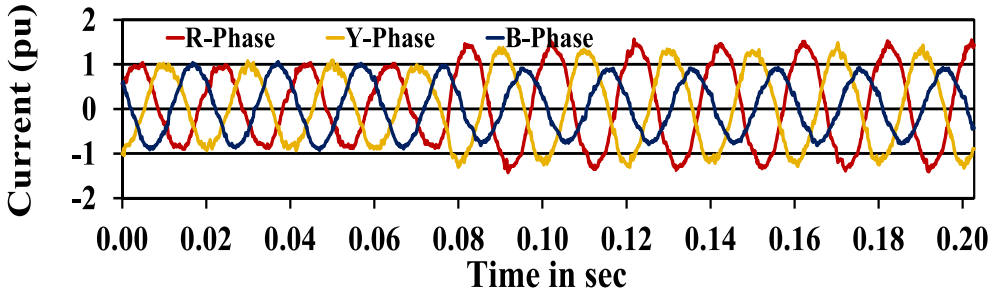


Figure 3.62: Three-phase currents for 8-turn short circuit in R-phase of a 3-hp induction motor under experimental case

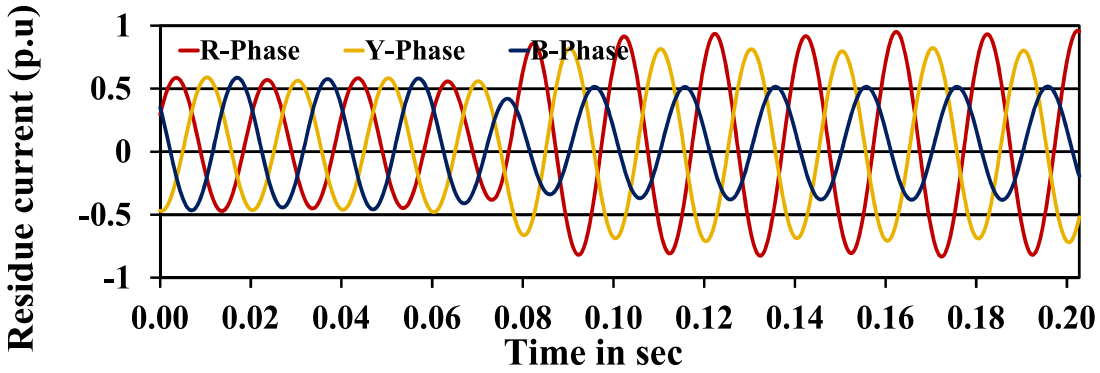


Figure 3.63: Three-phase residue currents for 8-turn short circuit in R-phase of a 3-hp induction motor under experimental case

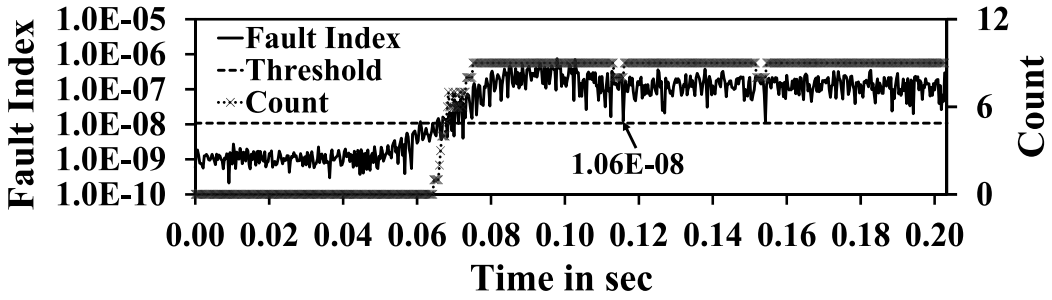


Figure 3.64: Variation in fault index for 8-turn short circuit in R-phase of a 3-hp induction motor under experimental case

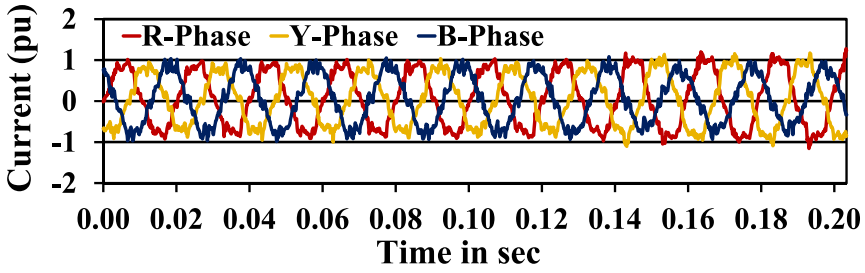


Figure 3.65: Three-phase currents for 8-turn short circuit in R-phase with 2% supply unbalance of a 3-hp induction motor under experimental case

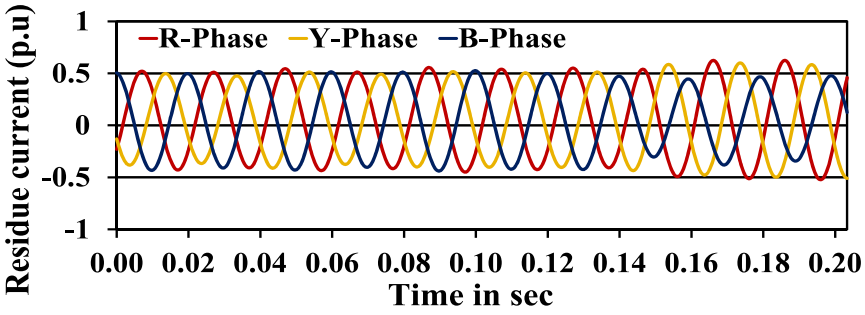


Figure 3.66: Three-phase residue currents for 8-turn short circuit in R-phase with 2% supply unbalance of a 3-hp induction motor under experimental case

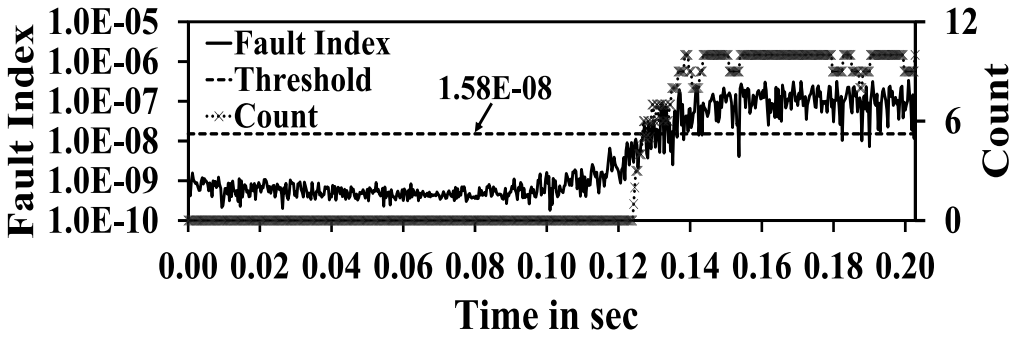


Figure 3.67: Variation in fault index for 8-turn short circuit in R-phase with 2% supply unbalance of a 3-hp induction motor under experimental case

The other cases of stator winding faults such as phase to ground and phase to phase faults are also considered for verifying the proposed method. The variation in captured three-phase currents, three-phase residues and fault indices and count values of stator phase faults (LG and LL) of simulation cases are shown in figures 3.74, 3.75, 3.76, 3.77, 3.78 and 3.79. Similarly, Figures 3.80, 3.81, 3.82, 3.83, 3.84 and 3.85 show the variation in three-phase currents, three-phase residues and fault indices and its count values of stator phase faults of experimental cases. The results proved that the proposed detection scheme is efficient for detecting the stator winding faults. Because all the discussed cases of simulation and experimental fault indices crosses the adaptive threshold and its count value is greater than 6 when the fault exists.

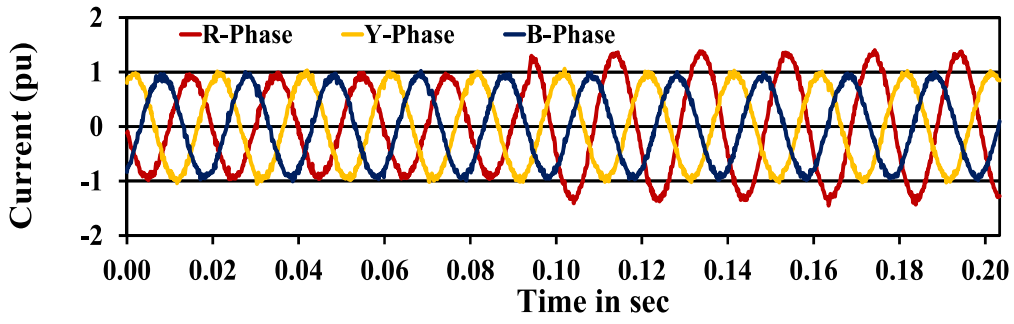


Figure 3.68: Three-phase currents for LG fault in R-phase of a 3-hp IM under simulation

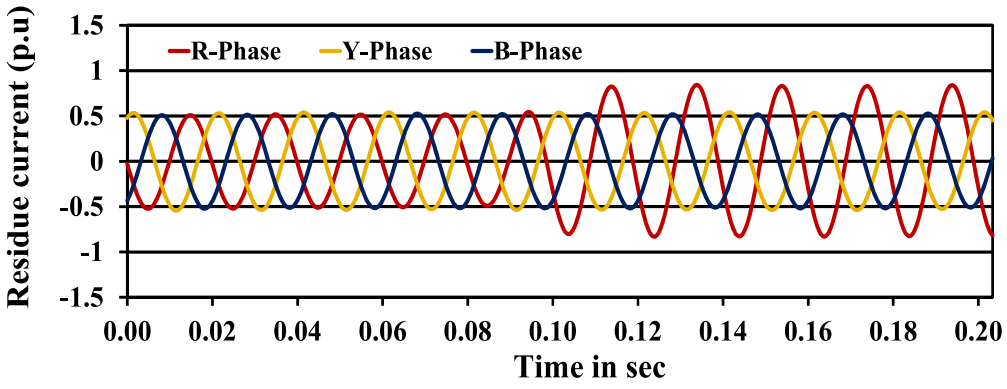


Figure 3.69: Three-phase residue currents for LG fault in R-phase of a 3-hp IM under simulation

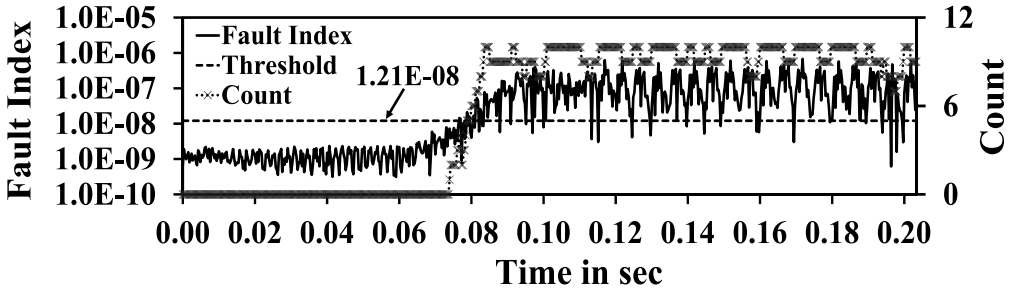


Figure 3.70: Variation in fault index for LG fault in R-phase of a 3-hp IM under simulation

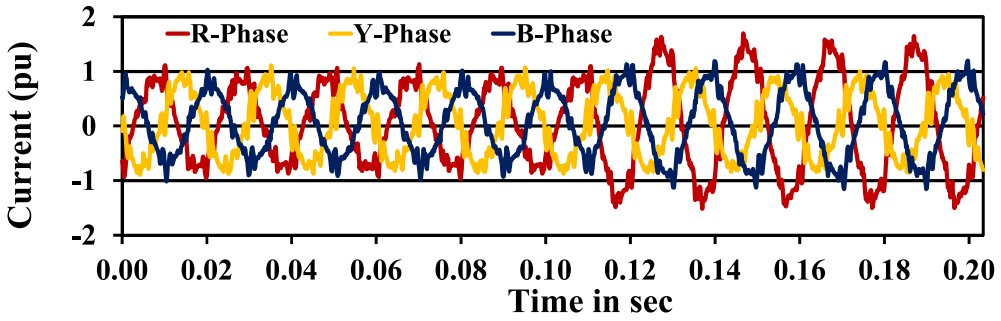


Figure 3.71: Three-phase currents for LL fault between R and Y phases of a 3-hp IM under simulation

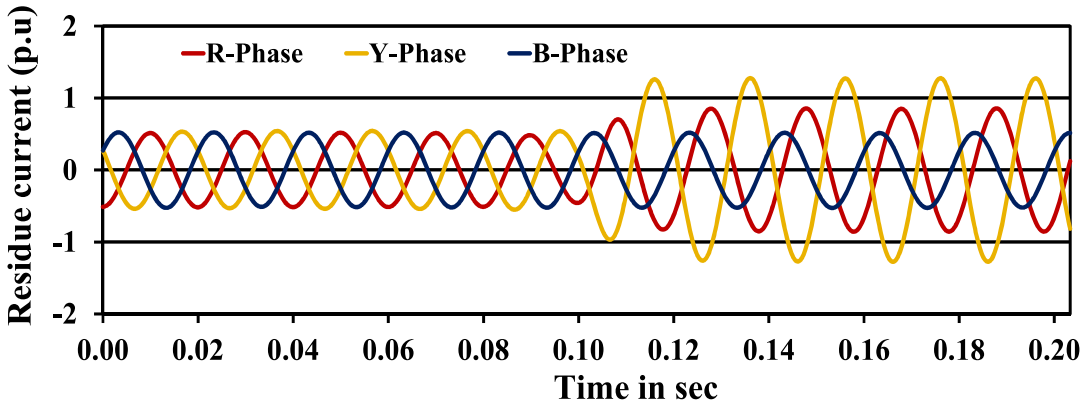


Figure 3.72: Three-phase residue currents for LL fault between R and Y phases of a 3-hp IM under simulation

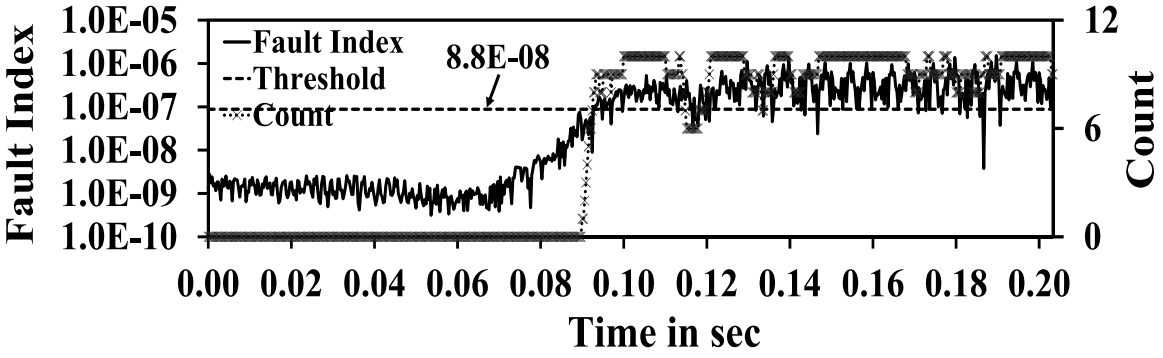


Figure 3.73: Variation in fault index for LL fault between R and Y phases of a 3-hp IM under simulation

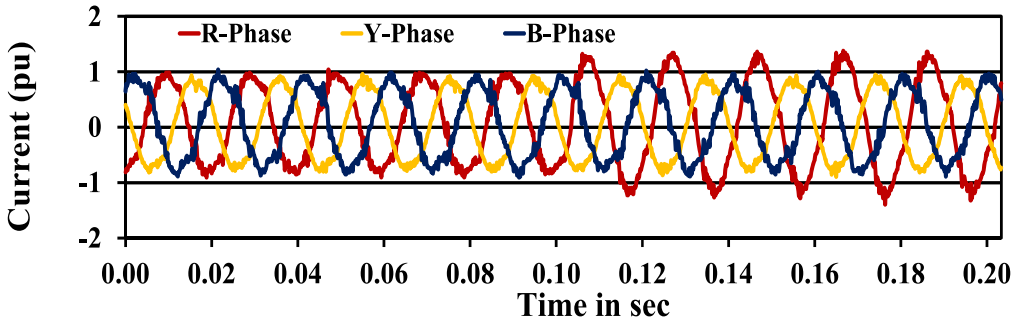


Figure 3.74: Three-phase currents for LG fault in R-phase of a 3-hp IM under experimental case

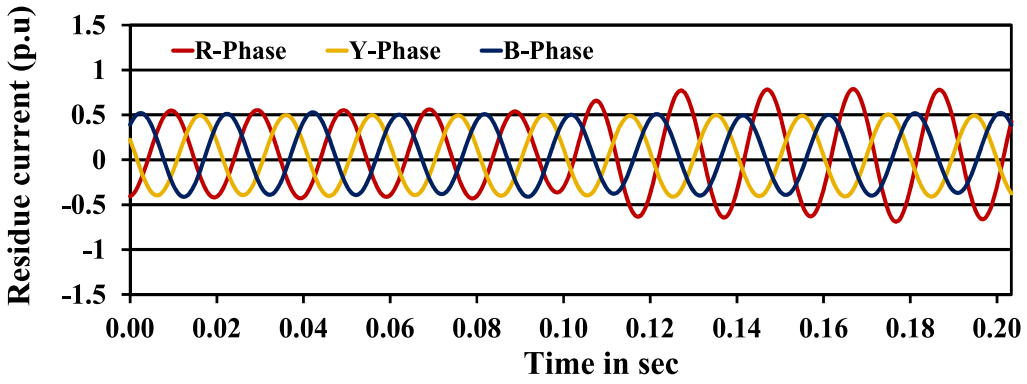


Figure 3.75: Three-phase residue currents for LG fault in R-phase of a 3-hp IM under experimental case

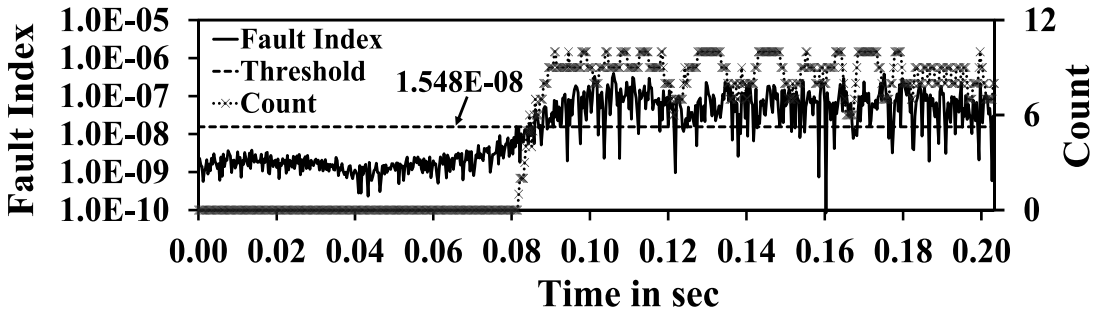


Figure 3.76: Variation in fault index for LG fault in R-phase of a 3-hp IM under experimental case

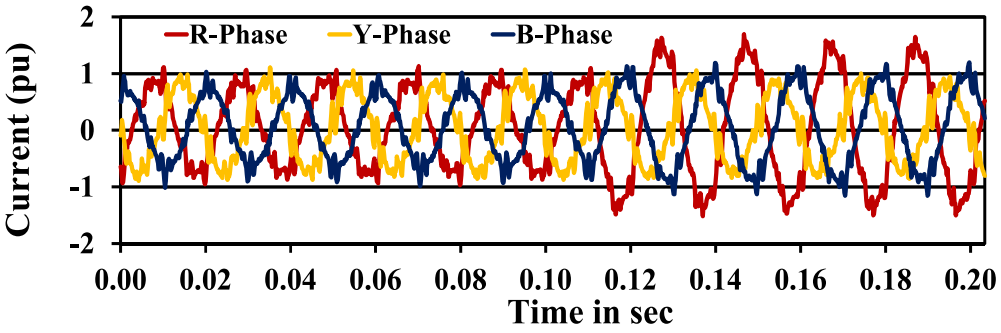


Figure 3.77: Three-phase currents for LL fault between R and Y phases of a 3-hp IM under experimental case

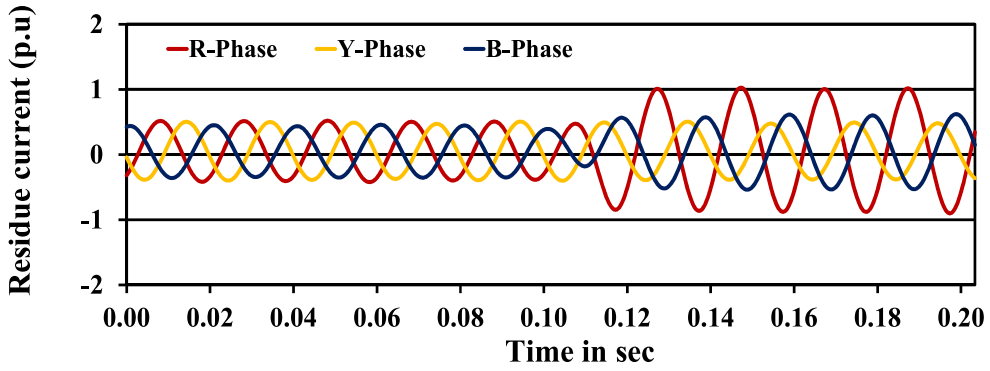


Figure 3.78: Three-phase residue currents for LL fault between R and Y phases of a 3-hp IM under experimental case

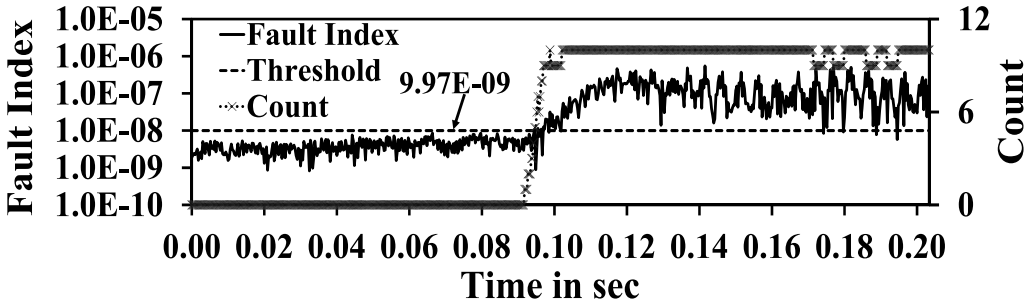


Figure 3.79: variation in fault index for LL fault between R and Y phases of a 3-hp IM under experimental case

#### 3.5.1.4 Comparison between Experimental and Simulation Results for a 3-hp Induction Motor

To validate the proposed detection algorithm, a comparison is made between the Relative Value of Maximum Fault Index *RMFI* and Relative Value of Adaptive Threshold *RAT* for various fault cases of practical and simulated studies. The *RMFI* and *RAT* are mathematically expressed using eq.3.17 and eq.3.18 respectively. The detection criteria for both experimental and simulation cases of different levels of stator inter-turn short circuits under balanced supply, 2% of supply unbalance and 50% of load condition are illustrated in Table 3.1. Table 3.2 shows the detection criteria for various

abnormal conditions other than stator inter-turn faults of

Table 3.1: Comparison of fault detection criteria for various practical and simulation cases of stator inter-turn faults

| **Cases** | **Practical** | | **Simulation** | |
|---|---|---|---|---|
| | *RMFI* | *RAT* | *RMFI* | *RAT* |
| 2-turn fault | 34.33 | 1.35 | 23.20 | 1.17 |
| 2-turn fault with 2% supply unbalance | 19.59 | 0.84 | 10.33 | 0.72 |
| 4-turn fault | 78.50 | 4.66 | 66.30 | 3.28 |
| 4-turn fault with 2% supply unbalance | 69.67 | 3.18 | 61.09 | 3.68 |
| 6-turn fault | 133.82 | 4.31 | 124.39 | 3.45 |
| 6-turn fault with 2% supply unbalance | 121.13 | 7.59 | 114.86 | 4.12 |
| 8-turn fault | 159.62 | 3.25 | 145.87 | 3.52 |
| 8-turn fault with 2% supply unbalance | 170.34 | 4.11 | 127.25 | 4.11 |
| 2-turn fault in R-phase with 50% load | 31.09 | 9.03 | 34.09 | 3.96 |
| 4-turn fault in R-phase with 50% load | 99.45 | 6.35 | 81.17 | 3.57 |
| 6-turn fault in R-phase with 50% load | 74.25 | 8.34 | 75.36 | 3.29 |
| 8-turn fault in R-phase with 50% load | 126.07 | 2.75 | 189.12 | 2.69 |

both experimental and simulation cases. Table 3.1 and 3.2 depict the effectiveness of the proposed algorithm for various cases under practical and simulation studies. From Table 3.1, even for small fault i.e 2-turn short circuit the RMFI in practical case is in good agreement with that of simulation case. The difference between the values of practical and simulation case is mainly due to considered constant noise variance in simulation which is not true in actual practice.

$$RMFI = \frac{Maximum\ value\ of\ I_f\ under\ fault\ condition}{Maximum\ value\ of\ I_f\ under\ healthy\ condition} \tag{3.17}$$

$$RAT = \frac{Th\ under\ fault\ condition}{Th\ under\ healthy\ condition} \tag{3.18}$$

Table 3.2: Comparison of fault detection criteria for various practical and simulation cases other than stator inter-turn faults

| **Cases** | **Practical** | | **Simulation** | |
|---|---|---|---|---|
| | *RMFI* | *RAT* | *RMFI* | *RAT* |
| 4-turn phase fault between RY phases | 206.44 | 3.01 | 469.02 | 2.28 |
| 6-turn phase fault between RY phases | 379.92 | 4.69 | 356.28 | 0.96 |
| 8-turn phase fault between RY phases | 269.48 | 8.20 | 603.89 | 5.02 |
| 4-turn ground fault in R-phase | 74.07 | 10.8 | 107.02 | 4.24 |
| 6-turn ground fault in R-phase | 143.52 | 6.83 | 356.11 | 5.76 |
| 8-turn ground fault in R-phase | 169.30 | 4.68 | 304.53 | 4.10 |
| Single phasing in R-phase | 812.78 | 3.66 | 899.34 | 3.67 |
| Single phasing in Y-phase | 474.06 | 5.16 | 624.59 | 6.48 |
| Single phasing in B-phase | 551.00 | 4.42 | 573.86 | 8.67 |
| 3% Supply unbalance in R-phase | 144.57 | 5.23 | 81.74 | 2.82 |
| 3% Supply unbalance in Y-phase | 166.19 | 5.50 | 84.01 | 0.35 |
| 3% Supply unbalance in B-phase | 159.20 | 4.31 | 93.30 | 2.78 |

#### 3.5.1.5 Experimental Results for a 10-hp Induction Motor

To check the reliability of the proposed detection criteria, another rating of 10-hp induction motor is also considered. Figures 3.80,3.81 3.82, 3.83, 3.84, 3.85, 3.86, 3.87, 3.88 and 3.92 demonstrate currents, residue currents and fault index under various experimental cases on a 10-hp induction motor of healthy, 2-turn fault, single phasing, under voltage and supply unbalance conditions respectively. From these results it is clear that the proposed algorithm has successfully detected the abnormal conditions of the motor. Hence, the proposed SWT and DWT based fault detection is

reliable and effective in detecting the faults because the rating and operating condition of the machine does not influence the detection criteria.

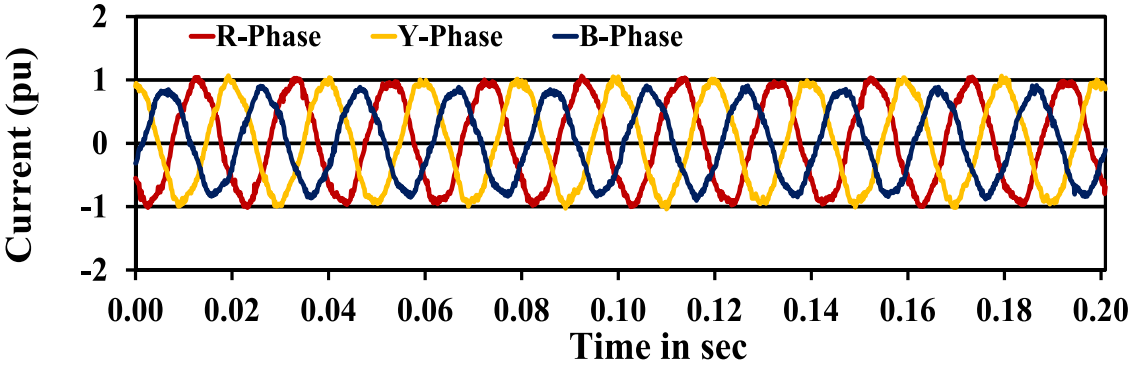


Figure 3.80: Three-phase currents for healthy of a 10-hp induction motor

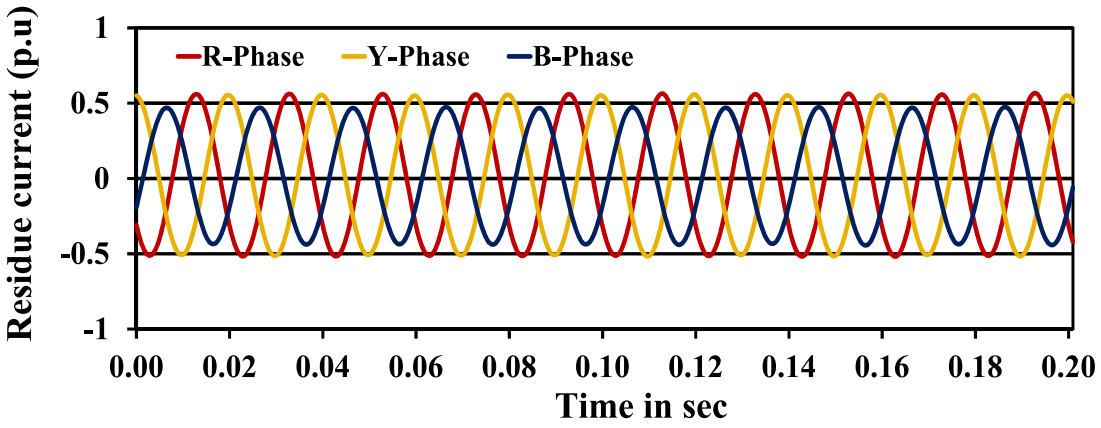


Figure 3.81: Three-phase residue currents for healthy of a 10-hp induction motor

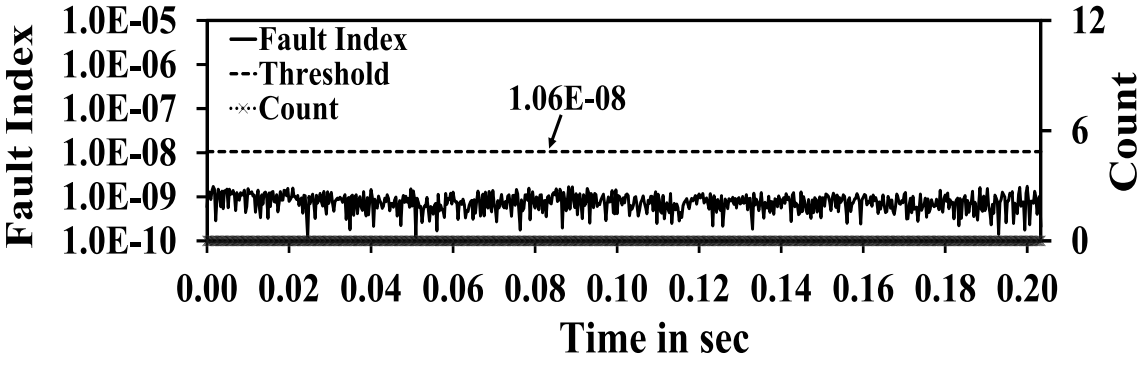


Figure 3.82: Variation in fault index for healthy of a 10-hp induction motor

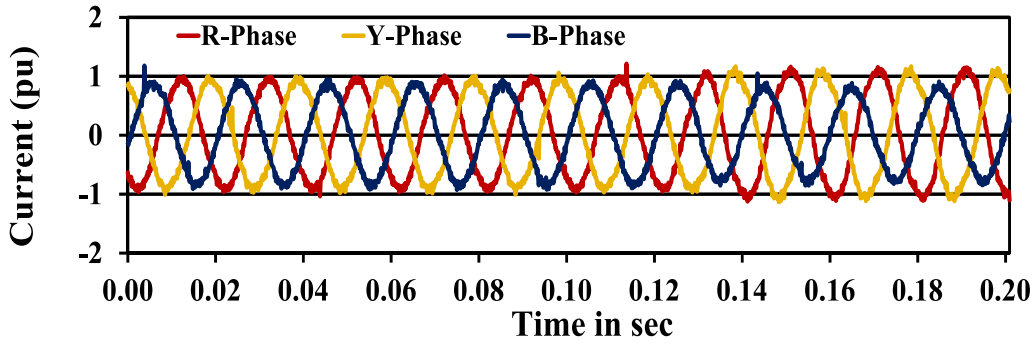


Figure 3.83: Three-phase currents for 2-turn fault in R-phase of a 10-hp induction motor

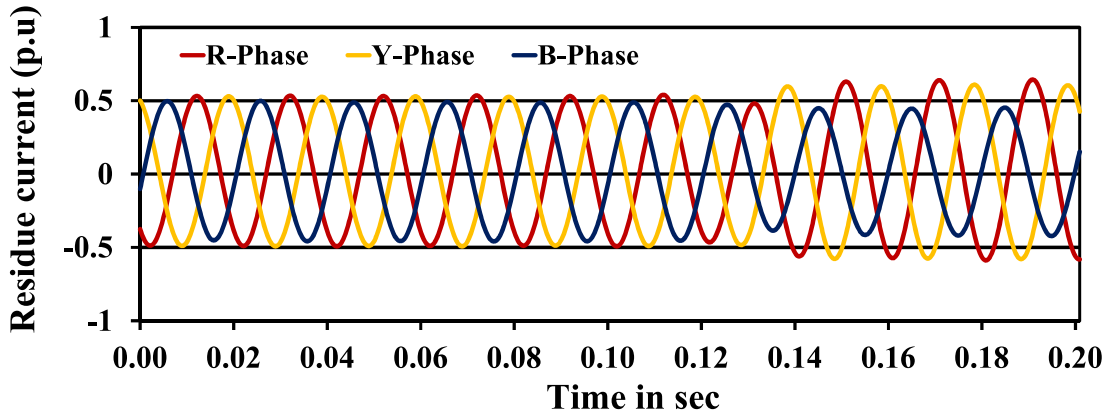


Figure 3.84: Three-phase residue currents for 2-turn fault in R-phase of a 10-hp induction motor

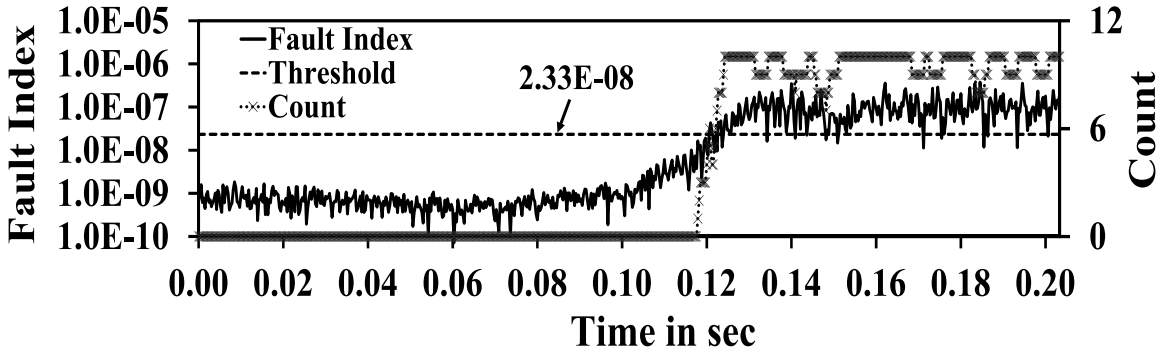


Figure 3.85: Variation in fault index for 2-turn fault in R-phase of a 10-hp induction motor

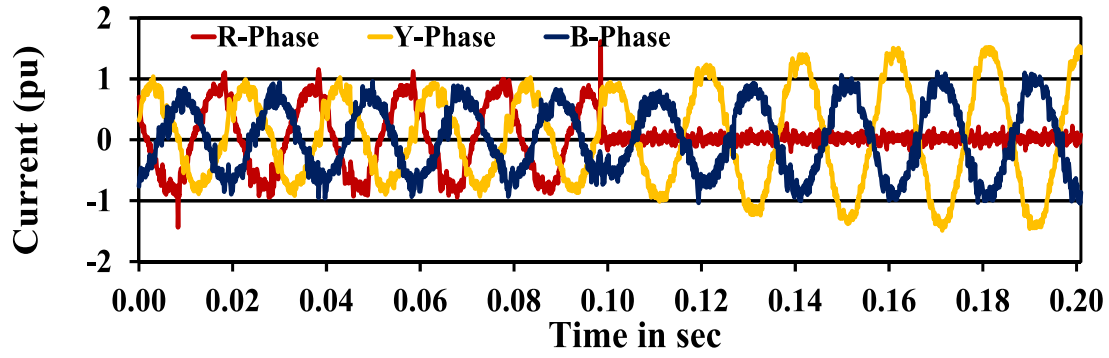


Figure 3.86: Three-phase currents for single phasing in R-phase of a 10-hp induction motor

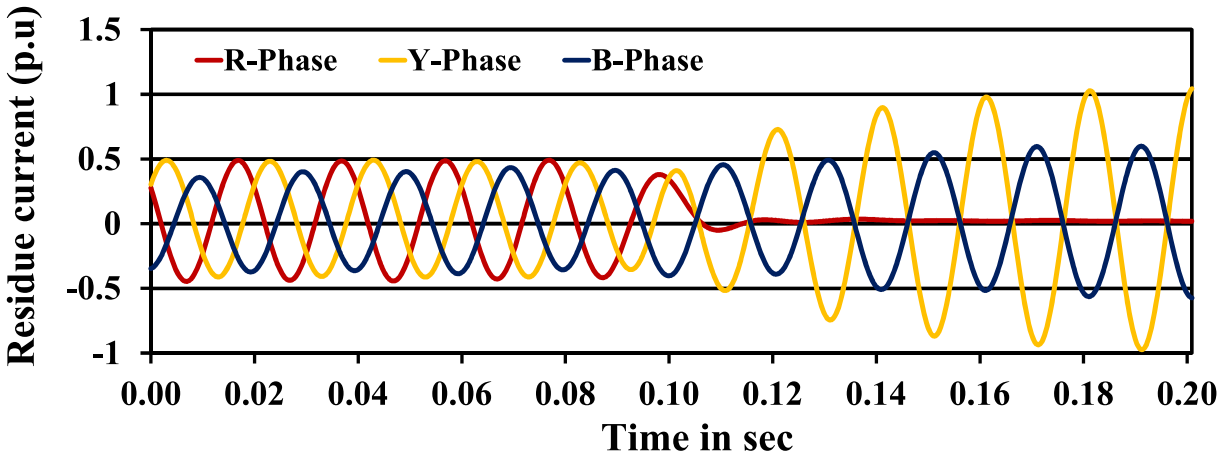


Figure 3.87: Three-phase residue currents for single phasing in R-phase of a 10-hp induction motor

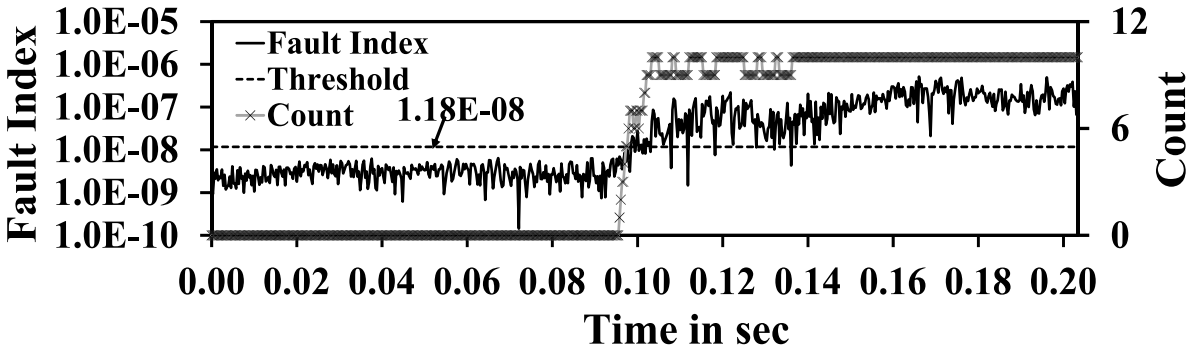


Figure 3.88: Variation in fault index for single phasing in R-phase of a 10-hp induction motor

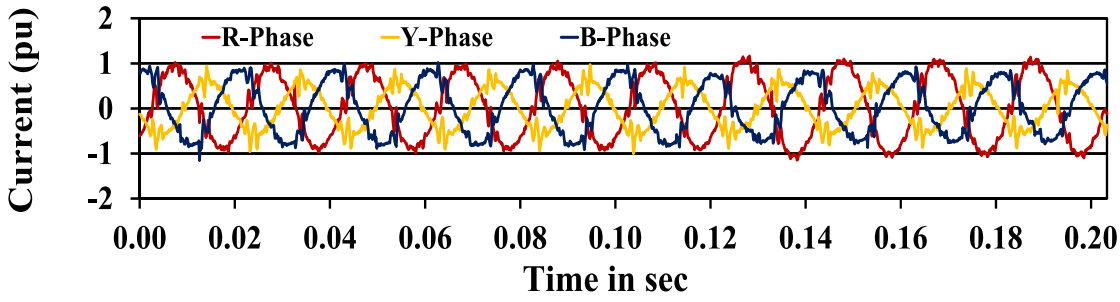


Figure 3.89: Three-phase currents for 2% supply unbalance of 10-hp induction motor

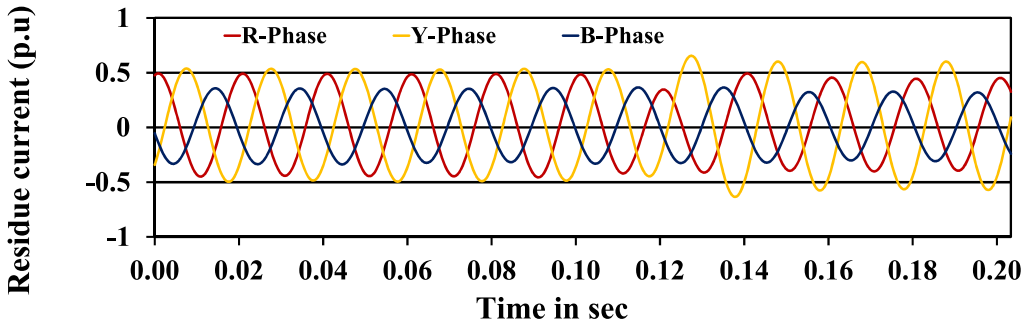


Figure 3.90: Three-phase residue currents for 2% supply unbalance of a 10-hp induction motor

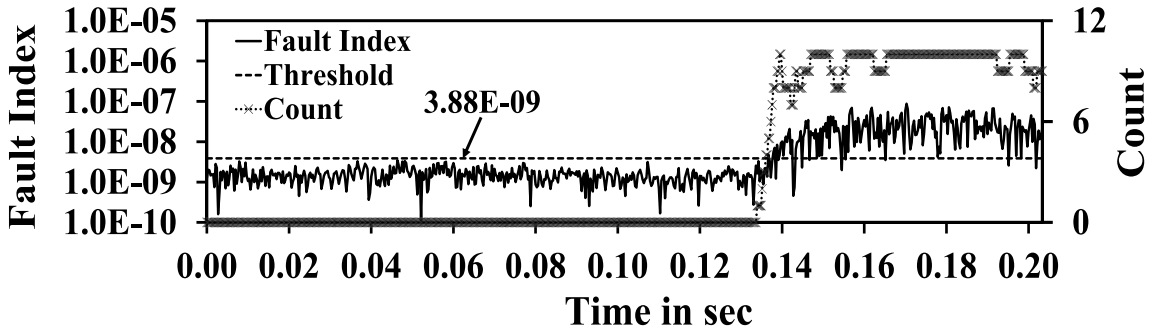


Figure 3.91: Variation in fault index for 2% supply unbalance of a 10-hp induction motor

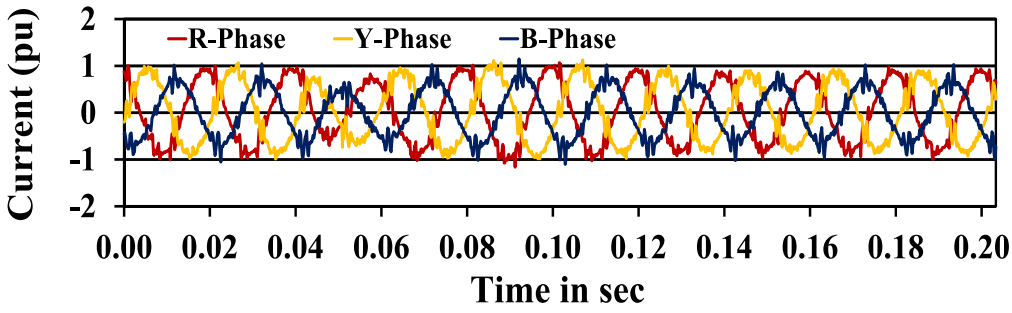


Figure 3.92: Three-phase currents for 7% under voltage of a 10-hp induction motor

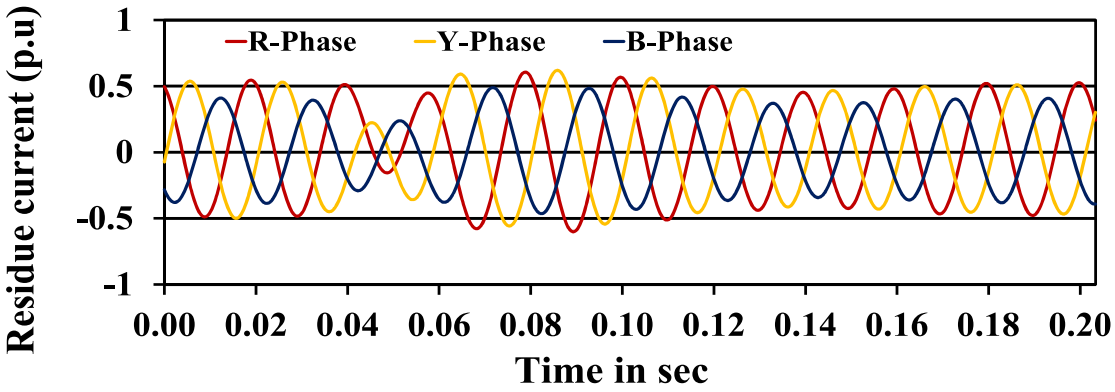


Figure 3.93: Three-phase residue currents for 7% under voltage of a 10-hp induction motor

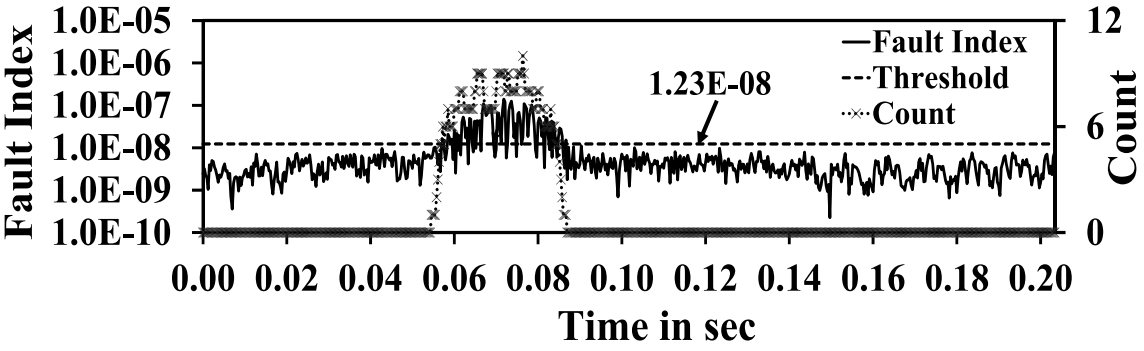


Figure 3.94: Variation in fault index for 7% under voltage of a 10-hp induction motor

## 3.6 Conclusions

In this chapter, two approaches are proposed for detecting the various stator and supply side faults using DWT and combination of SWT and DWT. From the results of simulation and experimental case, the following conclusions are made.

The proposed fault detection algorithm using DWT has been tested for various incidence angles. The exhaustive simulation studies proved that the proposed algorithm is simple and effective in detecting the various faults. However, it fails to detect the fault under noisy conditions.

Another proposed fault detection method based on SWT and DWT is developed to overcome the drawback of DWT based method. The simulation and experimental results demonstrated the efficacy of the proposed SWT and DWT based fault detection method on a 3-phase induction motors in presence of noise as well.

# Chapter 4

# Classification of Various Disturbances of a 3-Phase Induction Motor Using Wavelet and Modular Neural Network

## 4.1 Introduction

Rapid growth in automation increases the dependency on electric machines as drives and decreases the direct interaction between man and machine. This necessitates on line condition monitoring of motor to improve its reliability. The stator winding faults create unbalancing in the line current, and similar unbalancing is also created due to supply unbalances. However, the distinction between these two phenomena is highly challenging. Unbalancing condition in the motor could be due to stator winding insulation faults or due to sudden electrical load changes or single phasing or other conditions. Hence, a classifier is needed for segregating the various unbalances which are caused due to various faults. The detection, diagnoses and discrimination of stator turn to turn fault and unbalanced supply voltage fault in a three phase induction motors has been addressed

in [75]. But, it suffers from the drawback of taking so many measurements. In recent time, the accuracy of the classifier is improved by integrating the analysing techniques [76], [77]. This chapter proposes a classifier based on Wavelet and Modular Neural Network (MNN) to classify various faults such as stator phase-phase faults, stator phase-ground faults, single phasing, supply unbalance, under voltage and sudden load change.

## 4.2 Features for Disturbance Classifier

The schematic diagram of the proposed fault detection and classification is depicted in Figure 4.1. The proposed detection and classification method starts with data acquisition and then processing of signals to detect and classify the faults and its severity. In chapter 3, discussion on detection of fault is presented. The next process is classification and identification. In all totally three classifiers are considered to classify various disturbances, stator phase faults and stator inter-turn faults. This approach decreases the training time as the classifiers related to stator phase faults (ANN-2) and stator inter-turn faults (ANN-3) needs training only when the disturbance classifier recognizes the disturbance as related to the stator winding insulation faults which means that the faults are related to stator phase or stator inter-turn faults only.

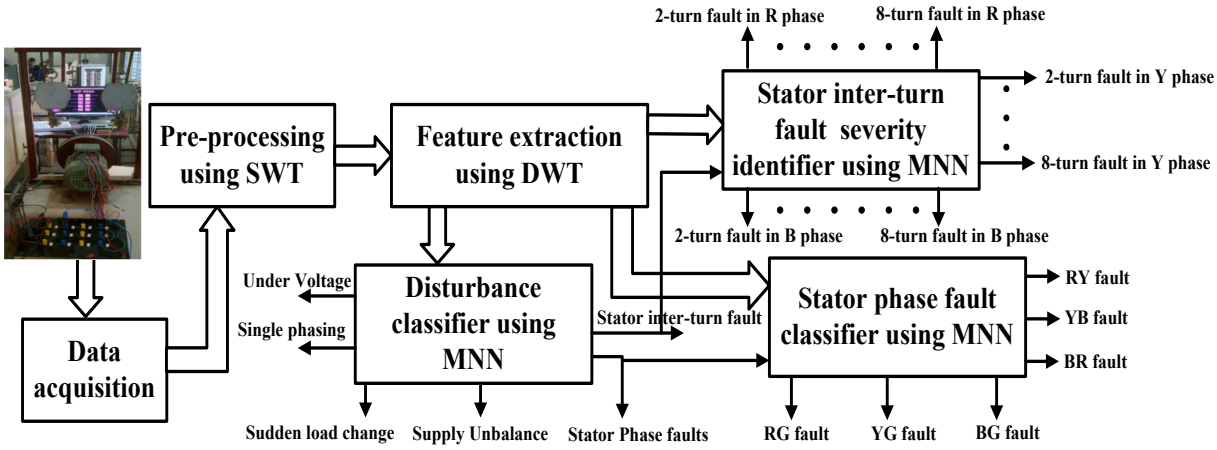


Figure 4.1: Proposed stator fault detector and classifier

This chapter mainly deals with disturbance classifier and extraction of features required for them. Stator phase fault and Stator inter-turn fault classifiers are explained in chapter 5 and chapter 6 respectively. Totally six types of disturbances are considered for disturbance classifier. To classify all these disturbances certain features are essential. The proposed classifier requires only three measurements and nine features. The three phase stator currents are the three measurements and are sensed for each of the disturbance and normal cases. These three phase currents are analysed with wavelet transform to detect the disturbance instant. After detecting the instant of disturbance, three statistical features of second level approximate coefficients of three phase residues are considered over a window of one cycle from the fault instant which are standard deviation, maximum and mean values. Totally, there are nine features such as feature 1, feature 2, feature 3, feature 4, feature 5, feature 6, feature 7, feature 8 feature 9 are defined as standard deviation of R-phase, standard deviation of Y-phase, standard deviation of B-phase, maximum value of R-phase, maximum value of Y-phase, maximum value of B-phase, mean value of R-phase,

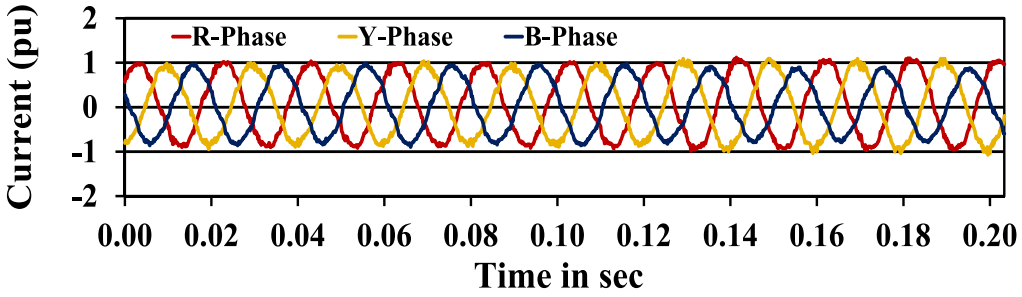


Figure 4.2: Three-phase stator currents of a 3-hp IM with 4-turn short circuit in R-phase

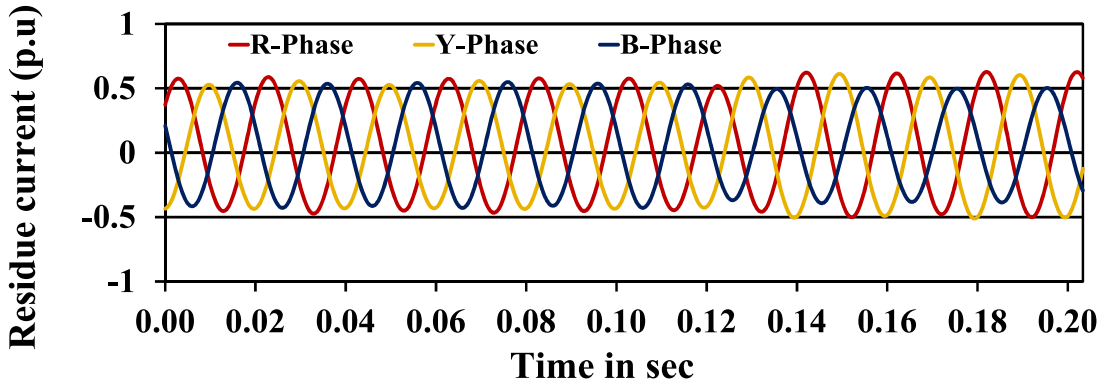


Figure 4.3: Variation in three-phase residues of a 3-hp IM with 4-turn short circuit in R-phase

mean value of Y-phase and mean value of B-phase respectively. These are given as inputs to the disturbance classifier for classifying the various disturbances on a 3-phase induction motor.

The feature extraction method is explained by considering stator winding faults and supply side faults. Figures 4.2 shows the variation in captured three-phase currents for 4-turn short circuit in R-phase of a 3-hp induction motor. To extract the disturbance features, the instant of fault occurrence and a2 coefficients of three-phase residues are to be required which are obtained by using proposed fault detection algorithm and as discussed in chapter 3. Figures 4.3 and 4.4 demonstrate the obtained three-phase residues and fault index for 4-turn short circuit in R-phase of a

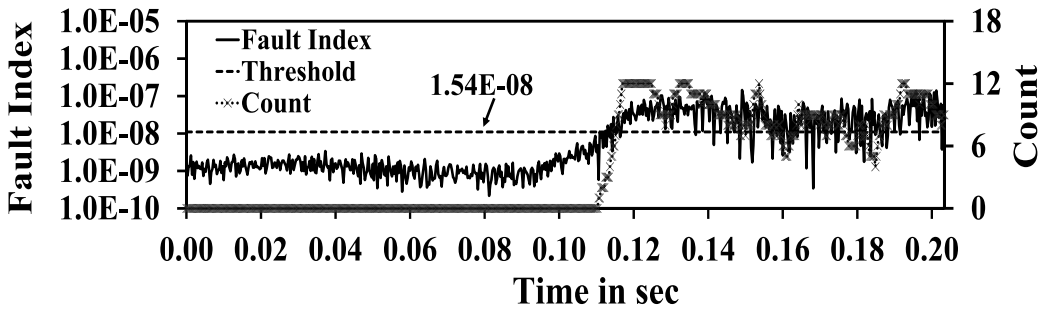


Figure 4.4: Variation in fault index of a 3-hp IM with 4-turn short circuit in R-phase

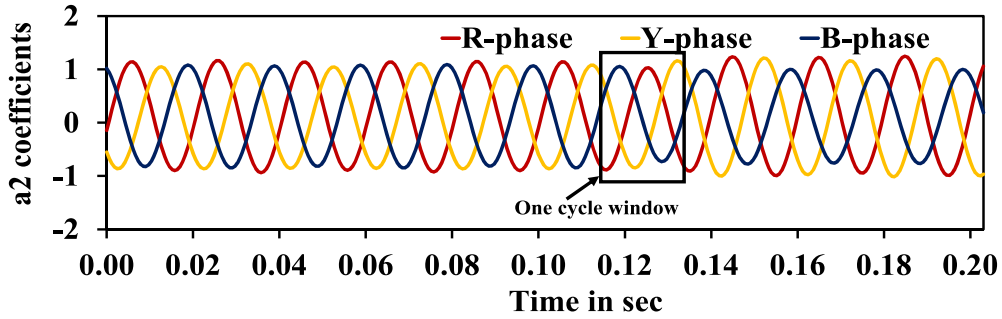


Figure 4.5: Variation in a2 coefficients of a 3-hp IM with 4-turn short circuit in R-phase

3-hp induction motor. Detection of fault and its instant occurrence is identified by comparing the fault index with adaptive threshold as presented in chapter 3. The 2nd level approximate coefficients of three-phase residues are obtained by decomposing the three-phase residues with DWT of Bior 5.5 mother wavelet. The variations in second level approximate coefficients of three-phase residues for 4-turn short circuit is shown in figure 4.5. From this figure, estimate the nine features over a window of one cycle from the fault instant. The estimated values of nine features corresponding to the 4-turn short circuit in R-phase of a 3-hp induction motor are 0.359, 0.358, 0.291, 1.24, 1.21, 1, 0.719, 0.709, and 0.57. These self normalized values are as input to the disturbance classifier which are 0.2904, 0.2895, 0.235, 1, 0.9822, 0.8093, 0.5813, 0.5735 and

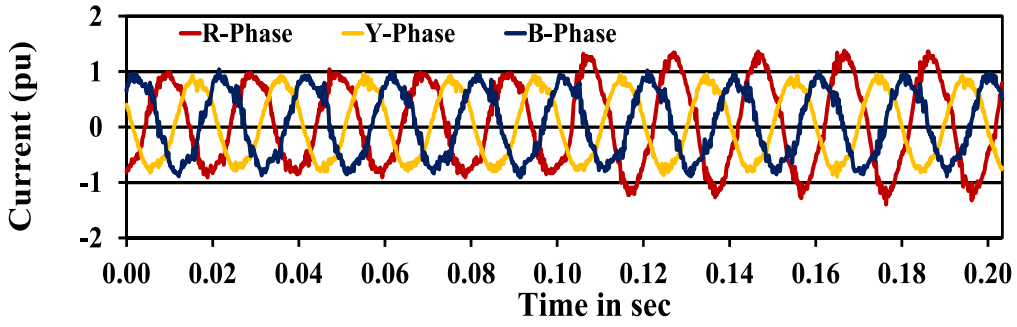


Figure 4.6: Three-phase stator currents of a 3-hp IM with 4-turn to ground fault in R-phase

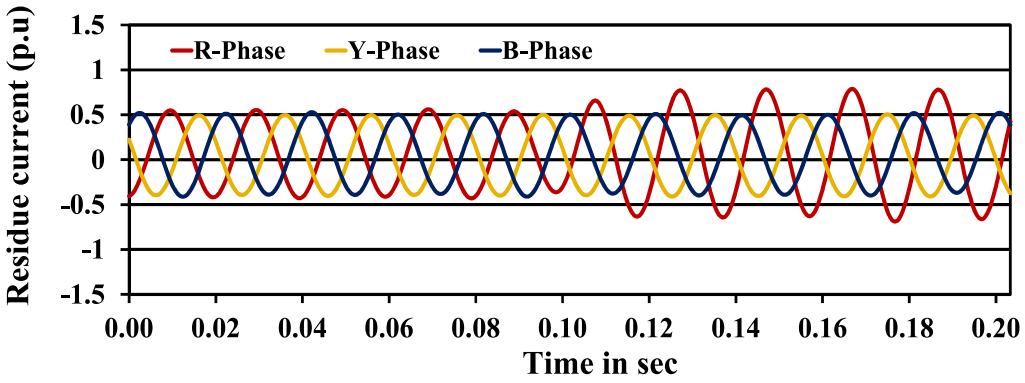


Figure 4.7: Variation in three-phase residues of a 3-hp IM with 4-turn to ground fault in R-phase

0.4610. The variations in three-phase currents, three-phase residues, fault index and a2 coefficients for 4-turn to ground fault of a 3-hp induction motor are illustrated in figures 4.6, 4.7, 4.8 and 4.9 respectively. Figures 4.10, 4.11, 4.12 and 4.13 are show the variations in three-phase currents, three-phase residues, fault index and a2 coefficients for 4-turn short circuit between R and Y phases of a 3-hp induction motor respectively. Similarly, the variations in three-phase currents, three-phase residues, fault index and a2 coefficients for supply unbalance case are shown in figures 4.14, 4.15, 4.16and 4.17 respectevely. The other two cases of under voltage and single phasing are demonstrated in figures 4.18, 4.19, 4.20, 4.21, 4.22, 4.23, 4.24 and 4.25.

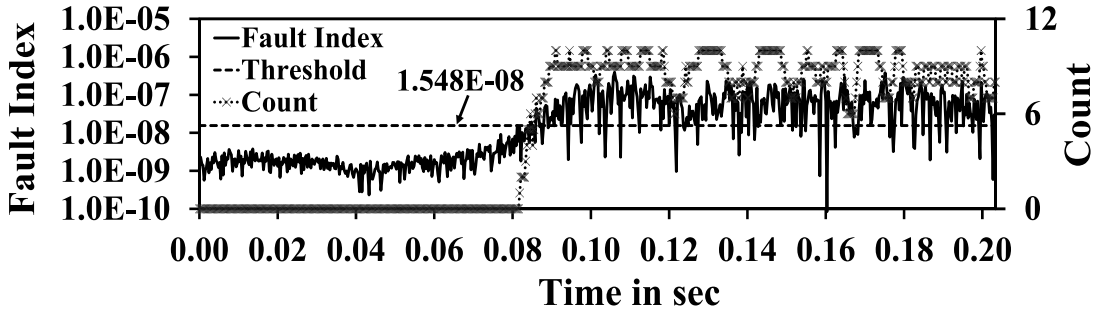


Figure 4.8: Variation in fault index of a 3-hp IM with 4-turn to ground fault in R-phase

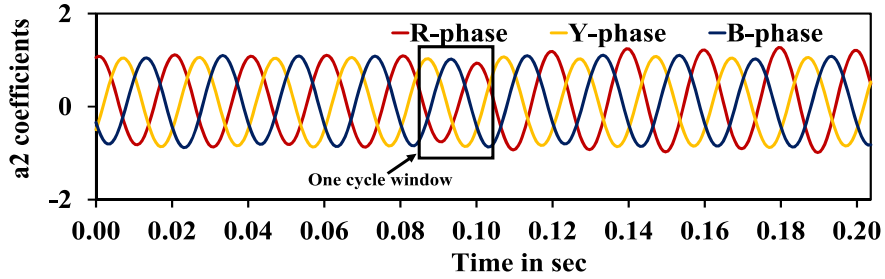


Figure 4.9: Variation in a2 coefficients of a 3-hp IM with 4-turn to ground fault in R-phase

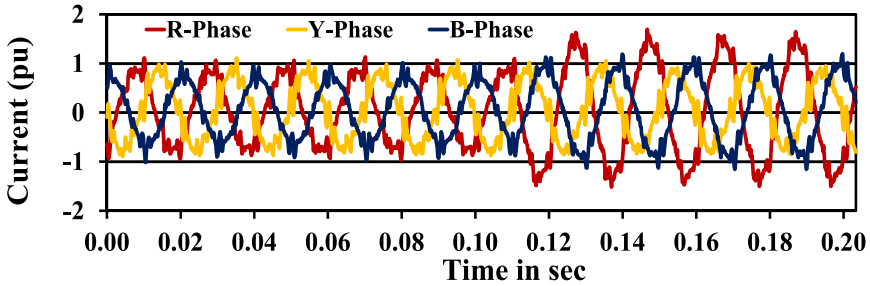


Figure 4.10: Three-phase stator currents of a 3-hp IM with 4-turn short circuit between R and Y phases

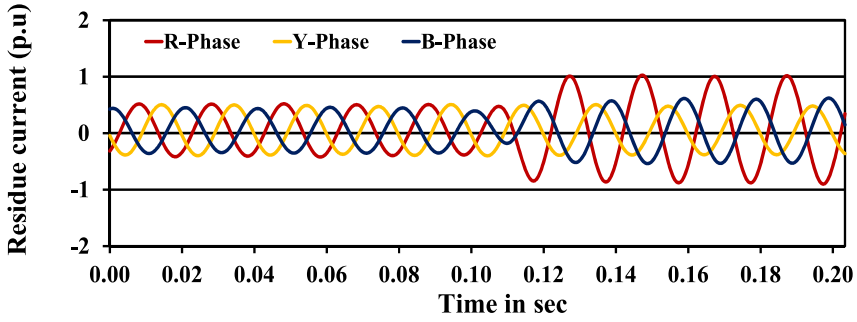


Figure 4.11: Variation in three-phase residues of a 3-hp IM with 4-turn short circuit between R and Y phases

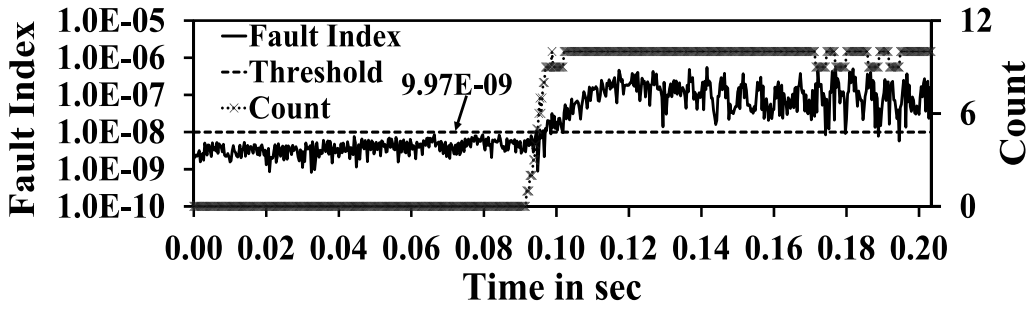


Figure 4.12: Variation in fault index of a 3-hp IM with 4-turn short circuit between R and Y phases

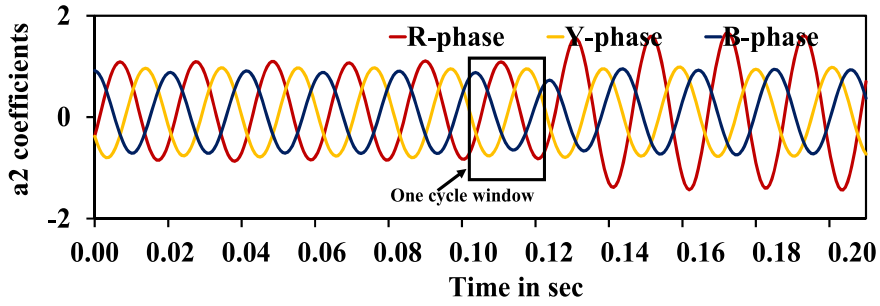


Figure 4.13: Variation in a2 coefficients of a 3-hp IM with 4-turn short circuit between R and Y phases

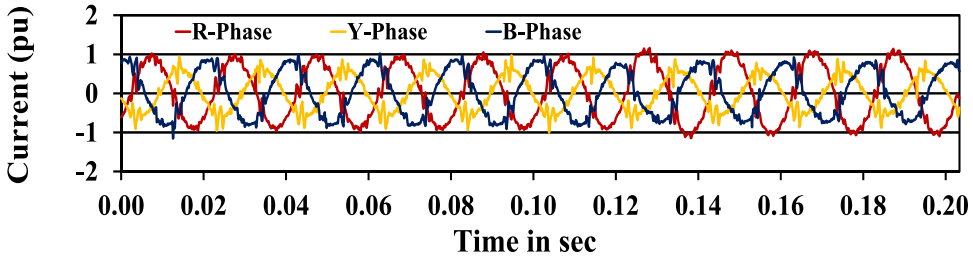


Figure 4.14: Three-phase stator currents of a 10-hp IM with 3% supply unbalance

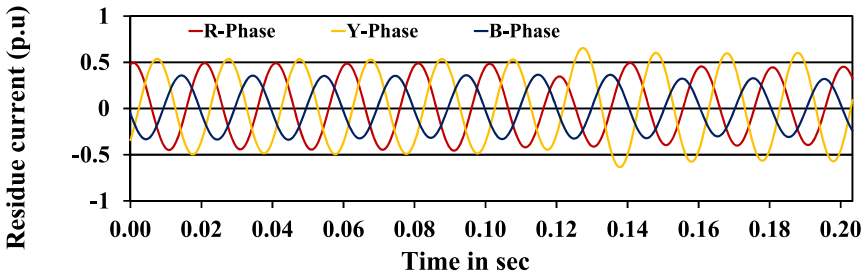


Figure 4.15: Variation in three-phase residues of a 10-hp IM with 3% supply unbalance

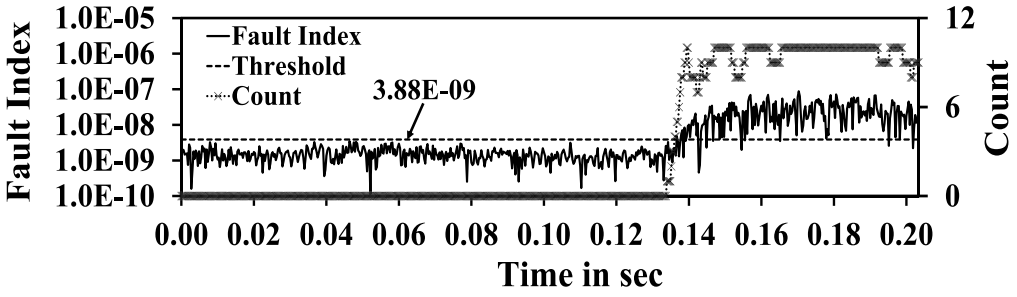


Figure 4.16: Variation in fault index of a 10-hp IM with 3% supply unbalance

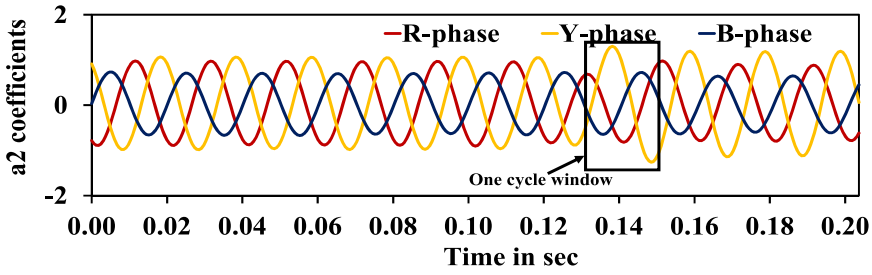


Figure 4.17: Variation in a2 coefficients of a 10-hp IM with 3% supply unbalance

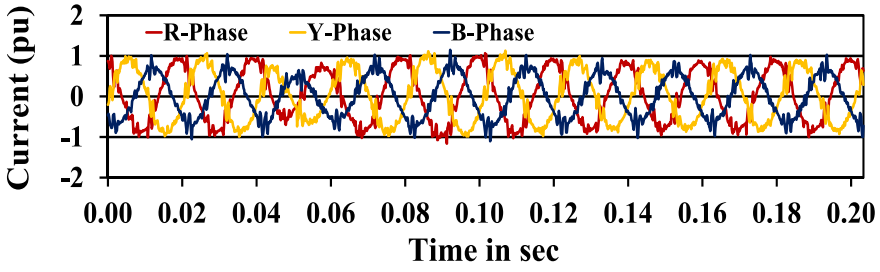


Figure 4.18: Three-phase stator currents of a 10-hp IM with 10%under voltage

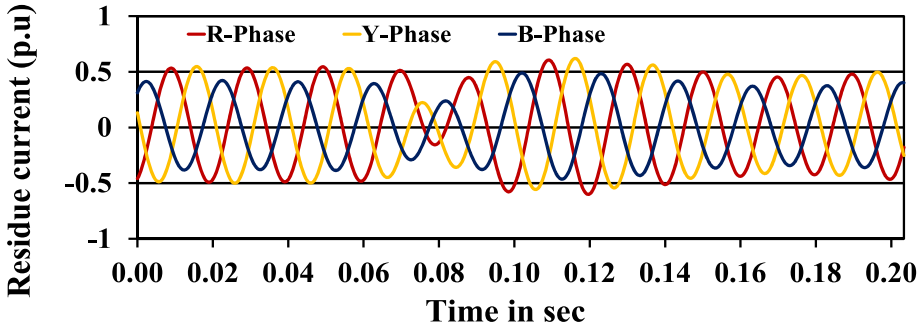


Figure 4.19: Variation in three-phase residues of a 10-hp IM with 10%under voltage

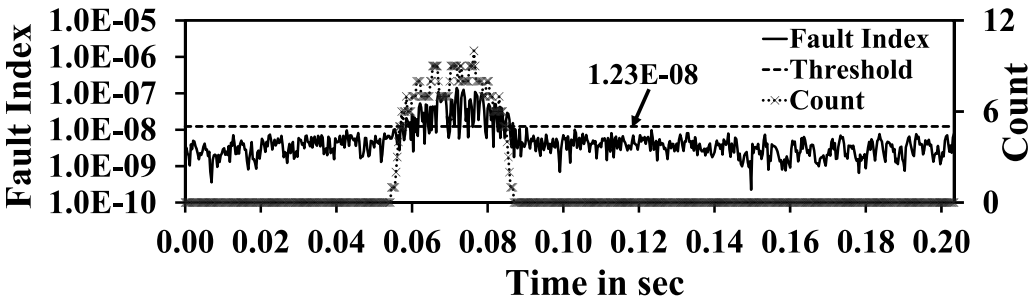


Figure 4.20: Variation in fault index of a 10-hp IM with 10%under voltage

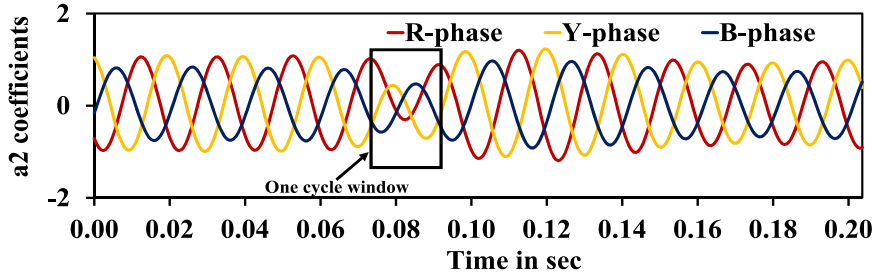


Figure 4.21: Variation in a2 coefficients of a 10-hp IM with 10%under voltage

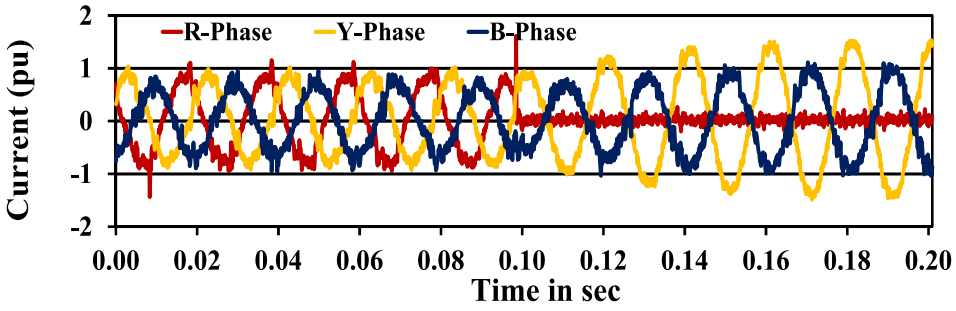


Figure 4.22: Three-phase stator currents of a 10-hp IM with single phasing

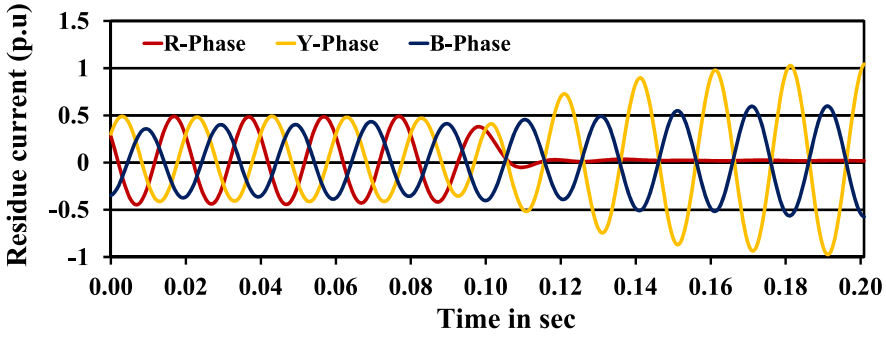


Figure 4.23: Variation in three-phase residues of a 10-hp IM with single phasing

From figures 4.4, 4.8, 4.12, 4.16, 4.20 and 4.24, it is observed that the instant of fault occurrence can be identified very accurately. The obtained value of instant of fault occurrence for each case is used to estimate the statistical features of a2 coefficients over a window of one cycle from the fault instant. The self normalized values of the nine features extracted for the six fault cases are tabulated in Table 4.1.

Apart from these, sudden electrical load change also gives unbalance in three-phases. Figure 4.26 demonstrate the variation in nine features for various disturbances like stator inter-turn fault (R, Y and B), stator phase faults (RG, YG, BG, RY, YB and BR), single phasing (R, Y and B), under voltage, supply unbalance (R, Y and B) and sudden load change conditions. The observation made from the figure 4.26 is that the nine

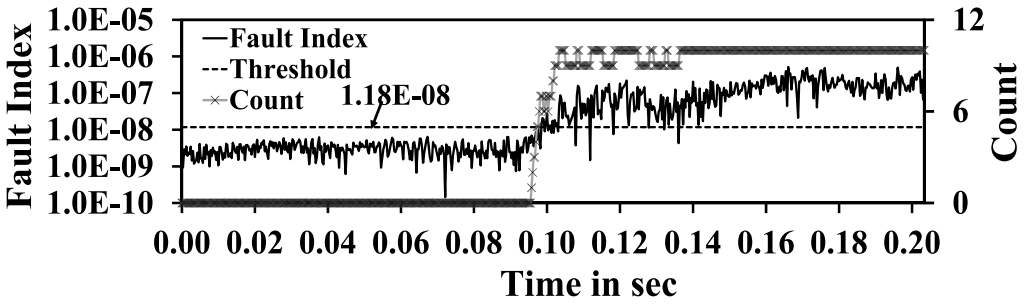


Figure 4.24: Variation in fault index of a 10-hp IM with single phasing

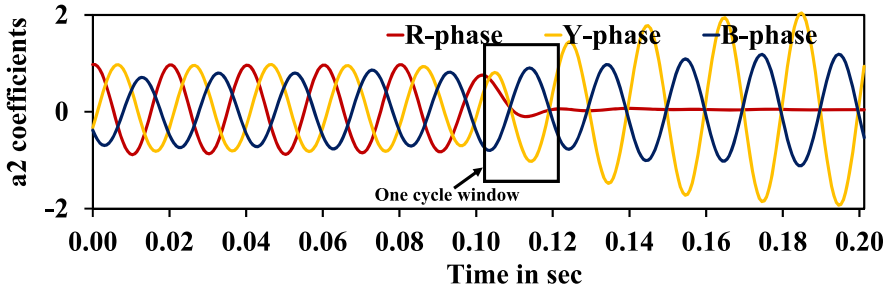


Figure 4.25: Variation in a2 coefficients of a 10-hp IM with single phasing

Table 4.1: Normalised features extracted from a2 coefficients

| Features | 4-turn fault in R-phase | RG fault | RY fault | Supply unbalance | Under voltage | Single phasing |
|---|---|---|---|---|---|---|
| Feature 1 | 0.29042 | 0.28991 | 0.29704 | 0.19779 | 0.25593 | 0.08377 |
| Feature 2 | 0.28953 | 0.25358 | 0.17895 | 0.29736 | 0.29394 | 0.27621 |
| Feature 3 | 0.23497 | 0.27213 | 0.18128 | 0.15351 | 0.27781 | 0.26451 |
| Feature 4 | 1 | 1 | 1 | 0.64192 | 0.91364 | 0.38264 |
| Feature 5 | 0.98217 | 0.86667 | 0.61389 | 1 | 1 | 1 |
| Feature 6 | 0.80928 | 0.93295 | 0.614 | 0.4936 | 0.92755 | 0.96998 |
| Feature 7 | 0.5813 | 0.57377 | 0.60465 | 0.40914 | 0.50725 | 0.12104 |
| Feature 8 | 0.57354 | 0.50517 | 0.33453 | 0.59954 | 0.46559 | 0.45205 |
| Feature 9 | 0.46101 | 0.51915 | 0.36005 | 0.31002 | 0.4851 | 0.49681 |

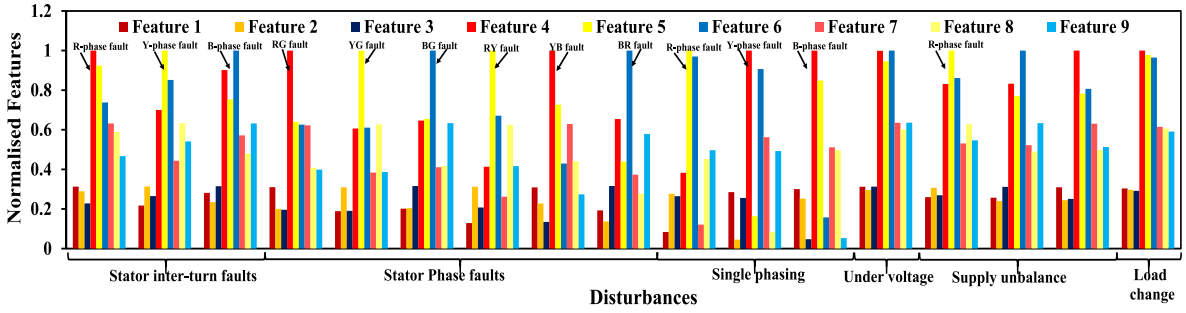


Figure 4.26: Variation in nine features for various disturbances

features of one case is different with other cases. The variations in nine features of different fault level for stator inter-turn faults, stator phase faults and supply unbalances are shown in figure 4.27. From this figure 4.27, it is an evidence that the nine features variation in a particular cases are in similar pattern. Hence, the selected features are insensitive to the operating conditions.

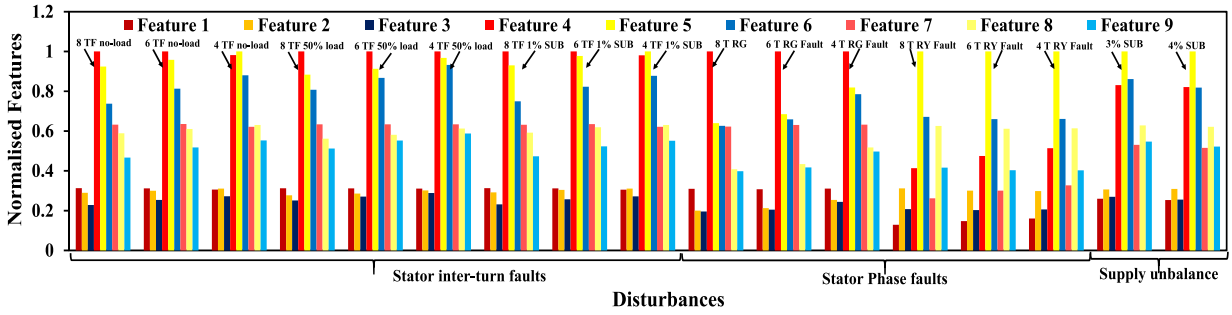


Figure 4.27: Variation in nine features for stator faults and supply unbalance

## 4.3 ANN Structures for Disturbance Classifier (ANN-1)

The schematic diagram for the proposed classifiers of a three-phase induction motor using Artificial Neural Network (ANN) is shown in figure 4.28. In this chapter, a multi layer feed forward back propagation network based classifier (ANN-1) is explained. The remaining two

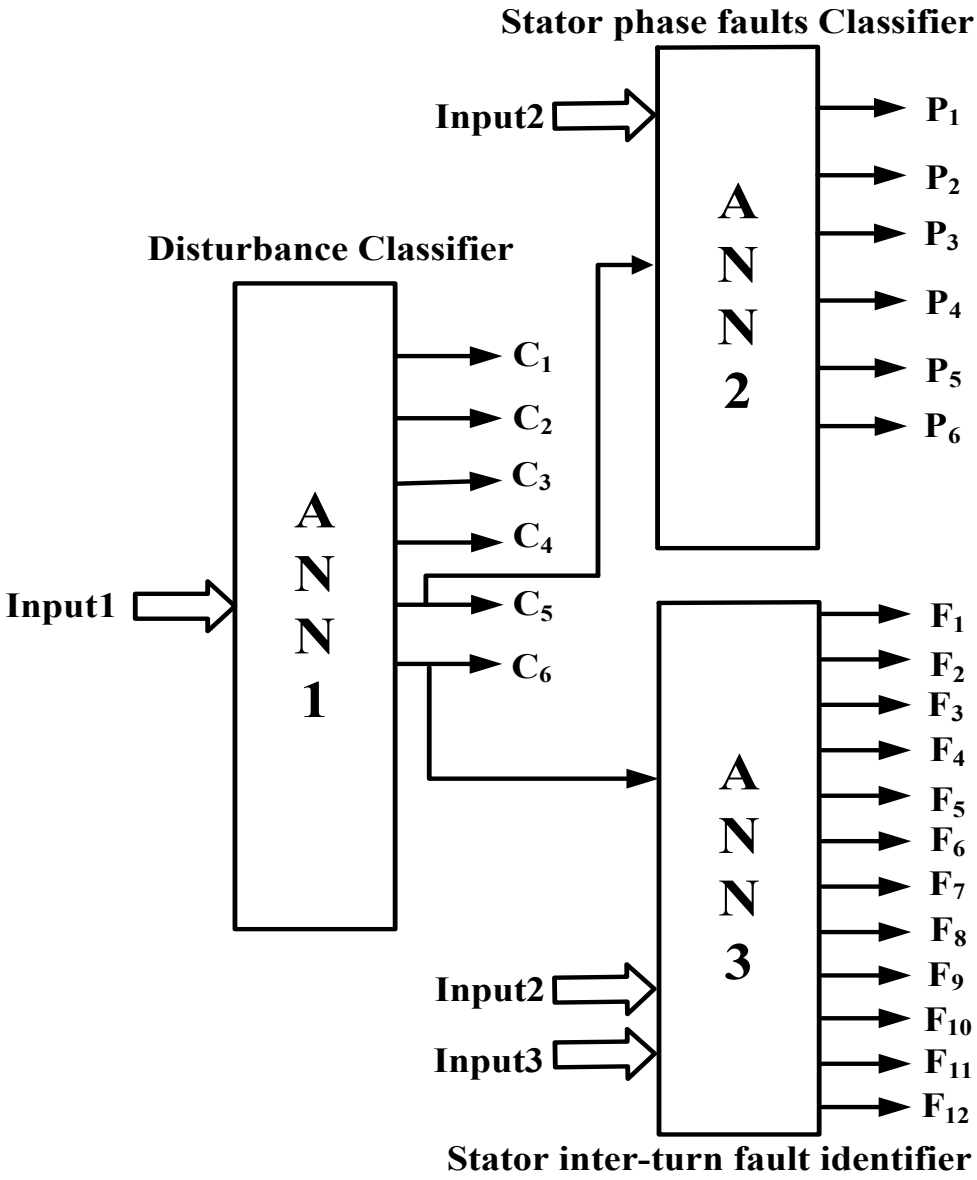


Figure 4.28: Proposed classifiers for classification of faults on a three-phase induction motor

networks are explained in chapter-5 and chapter-6 respectively. The inputs to the ANN-1 are the statistical features of second level approximate coefficients of three-phase residue currents of a motor, which are standard deviation, maximum value and mean value obtained over a window of one cycle from the fault instant. The output of ANN-1 classifies 6 classes (C1 to C6) of disturbances on three phase induction motor. the six classes of disturbances are as follows:

$C_1$ →Single phasing

$C_2$ →Supply unbalance

$C_3$ →Under voltage

$C_4$ →Sudden load change

$C_5$ →Stator phase fault

$C_6$ →Stator inter-turn fault

### 4.3.1 Training and Testing of ANN based Disturbance Classifier

For the simulation of ANN-1 in MATLAB, a tangent sigmoid (tansig) and log sigmoid (logsig) activation function are used and training goal is set at $10^{-6}$. First, the performance of single multilayer NN of ANN-1 is demonstrated. Various training and testing patterns are generated by using simulation and experimentation. The break up of experimental and simulation data sets of training and testing are given in Table 4.2. Totally 1287 patterns are carried out to train and test the ANN-1, out of 1287 sets 858 data sets are utilized for training i.e. two third of the total data sets remaining are used for testing. The training performance of single multilayer NN with respect to number of neurons variation in hidden layer is depicted in Table 4.3. From Table 4.3, it is observed that the training

accuracy for 12 hidden neurons and 14 hidden neurons are nearly same but number of epochs or 14 neurons is less than that for 12 neurons. Therefore, 14 hidden neurons are considered in ANN1.

Table 4.2: Training and testing data for various disturbances

| **Type of fault** | **No. of training patterns** | | **No. of testing patterns** | |
|---|---|---|---|---|
| | **Exp** | **Sim** | **Exp** | **Sim** |
| Single Phasing | 24 | 13 | 12 | 8 |
| Supply Unbalance | 60 | 54 | 30 | 27 |
| Under Voltage | 24 | 23 | 12 | 11 |
| Stator Inter-turn fault | 72 | 444 | 36 | 222 |
| Sudden load change | 18 | - | 8 | - |
| Phase Faults | 18 | 108 | 9 | 54 |
| Total | 216 | 642 | 107 | 322 |
| | 858 | | 429 | |

Table 4.3: Training performance of single multilayer ANN-1

| **Number of neurons in hidden layer** | **Learning epochs** | **Training accuracy** |
|---|---|---|
| 11 | 200 | 96.4% |
| 12 | 219 | 97.5% |
| 13 | 198 | 97.2% |
| 14 | 104 | 97.59% |
| 15 | 108 | 97.13% |
| 16 | 120 | 97.4% |

In any classifier, the performance evaluation requires specific measures which include accuracy, sensitivity and specificity. There are four additional terms should need to know that are the building blocks used in computing many evaluation measures. These are TP (True positives), TN

Table 4.4: Testing performance of single multilayer ANN-1

| Learning rate | Momentum | Testing accuracy | Training time in sec |
|---|---|---|---|
| 0.3 | 0.67 | 86.95% | 19 |
| 0.4 | | 90.21% | 14 |
| 0.5 | | 88.11% | 17 |
| 0.6 | | 86.71% | 4.07 |
| 0.3 | 0.68 | 86.95% | 16 |
| 0.4 | | 87.65% | 17 |
| 0.5 | | 90.61% | 7 |
| 0.6 | | 88.11% | 7 |
| 0.3 | 0.69 | 86.48% | 26 |
| 0.4 | | 90.68% | 11 |
| 0.5 | | 89.51% | 9 |
| 0.6 | | 89.74% | 9 |
| 0.3 | 0.7 | 85.05% | 18 |
| 0.4 | | 85.55% | 8 |
| o.5 | | 87.65% | 9 |
| 0.6 | | 89.04% | 16 |

(True negatives), FP (False positives) and FN (False negatives). The confusion matrix is a useful tool for analyzing how well the classifier can recognize tuples of different classes. The accuracy, sensitivity and specificity measures can be used, respectively, for identifying the performance of the classifier. These measures are defined as follows:

$$Sensitivity = \frac{TP}{P} \tag{4.1}$$

$$Specificity = \frac{TN}{N} \tag{4.2}$$

$$Accuracy = Sensitivity\frac{P}{P+N} + Specificity\frac{N}{P+N} \tag{4.3}$$

Table 4.5: Testing performance of multilayer ANN-1

| Number of neurons in hidden layer 1 and 2 | Learning rate | Momentum | Testing accuracy | Training time in sec |
|---|---|---|---|---|
| 14,10 | 0.4 | 0.69 | 92.31% | 37 |
| 14,20 | 0.4 | | 90.68% | 54 |
| 14,10 | 0.5 | 0.68 | 88.81% | 30 |
| 14,20 | 0.5 | | 91.38% | 86 |

The testing performance of ANN-1 is illustrated in Table 4.4 by making use of different learning rates and different values of momentums. From Table 6 it is observed that for momentum value of 0.69, 0.68 and learning rate of 0.4, 0.5 give better accuracy compared to remaining all. Similarly,

Table 4.6: Performance of ANN-1 in double multilayer of 14, 20

| Type of disturbance | Sensitivity | Specificity | Average |
|---|---|---|---|
| $C_1$ | 0.952 | 1 | |
| $C_2$ | 0.804 | 0.989 | Sensitivity: 0.786 |
| $C_3$ | 0.973 | 0.980 | |
| $C_4$ | 0.3 | 0.99 | Specificity: 0.977 |
| $C_5$ | 0.9 | 0.986 | |
| $C_6$ | 0.786 | 0.977 | |

same data is used to train and test the multilayer neural network with two hidden layers also, these results are shown in Table 4.5. From the results, it is proved that the testing accuracy of multilayer neural network is better compared with single multilayer neural network but the time taken to train the network is more. The other performance measures are also calculated using equations 4.1 and 4.2. Table 4.6 shows the performance measures

of sensitivity and specificity of 14, 20 configuration of double multilayer neural network with learning rate of 0.5 and momentum value of 0.68.

## 4.4 MNN Structure for Disturbance Classifier(MNN-1)

Artificial neural networks are broadly classified into monolithic networks and modular networks. In canonical implementations, most of the systems employ a monolithic network in order to solve the given task. However, when a system needs to process large amount of data or when the problem is highly complex, then it is not trivial, and sometimes unfeasible, to establish a good architecture and topology for a single network that can solve the problem.

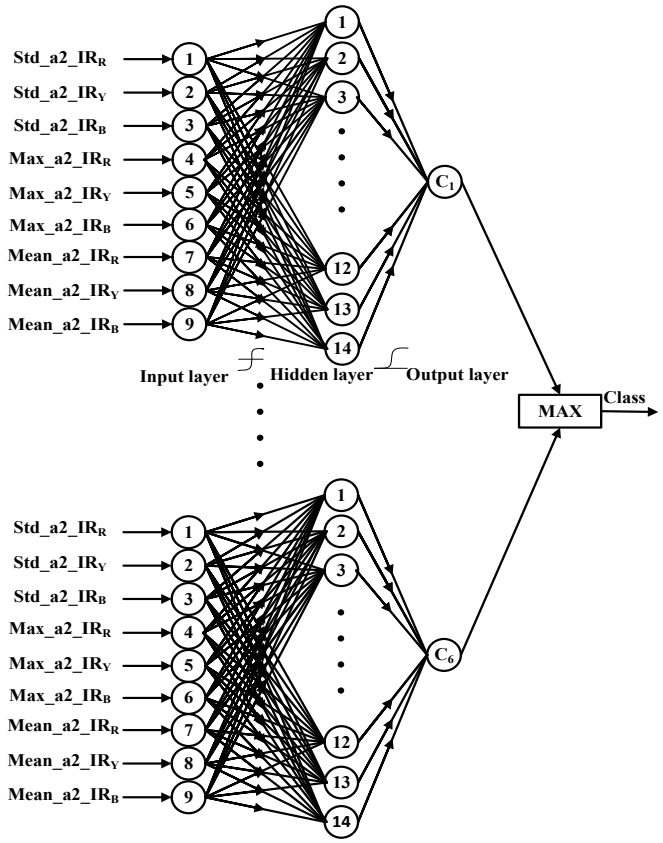


Figure 4.29: Proposed MNN-1 for disturbance classifier

In order to overcome some of the aforementioned shortcomings of monolithic ANNs, many researchers have proposed modular approaches [78] [79]. One of the major benefits of a modular neural network is the ability to reduce a large, unwieldy neural network to smaller, more manageable components. Other benefits of these networks are their efficiency, lower training time and robustness. In this connection, a modular multilayer neural network is implemented to classify various disturbances (MNN-1) of a three-phase induction motor. It is compared with artificial neural network (ANN) of a single multilayer neural network and double multilayer neural network through the simulation and experimentation. Figure 4.29 shows the MNN architecture for disturbance classifier.

### 4.4.1 Training and Testing of MNN based Disturbance Classifier

The implemented modular structure of disturbance classifier is trained and tested with same data sets to check the performance of the modular neural network. Six types of disturbances have been considered for classification, 6 modules of NN are required to form a modular neural network one (MNN-1). Each module of MNN-1 classifier classifies one class. During training process, features of a particular disturbance signal are applied to all modules with target as "1" to the corresponding neural module and target as "0" to the rest of the modules. During testing, outputs of all the NN modules are compared. The NN modules having largest output will represent the corresponding disturbance class. The performance of classifier MNN-1 is shown in Table 4.7. From this table the overall accuracy of the modular classifier of MNN-1 is 94.64% and this

Table 4.7: Confusion matrix for MNN-1

| | $C_1$ | $C_2$ | $C_3$ | $C_4$ | $C_5$ | $C_6$ |
|---|---|---|---|---|---|---|
| $C_1$ | 21 | 0 | 0 | 0 | 0 | 0 |
| $C_2$ | 2 | 50 | 0 | 0 | 1 | 3 |
| $C_3$ | 0 | 0 | 22 | 0 | 1 | 0 |
| $C_4$ | 0 | 0 | 0 | 9 | 0 | 1 |
| $C_5$ | 0 | 2 | 0 | 2 | 58 | 1 |
| $C_6$ | 1 | 4 | 2 | 2 | 1 | 246 |
| Overall accuracy = 94.64% | | | | | | |

performance is achieved within 4 sec. Hence, the results proved that the performance of MNN-1 is significantly higher (2.4%) as compared to multilayer neural network classifier of ANN-1.

## 4.5 Comparison of Performance between ANN-1 and MNN-1

The testing performance of ANN-1 and MNN-1 are compared based on the specific measures they are sensitivity and specificity which are defined in equation 4.1 and 4.2. Table 4.8 demonstrates the values of sensitivity and specificity for ANN-1 and MNN-1 based classifiers corresponding to 6 types of disturbances. From this table, it is proved that the modular structure of neural network has more capability to classify the various disturbances. Hence the modular based classifier is significantly far better than the multilayer neural network classifier.

Table 4.8: Performance for ANN-1 and MNN-1 in disturbance classification

| Type of network | Type of disturbance | Sensitivity | Specificity | Average |
|---|---|---|---|---|
| ANN-1 | $C_1$ | 0.952 | 0.995 | |
| | $C_2$ | 0.804 | 0.989 | Sensitivity: 0.858 |
| | $C_3$ | 0.913 | 0.980 | |
| | $C_4$ | 0.961 | 0.942 | Specificity: 0.98 |
| | $C_5$ | 0.6 | 0.998 | |
| | $C_6$ | 0.921 | 0.978 | |
| MNN-1 | $C_1$ | 1 | 0.993 | |
| | $C_2$ | 0.893 | 0.984 | Sensitivity: 0.939 |
| | $C_3$ | 0.957 | 0.995 | |
| | $C_4$ | 0.961 | 0.971 | Specificity:0.987 |
| | $C_5$ | 0.9 | 0.99 | |
| | $C_6$ | 0.921 | 0.992 | |

## 4.6 Conclusions

This chapter presents the underlying procedure for the extraction of nine features, from the operating conditions of induction motor, for the classification of faults that the motor is subjected to. Two classifiers, one based on multi layer neural network (ANN-1) and the other based on modular neural network (MNN-1) are proposed for classification of faults on induction motor. The following conclusions are drawn from the results of ANN-1 and MNN-1 classifiers.

Only three measurements are required to obtain the nine features fed as input to the proposed classifiers. Double multi layer ANN based disturbance classifier performed better when compared with single layer ANN based classifier. The over all accuracy of single multi layer ANN is 90.68% and

double layer ANN performance is improved by 1.63% when compared that of single layer ANN. But the time taken to achieve this performance is more.

The results revealed that there is an improvement in the accuracy of MNN-1 by 2.33% when compared with that of ANN-1.

# Chapter 5

# Classification of Stator Phase Faults

## 5.1 Introduction

The stator phase faults can be caused by the insulation failure between two phases or phase to ground of stator windings. These faults causes to lead the damage of winding or core of the machine. Hence, early detection and classification of stator phase faults along with faulty phase is essential to prevent permanent damage to the motor and to reduce motor down time. This chapter explains the ANN and MNN based classifier for stator phase faults.

## 5.2 Extraction of features for phase fault classification

The classification of phase faults also have equal importance as that of stator incipient faults, if phase faults occur towards the neutral point. Hence, identification and classification of phase faults are essential, before they lead to a major fault. Very little effort was made to address the classification of stator phase faults on a 3-phase Induction motor. In 2006, M. A. S. K Khan and et al. [56] have addressed the stator phase faults

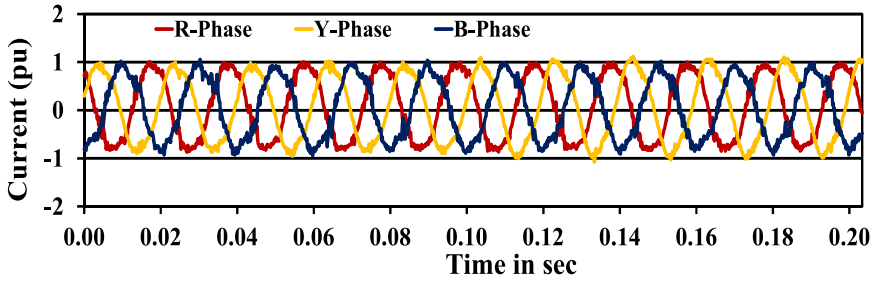


Figure 5.1: Three-phase currents for phase to ground fault in Y-phase of a 3-hp induction motor

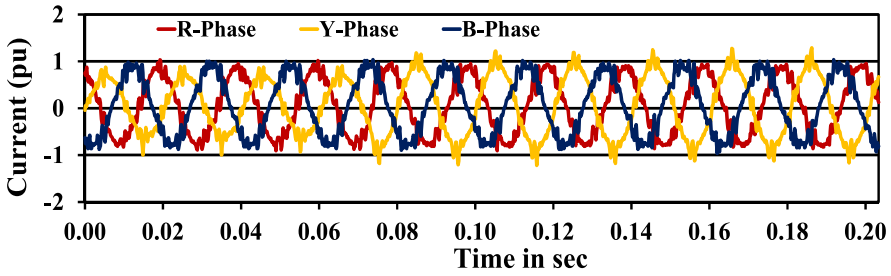


Figure 5.2: Three-phase currents for phase to phase fault between Y and B phases of a 3-hp induction motor

based on DWT. In general, classifier requires certain features which are insensitive to the operating conditions. Three features extracted from the slope of detail level coefficients of three-phase residues are considered for fault classification. These are the slopes of detail level coefficients of absolute peak values of three phase residue currents obtained over a window of 10 samples from the instant of fault occurrence. Figures 5.1 and 5.2 show the captured three-phase currents of the considered cases of phase to ground fault in Y-phase and phase to phase fault between Y and B phases. To identify the instant of fault occurrence is essential for extracting the features require to classify the phase faults. The SWT and DWT based fault detection criteria and identification of the instant of fault occurrence is already explained in chapter 3. With the help of that approach instant of

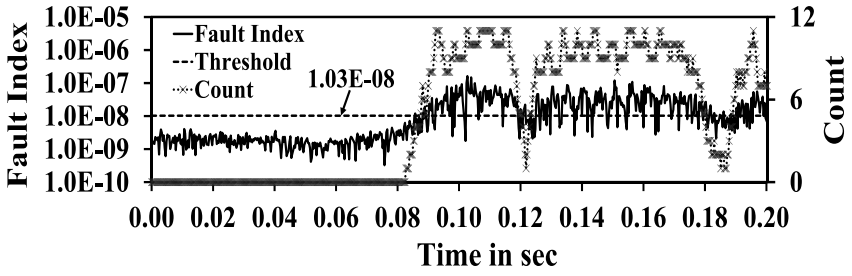


Figure 5.3: Variation in fault index for phase to ground fault in Y-phase of a 3-hp induction motor

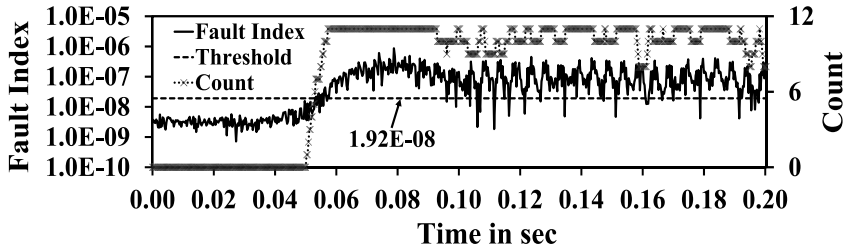


Figure 5.4: Variation in fault index for phase to phase fault between Y and B phases of a 3-hp induction motor

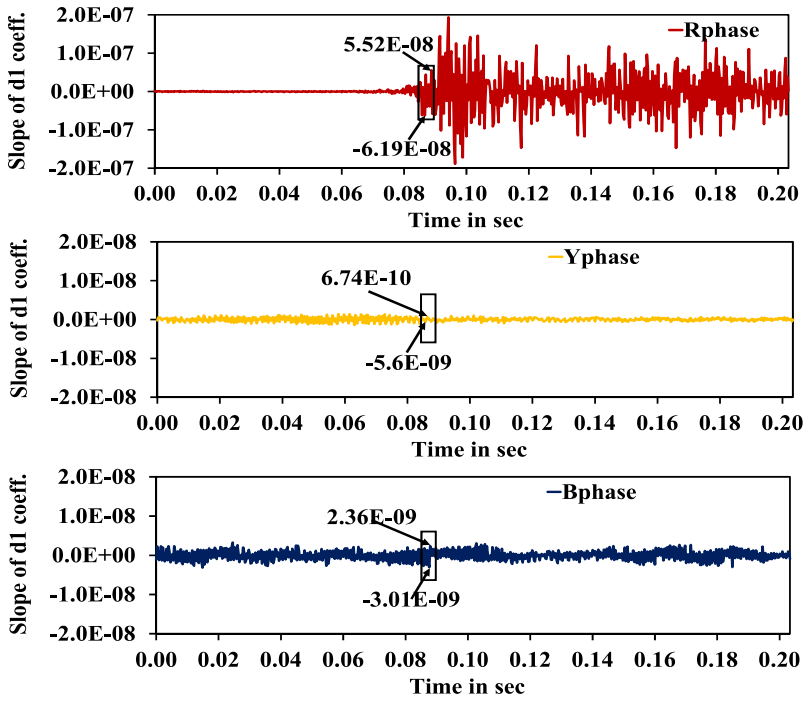


Figure 5.5: Variation in slope of detail level coefficients for phase to ground fault in Y-phase of a 3-hp induction motor

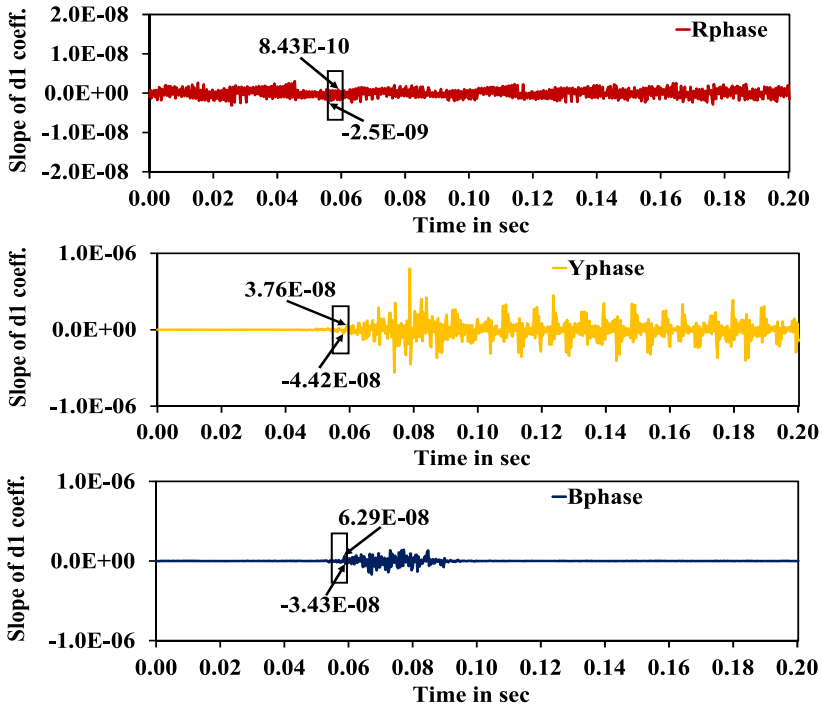


Figure 5.6: Variation in slope of detail level coefficients for phase to phase fault between Y and B phases of a 3-hp induction motor

fault occurrence is identified for the cases of phase to ground fault in Y-phase and phase to phase fault between Y and B phases and are demonstrated in figures 5.3 and 5.4 respectively. After getting the fault instant, features are calculated from the slope of detail level coefficients which are illustrated in figures5.5 and 5.6. From these figures, the absolute peak values of the slope of detail level coefficients of three-phase residues for YG fault are $6.19 \times 10^{-08}$, $6.74 \times 10^{-10}$ and $3.01 \times 10^{-09}$ and YB fault are $8.43 \times 10^{-10}$, $4.42 \times 10^{-08}$ and $6.29E \times 10^{-08}$ . Figure 5.7 shows the variation in normalised values of features for YG and YB fault cases. The results clearly demonstrate that the features of YG fault case is different from YB fault case. The variation in feature 1, feature 2 and feature 3 with respective to the various stator phase faults like phase to ground fault in R-phase, phase to ground fault in Y-phase, phase to ground fault in

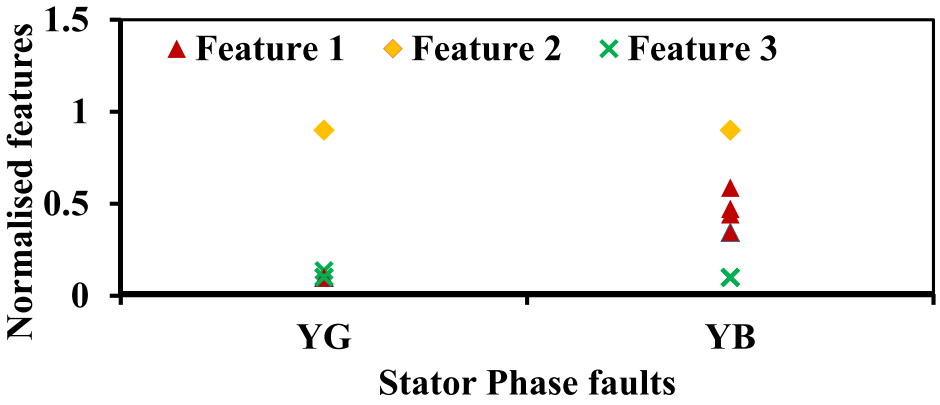


Figure 5.7: Variation in normalised features for YG and YB faults

B-phase, phase-phase fault between R and Y, phase-phase fault between Y and B and phase-phase fault between B and R are tabulated in Table 5.1. Interesting patterns that can be observed from the normalized feature values given in Table 5.1 are: for phase-ground fault two features assume low value and remaining third feature assumes higher value and for phase-phase fault two features assume high value and the remaining third feature assumes low value (quite opposite to the pattern observed for phase-ground fault). Figure 5.8 shows the variations in feature 1, feature 2 and feature 3 for various levels of stator phase faults such as 2-turn, 4-turn, 6-turn and 8-turn fault cases. The results gives an evidence that the features corresponding to the faulted phases are higher compared with healthy phase features. Hence, the selected features are good for segregating the various stator phase faults irrespective of its operating conditions because of the self normalization ability of the features.

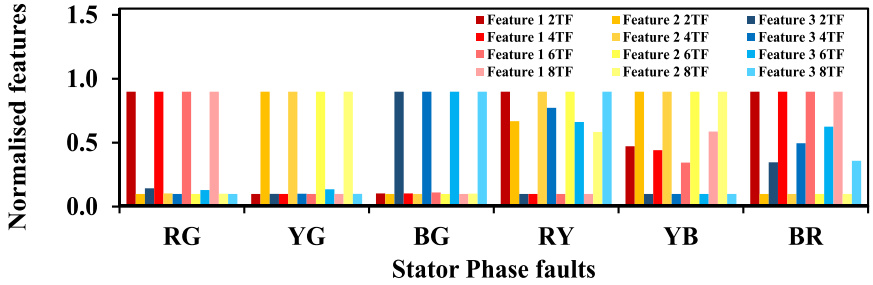


Figure 5.8: Variation in normalised features for stator phase faults

Table 5.1: Self normalised features for various stator phase faults

| Faulty phase | | RG fault | YG fault | BG fault | RY fault | YB fault | BR fault |
|---|---|---|---|---|---|---|---|
| Features | R-phase | 0.9 | 0.1 | 0.1 | 0.9 | 0.1 | 0.9 |
| in | Y-phase | 0.102 | 0.9 | 0.1 | 0.669 | 0.9 | 0.1 |
| simulation | B-phase | 0.1 | 0.101 | 0.9 | 0.1 | 0.898 | 0.347 |
| Features | R-phase | 0.9 | 0.1 | 0.105 | 0.9 | 0.1 | 0.9 |
| in | Y-phase | 0.1 | 0.9 | 0.1 | 0.52 | 0.9 | 0.1 |
| Experimental | B-phase | 0.136 | 0.137 | 0.9 | 0.1 | 0.821 | 0.396 |

## 5.3 ANN structure for phase fault classifier (ANN-2)

The classifier used for classifying the stator phase faults is named as ANN-2 which is already mentioned in chapter 4. Three detail level coefficients are fed as inputs to the ANN-2 when it is activated. The ANN-2 is active if and only if $C_5$ of ANN-1 is 1. The output of ANN-2 identify 6 classes of phase faults and these are as follows:

$P_1$ →Stator turn-turn fault between RY phases

$P_2$ →Stator turn-turn fault between YB phases

$P_3$ →Stator turn-turn fault between BR phases

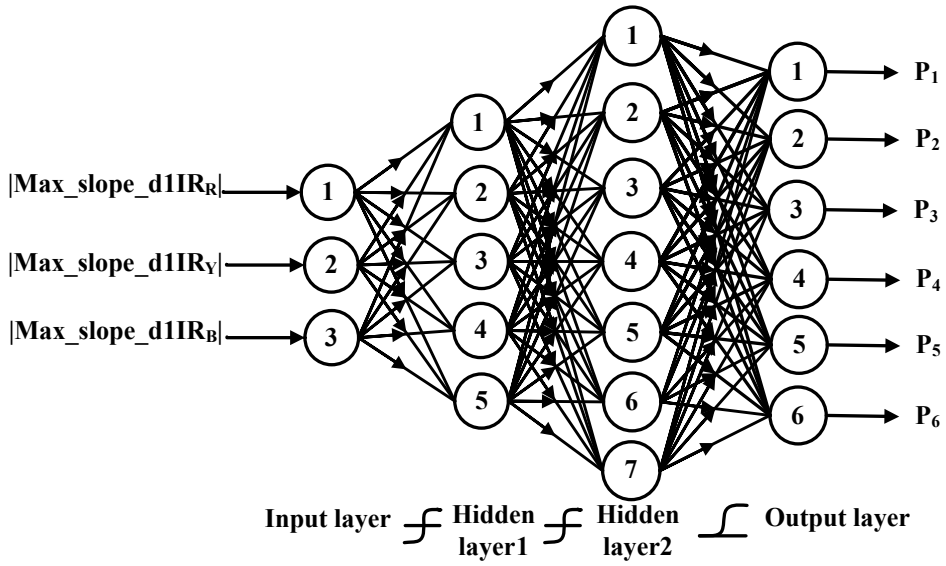


Figure 5.9: Proposed ANN-2 for classification of stator phase faults

$P_4$ →Stator turn-ground fault in R phase

$P_5$ →Stator turn-ground fault in Y phase

$P_6$ →Stator turn-ground fault in B phase

### 5.3.1 Training and Testing of ANN-2

ANN-2 is simulated in MATLAB with an activation functions of a tangent sigmoid (tansig) and log sigmoid (logsig) and training goal is set at $10^{-6}$. Number of training and test patterns used to train and test the classifier respectively are tabulated in Table 5.2. Out of 201 total patterns, 136 patterns are utilized for training the classifier and the remaining 66 patterns are used for testing. Approximately two thirds of the data set is used for training and one thirds of the data set is used for testing. Several multilayer neural network configurations are tested using MATLAB/Simulink software. Among all, the best performed configuration of multilayer neural network of ANN-2 has 3 (input neurons), 5 (hidden neurons), 7 (hidden

neurons) and 6 (output neurons). Figure 5.9 shows the proposed architecture for ANN-2. The testing performance of ANN-2 is demonstrated by using confusion matrix. The confusion matrix for the classifier is shown in Table 5.3. The overall accuracy is obtained as 89.39%.

Table 5.2: Training and testing data for stator phase faults classification

| **Type of stator phase fault** | **No. of training patterns** | | **No. of testing patterns** | |
|---|---|---|---|---|
| | **Exp** | **Sim** | **Exp** | **Sim** |
| Stator turn-ground fault in R phase | 6 | 18 | 2 | 9 |
| Stator turn-ground fault in Y phase | 6 | 18 | 2 | 9 |
| Stator turn-ground fault in B phase | 6 | 18 | 2 | 9 |
| Stator turn-turn fault between RY phase | 2 | 19 | 2 | 9 |
| Stator turn-turn fault between YB phase | 2 | 19 | 2 | 9 |
| Stator turn-turn fault between BR phase | 2 | 19 | 2 | 9 |
| Total | 24 | 111 | 12 | 54 |
| | 135 | | 66 | |

Table 5.3: Confusion matrix for ANN-2

| | $P_1$ | $P_2$ | $P_3$ | $P_4$ | $P_5$ | $P_6$ |
|---|---|---|---|---|---|---|
| $P_1$ | 10 | 0 | 1 | 0 | 0 | 0 |
| $P_2$ | 0 | 11 | 0 | 0 | 0 | 0 |
| $P_3$ | 2 | 0 | 11 | 0 | 0 | 0 |
| $P_4$ | 0 | 0 | 0 | 10 | 0 | 0 |
| $P_5$ | 0 | 2 | 0 | 0 | 8 | 0 |
| $P_6$ | 0 | 0 | 0 | 2 | 0 | 9 |
| Overall accuracy = 89.39% | | | | | | |

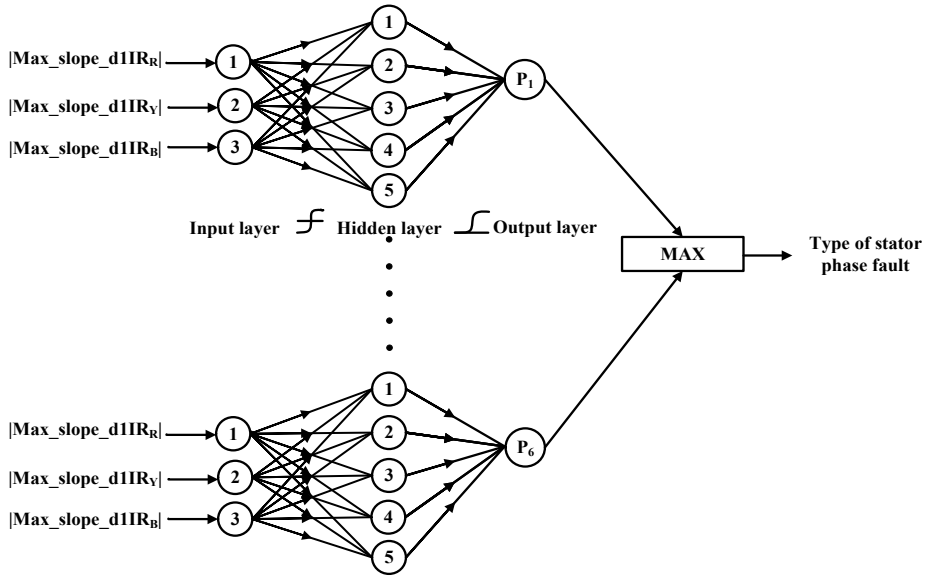


Figure 5.10: Proposed MNN-2 for classification of stator phase faults

## 5.4 MNN structure for phase fault classifier (MNN-2)

In this section, a modular structure of neural networks is implemented to classify various stator phase faults on a 3-phase Induction motor. Its performance is compared with that of ANN-2 for both simulation and experimental data. Figure 5.10 shows the proposed MNN configuration for stator phase fault classifier(MNN-2).

### 5.4.1 Training and Testing of MNN-2

To improve the stator phase fault classification performance a modular structure of neural network (NN) as shown in figure 5.10 is used. Training and testing data sets that are used for ANN-2, are also used to train and test the modular neural network respectively. Six modules of NN are required to form a modular neural network MNN-2. Each module of MNN-2 classifier classifies one class. During training phase, features of a stator phase fault signal are applied to all modules with target as 1 to the

corresponding phase fault neural module and target as 0 to the rest of the modules. During testing, outputs of all the NN modules are compared. The output of MNN-2 is same as the stator phase fault class corresponding to the NN module with largest output. The performance of MNN-2 classifier is shown in Table 5.4.

Table 5.4: Confusion matrix for MNN-2

| | $P_1$ | $P_2$ | $P_3$ | $P_4$ | $P_5$ | $P_6$ |
|---|---|---|---|---|---|---|
| $P_1$ | 11 | 0 | 0 | 0 | 0 | 0 |
| $P_2$ | 0 | 11 | 0 | 0 | 0 | 0 |
| $P_3$ | 0 | 0 | 11 | 0 | 0 | 0 |
| $P_4$ | 0 | 0 | 0 | 10 | 0 | 0 |
| $P_5$ | 0 | 0 | 0 | 0 | 10 | 0 |
| $P_6$ | 0 | 0 | 0 | 2 | 0 | 9 |
| Overall accuracy = 93.94% | | | | | | |

## 5.5 Comparison of performance between ANN-2 and MNN-2 for stator phase fault classification

A comparison is made between the performance of ANN-2 and that of MNN-2 based on the specific measures which are sensitivity and specificity. The values of sensitivity and specificity for ANN-2 and MNN-2 classifiers corresponding to 6 types of phase faults are tabulated in Table 5.5. The results clearly demonstrate that the modular structure of neural network has more capability to correctly classify the various stator phase faults. Hence the modular based classifier is significantly far better than the multilayer neural network classifier.

Table 5.5: Comparison of performance between ANN-2 and MNN-2

| Type of network | Type of disturbance | Sensitivity | Specificity | Average |
|---|---|---|---|---|
| **ANN-2** | $P_1$ | 0.909 | 0.964 | |
| | $P_2$ | 1 | 0.964 | Sensitivity: 0.896 |
| | $P_3$ | 0.846 | 0.981 | |
| | $P_4$ | 1 | 0.964 | Specificity: 0.979 |
| | $P_5$ | 0.8 | 1 | |
| | $P_6$ | 0.818 | 1 | |
| **MNN-2** | $P_1$ | 1 | 0.964 | |
| | $P_2$ | 1 | 1 | Sensitivity: 0.944 |
| | $P_3$ | 0.846 | 1 | |
| | $P_4$ | 1 | 0.964 | Specificity:0.988 |
| | $P_5$ | 1 | 1 | |
| | $P_6$ | 0.818 | 1 | |

## 5.6 Conclusions

This chapter presented the procedure for extraction of features and introduced two classifiers for stator phase fault classification on a 3-phase Induction motor. The features considered for stator phase fault classification are insensitive to the operating condition of a 3-phase Induction motor. Two classifiers based on ANN and MNN respectively are proposed. The following conclusions are drawn from the results of ANN-2 and MNN-2 classifiers.

The multi layer ANN of stator phase fault classifier attains an accuracy of 89.39% with minimum number of features. To improve the efficacy of the classifier a modular concept is introduced. The MNN based classifier has an edge over ANN based classifier for classifying stator phase faults.

The results revealed that there is an improvement in classifier accuracy by 4.55% when MNN is used in place of ANN.

# Chapter 6

# Identification of Faulty Phase and Estimation of Severity Level for Stator Inter-Turn Faults

## 6.1 Introduction

In recent times, the condition monitoring techniques are concentrated not only on the detection of faults but also on the identification of faulty phase and severity level of faults. Algorithms for fault detection and disturbance classification are discussed in chapter 3 and chapter 4 respectively. This chapter discusses and proposes an identifier based on ANN and MNN to identify the fault phase and to find severity level of stator inter-turn faults. Only four features, that are insensitive to the operating conditions, are used for identification of fault phase and to find severity level of fault.

## 6.2 Features used for identification of faulty phase and estimation of fault severity

Identification of faulty phase and estimation of severity of stator inter-turn faults are essential for induction motor fault diagnosis. In [77] and [80] discussion was made about assessment of fault severity based on CWT technique. But, for both the techniques the number of features required is more. Hence, an attempt is made to assess fault severity with minimum number of features which are selected from wavelet analysis and are insensitive to the operating conditions. Three features are extracted from the slope of detail level coefficients of three-phase residues and another feature is extracted from the mean energy values of $4^{th}$ level approximate coefficients of three-phase residues. The first three features are the slope of detail level coefficients of absolute peak values of three phase residue currents obtained over a window of 10 samples from the fault instant and are named as feature 1, feature 2 and feature 3. The other feature is the ratio of post fault and pre-fault mean energy values of $4^{th}$ level approximate coefficients and is named as feature 4.

To explain the selection process of the proposed features a 4-turn short circuit in R-phase is considered. The captured three-phase current signals of 4-turn short circuit in R-phase of experimental case are shown in figure 6.1 and their three-phase residues are obtained from SWT of Bior 5.5 mother wavelet which are shown in figure 6.2. The detail level coefficients of three-phase residues are obtained by decomposing the three-phase residue with DWT of Bior 5.5 mother wavelet. The instant of fault occurrence for extracting the features is estimated accurately by

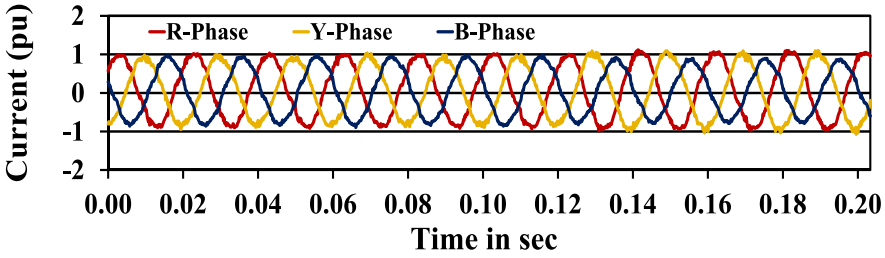


Figure 6.1: Three-phase currents for 4-turn short circuit in R-hase

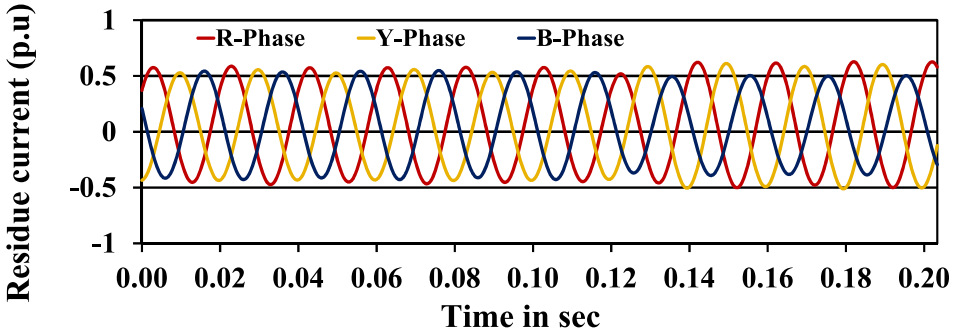


Figure 6.2: Three-phase residues for 4-turn short circuit in R-phase

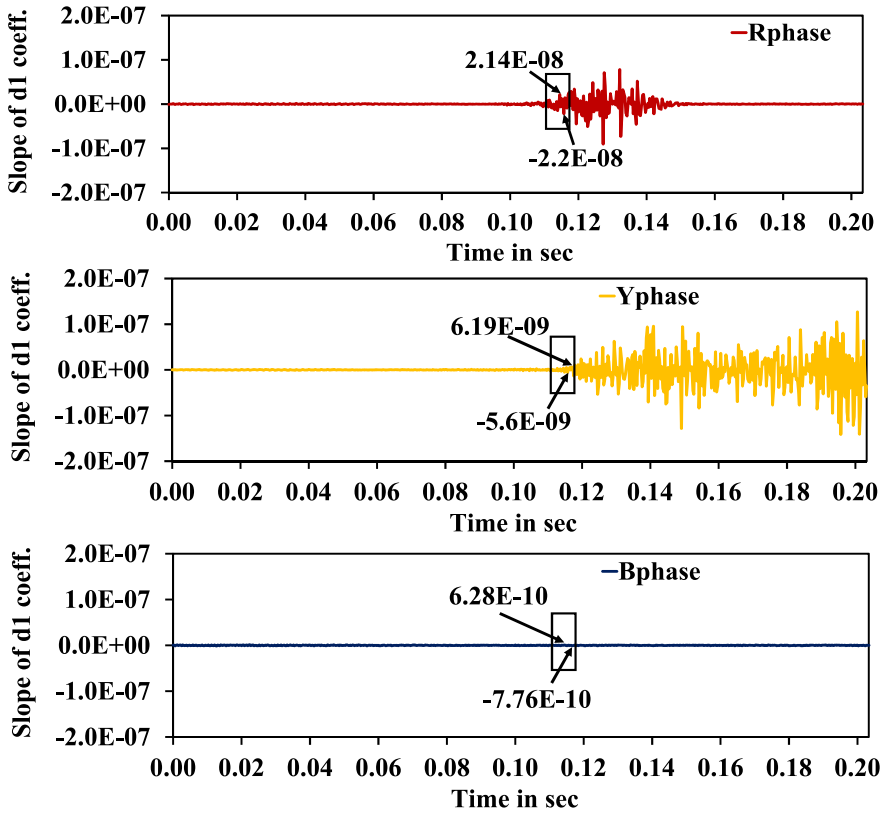


Figure 6.3: variation in slope of detail level coefficients for 4-turn short circuit in R-phase

Table 6.1: Features extracted from slope of detail level coefficients

| Faulty phase | | Rfault Exp. ($\times 10^{-9}$) | Yfault Exp. ($\times 10^{-9}$) | Bfault Exp. ($\times 10^{-9}$) | Rfault Sim. ($\times 10^{-9}$) | Yfault Sim. ($\times 10^{-9}$) | Bfault Sim. ($\times 10^{-9}$) |
|---|---|---|---|---|---|---|---|
| 2 turn fault features | R-phase | 10.36 | 1.117 | 1.529 | 49.49 | 1.386 | 2.025 |
| | Y-phase | 2.533 | 3.179 | 1.626 | 3.348 | 58.2 | 0.741 |
| | B-phase | 1.732 | 3.136 | 2.844 | 0.7426 | 7.329 | 21.53 |
| 4 turn fault features | R-phase | 33.74 | 1.652 | 26.19 | 30.92 | 0.5804 | 3.520 |
| | Y-phase | 0.7762 | 18.50 | 1.687 | 11.44 | 28.47 | 1.006 |
| | B-phase | 12.94 | 5.288 | 56.90 | 0.7325 | 0.5591 | 57.73 |
| 6 turn fault features | R-phase | 45.15 | 38.44 | 9.959 | 54.55 | 1.506 | 0.7698 |
| | Y-phase | 0.6834 | 192.0 | 2.939 | 0.4086 | 30.61 | 0.8719 |
| | B-phase | 5.414 | 27.84 | 61.51 | 0.4728 | 1.707 | 40.78 |
| 8 turn fault features | R-phase | 33.9 | 11.44 | 24.56 | 38.12 | 0.939 | 1.019 |
| | Y-phase | 3.329 | 51.97 | 31.95 | 0.5919 | 18.82 | 0.7379 |
| | B-phase | 0.8075 | 12.19 | 107.8 | 0.6292 | 1.227 | 23.62 |

calculating the ratio between the difference in sample values of the $d1$ coefficients of three phase residues over a moving window of 3 samples and difference in sample intervals. For a discrete signal the ratio between the difference in sample values and difference in sample intervals is called slope. A fault is detected by comparing the fault index with adaptive threshold which is already explained in chapter 3. Figure 6.3 illustrates the variations in slope of detail level coefficients of three phase residues for 4-turn short circuit in R-phase of a 3-hp induction motor. From figure 6.3, the positive and negative peak values of slope of detail coefficients three-phase residues over a window 10 samples are $2.14 \times 10^{-08}$ and $-2.2 \times 10^{-08}$ in R-phase, $6.19 \times 10^{-09}$ and $-5.6 \times 10^{-09}$ in Y-phase and

$6.28 \times 10^{-10}$ and $-7.76 \times 10^{-10}$ in B-phase for a 3-hp induction motor. From

Table 6.2: Self normalised features extracted from slope of detail level coefficients

| Faulty phase | | Rfault Exp. | Yfault Exp. | Bfault Exp. | Rfault Sim. | Yfault Sim. | Bfault Sim. |
|---|---|---|---|---|---|---|---|
| 2 turn fault features | R-phase | 0.9 | 0.1 | 0.192 | 0.9 | 0.1 | 0.100 |
| | Y-phase | 0.1423 | 0.9 | 0.1 | 0.17 | 0.9 | 0.1 |
| | B-phase | 0.1 | 0.184 | 0.9 | 0.1 | 0.153 | 0.9 |
| 4 turn fault features | R-phase | 0.9 | 0.101 | 0.119 | 0.9 | 0.1 | 0.432 |
| | Y-phase | 0.384 | 0.9 | 0.1 | 0.1 | 0.9 | 0.1 |
| | B-phase | 0.1 | 0.1 | 0.9 | 0.395 | 0.274 | 0.9 |
| 6 turn fault features | R-phase | 0.9 | 0.1 | 0.15 | 0.9 | 0.152 | 0.173 |
| | Y-phase | 0.1 | 0.9 | 0.1 | 0.1 | 0.9 | 0.1 |
| | B-phase | 0.101 | 0.106 | 0.9 | 0.185 | 0.1 | 0.9 |
| 8 turn fault features | R-phase | 0.9 | 0.1 | 0.11 | 0.9 | 0.1 | 0.1 |
| | Y-phase | 0.1 | 0.9 | 0.1 | 0.161 | 0.9 | 0.363 |
| | B-phase | 0.101 | 0.113 | 0.9 | 0.1 | 0.115 | 0.9 |

these values, it is clear that the faulty phase peak values are higher than those of healthy phases.

Table 6.1 and Table 6.2 demonstrate the actual and self normalized values of feature 1, feature 2 and feature 3 for various levels of stator inter-turn faults. The results from Table 6.1 and Table 6.2 show that, of all the three feature values the faulty phase feature has highest value. Hence, these three features are effective in identifying the faulty phase accurately. But severity level can not be identified from these features and is identified from feature 4, which can be obtained from $4^{th}$ level approximate coefficients. The variation in $4^{th}$ level approximate coefficients of three-phase residues and their energies for a 4-turn short circuit in R-phase are illustrated in figure6.4 and figure6.5 respectively. Figure 6.6 shows the

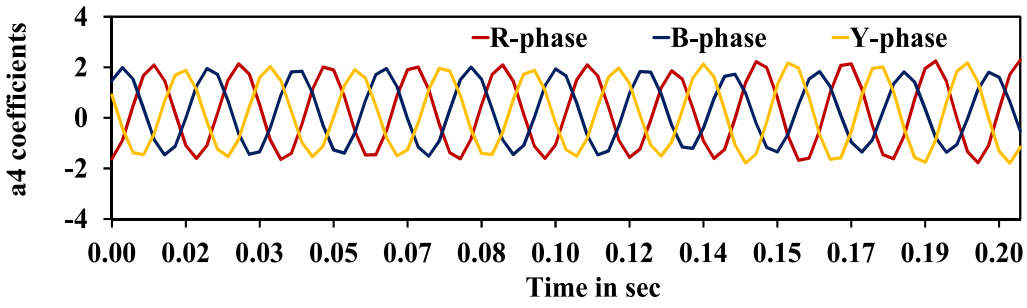


Figure 6.4: Variation in fourth level approximate coefficients for 4-turn short circuit in R-phase

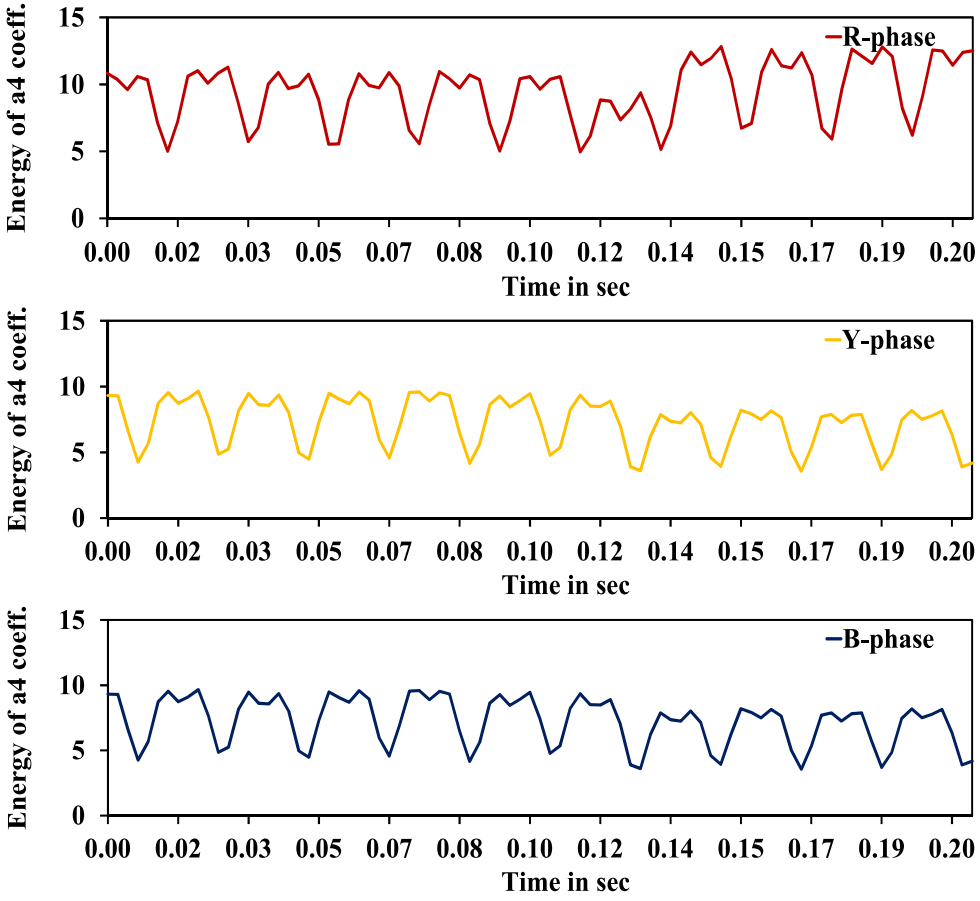


Figure 6.5: Variation in fourth level approximate coefficients for 4-turn short circuit in R-phase

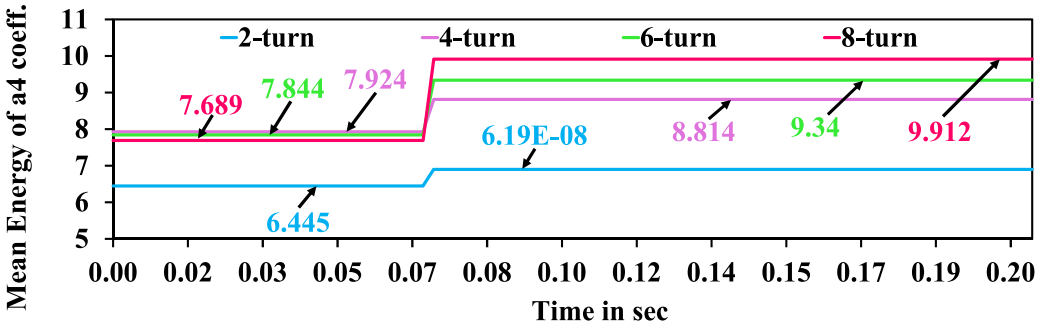


Figure 6.6: Variation in fourth level approximate coefficients for 4-turn short circuit in R-phase

Table 6.3: Feature 4 from fourth level approximate coefficients

| Faulty Phase | Feature 4 | | | |
|---|---|---|---|---|
| | 2-turn short circuit | 4-turn short circuit | 6-turn short circuit | 8-turn short circuit |
| Rfaultsim | 1.033704137 | 1.144667577 | 1.222547031 | 1.358542172 |
| Yfaultsim | 0.920199876 | 1.155779873 | 1.253613051 | 1.430107598 |
| Yfaultsim | 0.990207341 | 1.162978797 | 1.181858508 | 1.417702387 |
| Rfault prac | 1.070851345 | 1.112396703 | 1.190610055 | 1.890531044 |
| Yfault prac | 1.084232481 | 1.194048079 | 1.212579815 | 1.921602236 |
| Bfault prac | 1.100641357 | 1.108734934 | 1.157378489 | 1.910163369 |

mean energy values of various levels of stator inter-turn faults in R-phase. From this figure, it is clear that the severity level segregation is possible from variation in mean energy of fourth level approximate coefficients for various levels of stator inter-turn faults in R-phase. The variations in feature 4 for various levels of stator inter-turn faults in various phases of simulation and experimental cases are tabulated in Table 6.3. Figures 6.7 illustrates the variations in feature 4 for stator inter-turn faults in R-phase under various operating conditions such as no-load, 50% load, 100% load

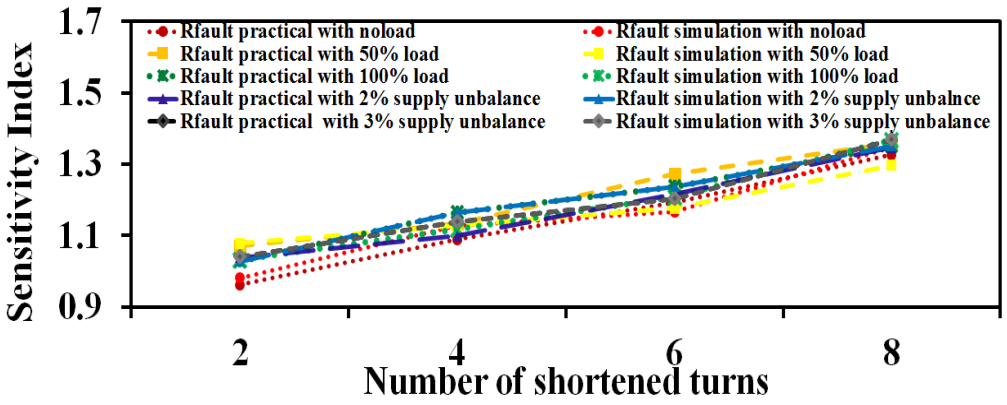


Figure 6.7: Variation in feature 4 for stator inter-turn fault in R-phase

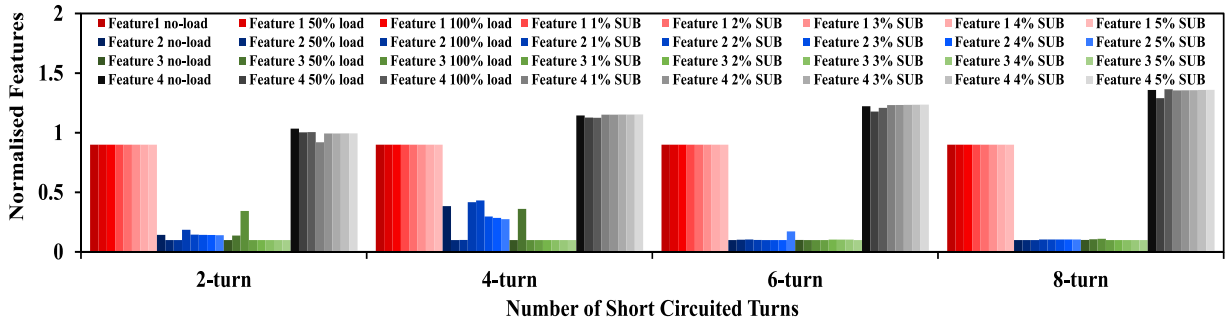


Figure 6.8: Variation in features for various level of stator inter-turn fault in R-phase

2% supply unbalance and 3% supply unbalance of simulation and experimental cases for a 3-hp induction motor.

The variations in feature 1, feature 2, feature 3 and feature 4 w.r.t the various severity levels of stator inter-turn faults like 2-turn, 4-turn, 6-turn and 8-turn faults of stator winding in R-phase under various operating conditions such as no-load, 50% of full load, 100% load, and supply unbalances from 1% to 5% are shown in figure 6.8. Similarly, figures 6.9 and 6.10 show the variations in features w.r.t the various severity levels of stator inter-turn fault in Y-phase and B-phase respectively. These figures provide evidence to the fact that the selected features are insensitive to the supply unbalance and load conditions. Hence, the selected features are

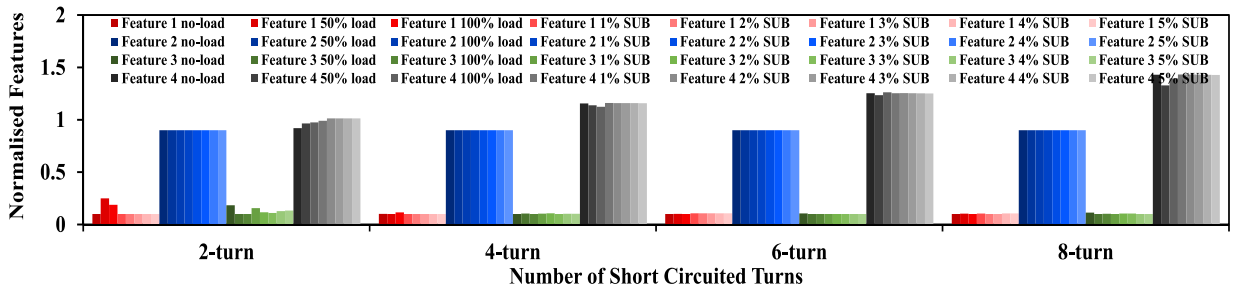


Figure 6.9: Variation in features for various level of stator inter-turn fault in Y-phase

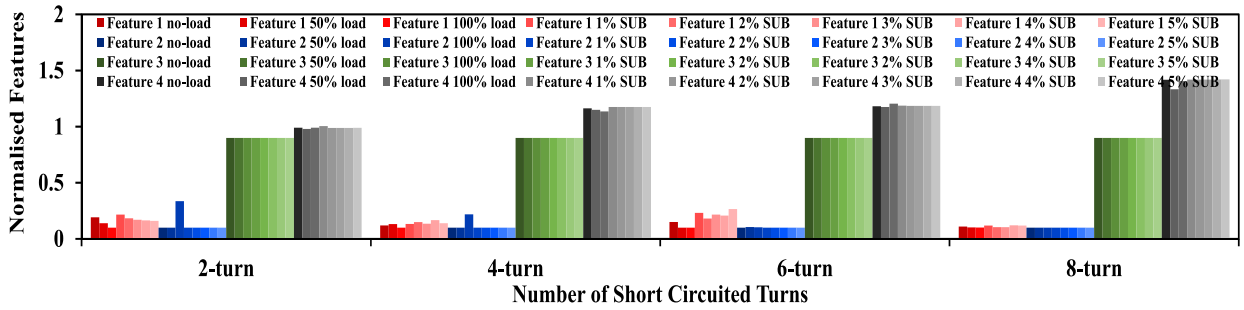


Figure 6.10: Variation in features for various level of stator inter-turn fault in B-phase

strong enough in segregating the stator inter-turn faults.

## 6.3 Proposed ANN based classifier for identification of faulty phase and estimation of fault severity of stator inter-turn faults

The proposed identifier (ANN-3) is modelled with four inputs and twelve outputs for identifying the stator inter-turn faults and its severity level. Figure **??** shows the configuration of ANN based identifier (ANN-3) for identifying faulty phase and severity level of stator inter-turn faults on a three-phase induction motor. The faulty phase and severity level identifier is triggered when the output of ANN-1 of $C_6$ becomes one. The features fed to the ANN-3 are the slope of detail level coefficients of absolute peak

values of three phase residue currents and ratio of post fault to pre-fault mean values of fourth level approximate coefficients. The twelve classes of outputs of ANN-3 are as follows:

$F_1$ →2-turns short circuit in R phase

$F_2$ →4-turns short circuit in R phase

$F_3$ →6-turns short circuit in R phase

$F_4$ →8-turns short circuit in R phase

$F_5$ →2-turns short circuit in Y phase

$F_6$ →4-turns short circuit in Y phase

$F_7$ →6-turns short circuit in Y phase

$F_8$ →8-turns short circuit in Y phase

$F_9$ →2-turns short circuit in B phase

$F_{10}$ →4-turns short circuit in B phase

$F_{11}$ →6-turns short circuit in B phase

$F_{12}$ →8-turns short circuit in B phase

### 6.3.1 Training and testing of the proposed ANN based method (ANN-3)

ANN-3 is simulated in MATLAB with an activation functions of a tangent sigmoid (tansig) and log sigmoid (logsig) and training goal is set at $10^{-6}$. Number of training and testing patterns used to train and test ANN-3 are tabulated in Table 6.4. Out of 762 patterns, 504 patterns are utilized for training the classifier and the remaining 258 patterns are used for testing. Approximately two thirds of the data set is used for training and one thirds of the data set is used for testing.

The performance of several multilayer neural network configurations

Table 6.4: Training and testing patterns used in ANN-3

| Type of stator phase fault | No. of training patterns | | No. of testing patterns | |
|---|---|---|---|---|
| | Exp | Sim | Exp | Sim |
| 2-turns short in R phase | 6 | 36 | 3 | 18 |
| 4-turns short in R phase | 6 | 36 | 3 | 19 |
| 6-turns short in R phase | 6 | 36 | 3 | 19 |
| 8-turns short in R phase | 6 | 36 | 3 | 18 |
| 2-turns short in Y phase | 6 | 36 | 3 | 18 |
| 4-turns short in Y phase | 6 | 36 | 3 | 19 |
| 6-turns short in Y phase | 6 | 36 | 3 | 19 |
| 8-turns short in Y phase | 6 | 36 | 3 | 18 |
| 2-turns short in B phase | 6 | 36 | 3 | 18 |
| 4-turns short in B phase | 6 | 36 | 3 | 19 |
| 6-turns short in B phase | 6 | 36 | 3 | 19 |
| 8-turns short in B phase | 6 | 36 | 3 | 18 |
| Total | 72 | 432 | 36 | 222 |
| | 504 | | 258 | |

are studied using MATLAB/Simulink. Among all, the best performed configuration of multilayer neural network ANN-3 as 3 (input neurons), 5 (hidden neurons), 9 (hidden neurons) and 12 (output neurons). Figure **??** shows the pconfiguration of best performed multi layer neural network ANN-3. he confusion matrix for the classifier ANN-3 is shown in Table6.5. From Table6.5 the accuracy of the classifier is 95.73%. This result proved the efficacy of the proposed ANN-3.

Table 6.5: Confusion matrix for ANN-3

| | $F_1$ | $F_2$ | $F_3$ | $F_4$ | $F_5$ | $F_6$ | $F_7$ | $F_8$ | $F_9$ | $F_{10}$ | $F_{11}$ | $F_{12}$ |
|---|---|---|---|---|---|---|---|---|---|---|---|---|
| $F_1$ | 21 | 0 | 0 | 0 | 0 | 0 | 0 | 0 | 0 | 0 | 0 | 0 |
| $F_2$ | 0 | 21 | 0 | 0 | 0 | 1 | 0 | 0 | 0 | 0 | 0 | 0 |
| $F_3$ | 0 | 0 | 22 | 0 | 0 | 0 | 0 | 0 | 0 | 0 | 0 | 0 |
| $F_4$ | 0 | 0 | 0 | 21 | 0 | 0 | 0 | 0 | 0 | 0 | 0 | 0 |
| $F_5$ | 0 | 0 | 0 | 0 | 20 | 0 | 0 | 0 | 1 | 0 | 0 | 0 |
| $F_6$ | 0 | 0 | 0 | 0 | 0 | 22 | 0 | 0 | 0 | 0 | 0 | 0 |
| $F_7$ | 0 | 0 | 0 | 0 | 0 | 2 | 20 | 0 | 0 | 0 | 0 | 0 |
| $F_8$ | 0 | 0 | 0 | 0 | 0 | 0 | 0 | 21 | 0 | 0 | 0 | 0 |
| $F_9$ | 0 | 1 | 0 | 0 | 0 | 0 | 0 | 0 | 19 | 1 | 0 | 0 |
| $F_{10}$ | 0 | 0 | 0 | 0 | 0 | 0 | 0 | 0 | 0 | 21 | 1 | 0 |
| $F_{11}$ | 0 | 0 | 0 | 0 | 0 | 0 | 0 | 0 | 0 | 3 | 19 | 0 |
| $F_{12}$ | 0 | 0 | 0 | 0 | 0 | 0 | 0 | 1 | 0 | 0 | 0 | 20 |

Overall accuracy = 95.73%

## 6.4 Proposed MNN based classifier for identification of faulty phase and estimation of fault severity of stator inter-turn faults

A modular structure of neural network (NN) is implemented for identification of faulty phase and estimation of fault severity of stator inter-turn faults on a three-phse induction motor. Figure 6.11 shows the MNN configuration for stator inter-turn faults identifier (MNN-3).

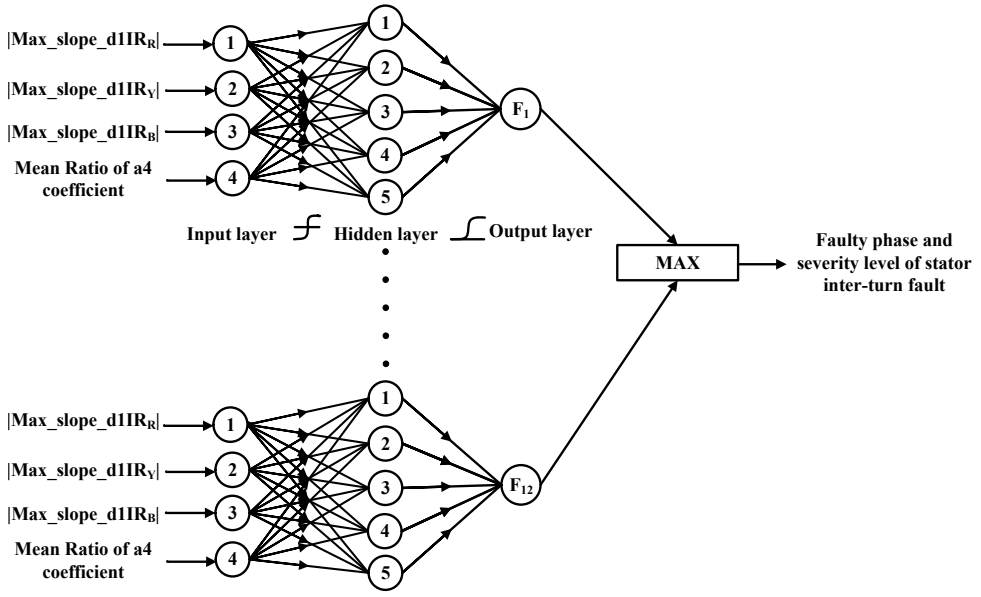


Figure 6.11: Proposed MNN-3 classifier dentification of faulty phase and estimation of fault severity of stator inter-turn faults

### 6.4.1 Training and testing of the proposed MNN based classifier (MNN-3)

Same training and testing data sets that are used for ANN-3, are also used to train and test the modular neural network respectively. Twelve types of severity levels of stator inter-turn faults have been considered for identification, 12 modules of NN are used to form one modular neural network (MNN-3). Each module of MNN-3 classifier identifies one class. Table 6.6 shows the performance of MNN-3. The overall accuracy of the classifier of MNN-3 is 94.64% and this performance is achieved within 4 sec. The results proved that the performance of classifier MNN-3 is better when compared with that of classifier ANN-3.

Table 6.6: Confusion matrix for MNN-3

| | $F_1$ | $F_2$ | $F_3$ | $F_4$ | $F_5$ | $F_6$ | $F_7$ | $F_8$ | $F_9$ | $F_{10}$ | $F_{11}$ | $F_{12}$ |
|---|---|---|---|---|---|---|---|---|---|---|---|---|
| $F_1$ | 21 | 0 | 0 | 0 | 0 | 0 | 0 | 0 | 0 | 0 | 0 | 0 |
| $F_2$ | 0 | 21 | 1 | 0 | 0 | 0 | 0 | 0 | 0 | 0 | 0 | 0 |
| $F_3$ | 0 | 0 | 22 | 0 | 0 | 0 | 0 | 0 | 0 | 0 | 0 | 0 |
| $F_4$ | 0 | 0 | 0 | 21 | 0 | 0 | 0 | 0 | 0 | 0 | 0 | 0 |
| $F_5$ | 0 | 0 | 0 | 0 | 20 | 0 | 0 | 0 | 0 | 1 | 0 | 0 |
| $F_6$ | 0 | 0 | 0 | 0 | 0 | 22 | 0 | 0 | 0 | 0 | 0 | 0 |
| $F_7$ | 0 | 0 | 0 | 0 | 0 | 2 | 20 | 0 | 0 | 0 | 0 | 0 |
| $F_8$ | 0 | 0 | 1 | 0 | 0 | 0 | 0 | 20 | 0 | 0 | 0 | 0 |
| $F_9$ | 0 | 0 | 0 | 0 | 0 | 1 | 0 | 0 | 20 | 0 | 0 | 0 |
| $F_{10}$ | 0 | 0 | 0 | 0 | 0 | 0 | 0 | 0 | 0 | 22 | 0 | 0 |
| $F_{11}$ | 0 | 0 | 0 | 0 | 0 | 0 | 0 | 0 | 0 | 0 | 20 | 0 |
| $F_{12}$ | 0 | 0 | 0 | 0 | 0 | 0 | 0 | 0 | 0 | 0 | 0 | 21 |
| Overall accuracy = 96.9% | | | | | | | | | | | | |

## 6.5 Comparison of performance between ANN-3 and MNN-3 for fault classification

Table 6.7: Performance for ANN-3 and MNN-3 in stator inter-turn fault classification

| Type of network | Type of disturbance | Sensitivity | Specificity | Average |
|---|---|---|---|---|
| ANN-3 | $F_1$ | 1 | 1 | |
| | $F_2$ | 0.954 | 0.996 | |
| | $F_3$ | 1 | 1 | |
| | $F_4$ | 1 | 1 | Specificity: 0.957 |
| | $F_5$ | 0.952 | 1 | |
| | $F_6$ | 1 | 0.987 | |
| | $F_7$ | 0.909 | 1 | |
| | $F_8$ | 1 | 0.996 | |
| | $F_9$ | 0.905 | 0.996 | Specificity: 0.996 |
| | $F_{10}$ | 0.954 | 0.983 | |
| | $F_{11}$ | 0.864 | 0.995 | |
| | $F_{12}$ | 0.952 | 1 | |
| MNN-3 | $F_1$ | 1 | 1 | |
| | $F_2$ | 0.954 | 1 | |
| | $F_3$ | 1 | 0.991 | |
| | $F_4$ | 1 | 1 | Specificity: 0.969 |
| | $F_5$ | 0.952 | 1 | |
| | $F_6$ | 1 | 0.987 | |
| | $F_7$ | 0.909 | 1 | |
| | $F_8$ | 0.952 | 1 | |
| | $F_9$ | 0.952 | 1 | Specificity: 0.997 |
| | $F_{10}$ | 1 | 0.987 | |
| | $F_{11}$ | 0.909 | 1 | |
| | $F_{12}$ | 1 | 1 | |

The performances of ANN-3 and MNN-3 are compared based on the specific measures that is sensitivity and specificity. Table 6.7 shows the values of sensitivity and specificity for ANN-3 and MNN-3 corresponding to 12 types of stator inter-turn faults. The average sensitivity of MNN-3 is 0.969 and average specificity is 0.997 which are better than those of ANN-3. The results proved that the modular neural network based classifiers are better when compared to neural network based classifiers in identifying faulty phase and estimating the severity level of stator inter-turn fault.

## 6.6 Conclusions

In this chapter the procedure for extraction of features and two proposed classifiers based on neural networks and modular neural networks for classifying stator inter-turn faults are explained. The four features, that are used as inputs to classifiers, are insensitive to the supply unbalances and load conditions. From the performance results of two classifiers ANN-3 and MNN-3, the following conclusions are drawn.

The multi layer classifier of ANN-3 attains an accuracy of 95.73% with minimum number of features. To improve the performance of the classifier further a modular concept is introduced and an overall accuracy of 96.9% is achieved. The results revealed that there is an improvement in the accuracy by 1.17% when MNN-3 is used in place of ANN-3 for classifying stator inter-turn fault.

# Chapter 7

# Conclusions and Future Scope

## 7.1 Conclusions

Rapid industrialization enhances the usage of induction motors especially in processes industries. To improve the reliability of motors, for a good return on investment, they need continuous condition monitoring. A reliable condition monitoring method for detecting, classifying and identifying the supply side faults and stator winding insulation faults at the earliest without effecting the motor operation, is the focus on this thesis.

Common types of faults and their root causes in induction motor are studied in this research work. Various types of model and model-free techniques are reviewed and summarized in this thesis. From the literature survey, it is inferred that till now there is no algorithm for detecting multiple faults with single diagnosis technique and minimum number of measurements and features. Even though the multi function digital relays are responding well but it does not respond to the incipient faults in presence of supply unbalance and machine unbalances. Hence, in this thesis, an attempt has been made to propose reliable fault diagnosis schemes for a three-phase induction motor with a focus on detection,

classification and identification of various faults such as stator winding insulation faults and supply side faults. The present research is organized into five stages.

The first stage of research work focuses on development of distributed parameter model and its validation for a three-phase induction motor. The distributed parameters are estimated physically for a 5-hp and 3-hp induction motors by conducting no-load, blocked rotor, differential mode and common mode tests, as presented in chapter 2. The model is validated by comparing the frequency responses obtained from simulation and experimental setup. The results proved that the developed distributed parameter model is applicable for transient analysis.

The second stage of research work focuses on fault detection algorithms based on three-phase current measurements and wavelet analysis. Using the developed model, the stator winding insulation faults and supply side faults in an induction machine are simulated, by taking into account various fault switching instants, in MATLAB/Simulink environment. The DWT based fault detection algorithm is validated through simulation data and proved to be effective in detecting the faults. This algorithm fails to detect the fault under noisy conditions. For more realistic study, another fault detection algorithm based on SWT and DWT is considered. The sequence of steps for fault detection using this method is signal reconstruction (using SWT), decomposition (using DWT), and calculation of fault index and adaptive threshold. The observations made from the reconstruction of the captured signals indicated that the SWT has clear advantage over the DWT to extract the fault residues in the presence of noise and supply unbalances. The instant at which disturbance starts can be

identified accurately by comparing the fault indices with adaptive threshold and count value as discussed in chapter 3. Experimental setup is built with two three-phase induction motor machines of 3-hp and 10-hp ratings. The stator winding faults are created by short circuiting the tap points, which are already brought from each phase of the winding. The effectiveness of the proposed SWT and DWT based fault detection algorithm is verified by simulation and experimental data as presented in chapter 3. The results proved that the proposed SWT and DWT based fault detection algorithm is insensitive to the operating conditions because of adaptive threshold logic.

Classification of disturbances in a three-phase induction motor is discussed in the third stage. Two classifiers are implemented in MATLAB/Simulink to classify various faults. One classifier is based on ANN and another one is based on modular neural network (MNN). Nine features are selected to classify 6 types of disturbances on a three-phase induction motor. The normalised features are fed as input to the ANN disturbance classifier and various structures of ANN are considered for finding best performed ANN structure. The best performance is achieved by using double multilayer ANN as presented in chapter 3. The results demonstrates that the proposed algorithm classifies the disturbances irrespective of operating conditions. However, the accuracy of the classifier is observed to 92.31%, which is not satisfactory. Hence, the modular concept is introduced to NN for enhancing efficacy and reducing task complexity of the disturbance classifier. The results proved that the performance of MNN in disturbance classification is significantly higher as compared to that of ANN and an increase in performance by 2.33% in overall accuracy, 8% in sensitivity, and 0.7% in specificity, is achieved in

minimum time as demonstrated in chapter 3.

The fourth stage of research focuses on classification of stator phase faults using two methods, one based on ANN and the other one based on MNN. Six types of phase faults are classified with only three features, which are extracted from slope of detail level coefficients. The performance of MNN in stator phase faults classification is accurate, simple and insensitive to the operating conditions because of self normalised features. The results proved that the performance of MNN classifier of stator phase faults is higher than ANN classifier for stator phase faults and an increase in performance by 4.55% in overall accuracy, 4.85% in sensitivity and 0.9% in specificity is observed. The details are given in Chapter 4..

Finally, identifiers are developed for identification of faulty phase and severity level of stator inter-turn faults based on ANN and MNN. Experimentations and exhaustive simulation studies are conducted to check reliability of the proposed identifiers. Identifying the faulty phase and severity level of stator inter-turn faults using features of slope of detail level coefficients of absolute peak values of three phase residue currents and ratio of post fault and pre-fault mean energy values of $4^{th}$ level approximate coefficients. The results are found to be efficient and reliable because these feature are insensitive to the operating conditions. The performance of MNN is better than that of ANN in identifying faulty phase and severity level of stator inter-turn faults. An increase in performance by 1.17% in accuracy, 1.15% in sensitivity and 0.1% in specificity is observed for MNN based identifier when compared with the performance of ANN based identifier.

## 7.2 Future Scope

The proposed algorithms were tested on practical induction motors of 3-hp and 10-hp. These schemes can be extended to be part of on-line condition monitoring and to be assessed for various operating conditions faced by the induction motor during its life time.

The proposed protection schemes are tested only on low voltage motors. The same methodologies can also be extended to medium and high voltage motors with further study.

The proposed techniques can be extended to generators as well, but it requires further study.

# Bibliography

[1] R. Bell, D. McWilliams, P. O'donnell, C. Singh, and S. Wells, "Report of large motor reliability survey of industrial and commercial installations. i," *IEEE Transactions on Industry applications*, vol. 21, no. 4, pp. 853–864, 1985.

[2] R. Bell, C. Heising, P. O'donnell, C. Singh, and S. Wells, "Report of large motor reliability survey of industrial and commercial installations. ii," *IEEE Transactions on Industry applications*, vol. 21, no. 4, pp. 865–872, 1985.

[3] W. Kersting and W. Phillips, "Phase frame analysis of the effects of voltage unbalance on induction machines," *IEEE transactions on Industry Applications*, vol. 33, no. 2, pp. 415–420, 1997.

[4] M. El Hachemi Benbouzid, "A review of induction motors signature analysis as a medium for faults detection," *IEEE Transactions on Industrial Electronics*, vol. 47, no. 5, pp. 984–993, 2000.

[5] A. Siddique, G. Yadava, and B. Singh, "A review of stator fault monitoring techniques of induction motors," *IEEE Transactions on Energy conversion*, vol. 20, no. 1, pp. 106–114, 2005.

[6] S. Nandi, H. A. Toliyat, and X. Li, "Condition monitoring and fault diagnosis of electrical motors-a review," *IEEE Transactions on Energy Conversion*, vol. 20, no. 4, pp. 719–729, 2005.

[7] S. Grubic, J. M. Aller, B. Lu, and T. G. Habetler, "A survey on testing and monitoring methods for stator insulation systems of low-voltage induction machines focusing on turn insulation problems," *IEEE Transactions on Industrial Electronics*, vol. 55, no. 12, pp. 4127–4136, 2008.

[8] S. Ding, *Model-based fault diagnosis techniques: design schemes, algorithms, and tools*. Springer Science & Business Media, 2008.

[9] S. Bachir, S. Tnani, J.-C. Trigeassou, and G. Champenois, "Diagnosis by parameter estimation of stator and rotor faults occurring in induction machines," *IEEE Transactions on Industrial Electronics*, vol. 53, no. 3, pp. 963–973, 2006.

[10] S. Bachir, S. Tnani, T. Poinot, and J. Trigeassou, "Stator fault diagnosis in induction machines by parameter estimation," *IEEE International SDEMPED01*, pp. 235–239, 2001.

[11] J. Gertler, "Fault detection and isolation using parity relations," *Control engineering practice*, vol. 5, no. 5, pp. 653–661, 1997.

[12] I. Hwang, S. Kim, Y. Kim, and C. E. Seah, "A survey of fault detection, isolation, and reconfiguration methods," *IEEE Transactions on Control Systems Technology*, vol. 18, no. 3, pp. 636–653, 2010.

[13] J. Gertler, *Fault detection and diagnosis in engineering systems*. CRC press, 1998.

[14] R. Isermann, *Fault-diagnosis systems: an introduction from fault detection to fault tolerance*. Springer Science & Business Media, 2006.

[15] R. N. Clark, D. C. Fosth, and V. M. Walton, "Detecting instrument malfunctions in control systems," *IEEE Transactions on Aerospace and Electronic Systems*, no. 4, pp. 465–473, 1975.

[16] R. Isermann, "Process fault detection based on modeling and estimation methodsa survey," *Automatica*, vol. 20, no. 4, pp. 387–404, 1984.

[17] R. K. Mehra and J. Peschon, "An innovations approach to fault detection and diagnosis in dynamic systems," *Automatica*, vol. 7, no. 5, pp. 637–640, 1971.

[18] R. Isermann, "Fault diagnosis of machines via parameter estimation and knowledge processingtutorial paper," *Automatica*, vol. 29, no. 4, pp. 815–835, 1993.

[19] P. Zhang, Y. Du, T. G. Habetler, and B. Lu, "A survey of condition monitoring and protection methods for medium-voltage induction motors," *IEEE Transactions on Industry Applications*, vol. 47, no. 1, pp. 34–46, 2011.

[20] M. E. H. Benbouzid, "A review of induction motors signature analysis as a medium for faults detection," *IEEE transactions on industrial electronics*, vol. 47, no. 5, pp. 984–993, 2000.

[21] P. Tavner, "Review of condition monitoring of rotating electrical machines," *IET Electric Power Applications*, vol. 2, no. 4, pp. 215–247, 2008.

[22] B.-S. Yang and K. J. Kim, "Application of dempster–shafer theory in fault diagnosis of induction motors using vibration and current signals," *Mechanical Systems and Signal Processing*, vol. 20, no. 2, pp. 403–420, 2006.

[23] O. N. G. S Gunal, D G Ece, "Induction machine condition monitoring using notch-filtered motor current," *Mechanical Systems and Signal Processing*, vol. 23, pp. 2658–2670, 2009.

[24] Y. Lei, Z. He, and Y. Zi, "A new approach to intelligent fault diagnosis of rotating machinery," *Expert Systems with Applications*, vol. 35, no. 4, pp. 1593–1600, 2008.

[25] A. Bellini, F. Filippetti, C. Tassoni, and G.-A. Capolino, "Advances in diagnostic techniques for induction machines," *IEEE Transactions on Industrial Electronics*, vol. 12, no. 55, pp. 4109–4126, 2008.

[26] F. Immovilli, M. Cocconcelli, A. Bellini, and R. Rubini, "Detection of generalized-roughness bearing fault by spectral-kurtosis energy of vibration or current signals," *IEEE Transactions on Industrial Electronics*, vol. 56, no. 11, pp. 4710–4717, 2009.

[27] S. Rajagopalan, J. M. Aller, J. A. Restrepo, T. G. Habetler, and R. G. Harley, "Detection of rotor faults in brushless dc motors operating under nonstationary conditions," *IEEE Transactions on Industry Applications*, vol. 42, no. 6, pp. 1464–1477, 2006.

[28] V. Climente-Alarcon, J. Antonino-Daviu, M. Riera-Guasp, J. Pons-Llinares, J. Roger-Folch, P. Jover-Rodriguez, and A. Arkkio, "Transient tracking of low and high-order eccentricity-related components in induction motors via tfd tools," *Mechanical Systems and Signal Processing*, vol. 25, no. 2, pp. 667–679, 2011.

[29] V. Climente-Alarcon, J. Antonino-Daviu, M. Riera-Guasp, R. Puche-Panadero, and L. Escobar, "Application of the wigner–ville distribution for the detection of rotor asymmetries and eccentricity through high-order harmonics," *Electric Power Systems Research*, vol. 91, pp. 28–36, 2012.

[30] M. Blodt, D. Bonacci, J. Regnier, M. Chabert, and J. Faucher, "On-line monitoring of mechanical faults in variable-speed induction motor drives using the wigner distribution," *IEEE Transactions on Industrial Electronics*, vol. 55, no. 2, pp. 522–533, 2008.

[31] M. Blodt, J. Regnier, and J. Faucher, "Distinguishing load torque oscillations and eccentricity faults in induction motors using stator current wigner distributions," *IEEE Transactions on Industry Applications*, vol. 45, no. 6, pp. 1991–2000, 2009.

[32] Z. Peng and F. Chu, "Application of the wavelet transform in machine condition monitoring and fault diagnostics: a review with bibliography," *Mechanical systems and signal processing*, vol. 18, no. 2, pp. 199–221, 2004.

[33] S. G. Mallat, "A theory for multiresolution signal decomposition: the wavelet representation," *IEEE transactions on pattern analysis and*

*machine intelligence*, vol. 11, no. 7, pp. 674–693, 1989.

[34] J. Pons-Llinares, J. A. Antonino-Daviu, M. Riera-Guasp, M. Pineda-Sanchez, and V. Climente-Alarcon, "Induction motor diagnosis based on a transient current analytic wavelet transform via frequency b-splines," *IEEE Transactions on Industrial Electronics*, vol. 58, no. 5, pp. 1530–1544, 2011.

[35] A. Graps, "An introduction to wavelets," *IEEE computational science and engineering*, vol. 2, no. 2, pp. 50–61, 1995.

[36] M. A. Awadallah and M. M. Morcos, "Application of ai tools in fault diagnosis of electrical machines and drives-an overview," *IEEE Transactions on energy conversion*, vol. 18, no. 2, pp. 245–251, 2003.

[37] X. Z. Gao and S. J. Ovaska, "Soft computing methods in motor fault diagnosis," *Applied soft computing*, vol. 1, no. 1, pp. 73–81, 2001.

[38] M. Ghazal and J. Poshtan, "Robust stator winding fault detection in induction motors," in *Power Electronics, Drive Systems and Technologies Conference (PEDSTC), 2011 2nd*. IEEE, 2011, pp. 163–168.

[39] M. S. Ballal, Z. J. Khan, H. M. Suryawanshi, and R. L. Sonolikar, "Adaptive neural fuzzy inference system for the detection of inter-turn insulation and bearing wear faults in induction motor," *IEEE Transactions on Industrial Electronics*, vol. 54, no. 1, pp. 250–258, 2007.

[40] S. Altug, M.-Y. Chen, and H. J. Trussell, "Fuzzy inference systems implemented on neural architectures for motor fault detection and

diagnosis," *IEEE transactions on industrial electronics*, vol. 46, no. 6, pp. 1069–1079, 1999.

[41] P. Akhlaghi, A. R. Kashanipour, and K. Salahshoor, "Complex dynamical system fault diagnosis based on multiple anfis using independent component," in *Control and Automation, 2008 16th Mediterranean Conference on*. IEEE, 2008, pp. 1798–1803.

[42] P. V. Goode and M.-Y. Chow, "Using a neural/fuzzy system to extract heuristic knowledge of incipient faults in induction motors. part i-methodology," *IEEE Transactions on Industrial Electronics*, vol. 42, no. 2, pp. 131–138, 1995.

[43] G. Auda, M. Kamel, and H. Raafat, "Modular neural network architectures for classification," in *Neural Networks, 1996., IEEE International Conference on*, vol. 2. IEEE, 1996, pp. 1279–1284.

[44] B.-L. Lu and M. Ito, "Task decomposition and module combination based on class relations: a modular neural network for pattern classification," *IEEE Transactions on Neural Networks*, vol. 10, no. 5, pp. 1244–1256, 1999.

[45] G. M. Joksimovic and J. Penman, "The detection of inter-turn short circuits in the stator windings of operating motors," *IEEE Transactions on Industrial Electronics*, vol. 47, no. 5, pp. 1078–1084, 2000.

[46] S. Mallat, *A wavelet tour of signal processing*. Academic press, 1999.

[47] T. W. Chow and S. Hai, "Induction machine fault diagnostic analysis with wavelet technique," *IEEE Transactions on Industrial Electronics*, vol. 51, no. 3, pp. 558–565, 2004.

[48] R. A. K. G. B. Kliman, W. J. Premerlani and D. Hoeweler, "A new approach to on-line turn fault detection in ac motors," *in Conf. Rec. 31st, IEEE IAS Annu. Meeting*, vol. vol. 1, pp. pp. 687–693, 1996.

[49] B. Mirafzal and N. A. Demerdash, "On innovative methods of induction motor inter-turn and broken-bar fault diagnostics," in *IEEE International Conference on Electric Machines and Drives, 2005.* IEEE, 2005, pp. 762–769.

[50] S. M. Cruz and A. M. Cardoso, "Stator winding fault diagnosis in three-phase synchronous and asynchronous motors, by the extended park's vector approach," *IEEE Transactions on Industry applications*, vol. 37, no. 5, pp. 1227–1233, 2001.

[51] A. M. Da Silva, R. J. Povinelli, and N. A. Demerdash, "Induction machine broken bar and stator short-circuit fault diagnostics based on three-phase stator current envelopes," *IEEE Transactions on Industrial Electronics*, vol. 55, no. 3, pp. 1310–1318, 2008.

[52] B. Mirafzal, R. J. Povinelli, and N. A. Demerdash, "Interturn fault diagnosis in induction motors using the pendulous oscillation phenomenon," *IEEE Transactions on Energy Conversion*, vol. 21, no. 4, pp. 871–882, 2006.

[53] C. H. De Angelo, G. R. Bossio, S. J. Giaccone, M. I. Valla, J. A. Solsona, and G. O. García, "Online model-based stator-fault detection and identification in induction motors," *IEEE Transactions on Industrial Electronics*, vol. 56, no. 11, pp. 4671–4680, 2009.

[54] S. Nandi and H. A. Toliyat, "Novel frequency-domain-based technique to detect stator interturn faults in induction machines using stator-induced voltages after switch-off," *IEEE Transactions on Industry Applications*, vol. 38, no. 1, pp. 101–109, 2002.

[55] M. K. Khan and M. Rahman, "Discrete wavelet transform based detection of disturbances in induction motors," in *2006 International Conference on Electrical and Computer Engineering*. IEEE, 2006, pp. 462–465.

[56] M. Khan, T. S. Radwan, and M. A. Rahman, "Real-time implementation of wavelet packet transform-based diagnosis and protection of three-phase induction motors," *IEEE Transactions on Energy Conversion*, vol. 22, no. 3, pp. 647–655, 2007.

[57] O. Hernández and E. Olvera, "Noise cancellation on ecg and heart rate signals using the undecimated wavelet transform," in *International Conference on eHealth, Telemedicine, and Social Medicine, 2009. eTELEMED'09.* IEEE, 2009, pp. 145–150.

[58] N. Akshay, N. A. V. Jonnabhotla, N. Sadam, and N. D. Yeddanapudi, "Ecg noise removal and qrs complex detection using uwt," in *International Conference on Electronics and Information Engineering (ICEIE), 2010*, vol. 2. IEEE, 2010, pp. V2–438.

[59] "Ieee standard test procedure for polyphase induction motors and generators," *IEEE Power Engineering Society Sponsored by the Electric Machinery Committee*, 2004.

[60] B. Mirafzal, G. Skibinski, R. Tallam, D. Schlegel, and R. Lukaszewski, "Universal induction motor model with low-to-high frequency-response characteristics," *IEEE Transactions on Industry Applications*, vol. 43, no. 5, pp. 1233–1246, 2007.

[61] J. Das, "Effects of momentary voltage dips on the operation of induction and synchronous motors," *IEEE Transactions on Industry Applications*, vol. 26, no. 4, pp. 711–718, 1990.

[62] W. H. Kersting, "Causes and effects of single-phasing induction motors," *IEEE Transactions on industry applications*, vol. 41, no. 6, pp. 1499–1505, 2005.

[63] M. Sudha and P. Anbalagan, "A novel protecting method for induction motor against faults due to voltage unbalance and single phasing," in *Industrial Electronics Society, 2007. IECON 2007. 33rd Annual Conference of the IEEE*. IEEE, 2007, pp. 1144–1148.

[64] P. Albrecht, J. Appiarius, R. McCoy, E. Owen, and D. Sharma, "Assessment of the reliability of motors in utility applications-updated," *IEEE Transactions on Energy Conversion*, no. 1, pp. 39–46, 1986.

[65] M. Sin, W. Soong, and N. Ertugrul, "Induction machine on-line condition monitoring and fault diagnosis–a survey," in *Australasian Universities Power Engineering Conference*, vol. 28, 2003, pp. 1–6.

[66] R. M. Tallam, S. B. Lee, G. C. Stone, G. B. Kliman, J. Yoo, T. G. Habetler, and R. G. Harley, "A survey of methods for detection of

stator-related faults in induction machines," *IEEE Transactions on Industry Applications*, vol. 43, no. 4, pp. 920–933, 2007.

[67] M. Sifuzzaman, M. Islam, and M. Ali, "Application of wavelet transform and its advantages compared to fourier transform," 2009.

[68] W. A. Wilkinson and M. Cox, "Discrete wavelet analysis of power system transients," *IEEE Transactions on Power systems*, vol. 11, no. 4, pp. 2038–2044, 1996.

[69] A. W. Galli and O. M. Nielsen, "Wavelet analysis for power system transients," *IEEE Computer Applications in Power*, vol. 12, no. 1, pp. 16–18, 1999.

[70] O. A. Youssef, "Online applications of wavelet transforms to power system relaying," *IEEE Transactions on Power Delivery*, vol. 18, no. 4, pp. 1158–1165, 2003.

[71] H. A. Darwish, M. Hesham, A.-M. Taalab, and N. M. Mansour, "Close accord on dwt performance and real-time implementation for protection applications," *IEEE Transactions on Power Delivery*, vol. 25, no. 4, pp. 2174–2183, 2010.

[72] D. L. Donoho and I. M. Johnstone, "Threshold selection for wavelet shrinkage of noisy data," in *International Conference on Engineering Advances: New Opportunities for Biomedical Engineers 1994*. IEEE, 1994, pp. A24–A25.

[73] A. R. F. da Silva, "Wavelet denoising with evolutionary algorithms," *Digital signal processing*, vol. 15, no. 4, pp. 382–399, 2005.

[74] D. Giaouris and J. Finch, "Denoising using wavelets on electric drive applications," *Electric Power Systems Research*, vol. 78, no. 4, pp. 559–565, 2008.

[75] S. S. Refaat, H. Abu-Rub, M. Saad, E. M. Aboul-Zahab, and A. Iqbal, "Detection, diagnoses and discrimination of stator turn to turn fault and unbalanced supply voltage fault for three phase induction motors," in *Power and Energy (PECon), 2012 IEEE International Conference on*. IEEE, 2012, pp. 910–915.

[76] S. Das, P. Purkait, D. Dey, and S. Chakravorti, "Monitoring of inter-turn insulation failure in induction motor using advanced signal and data processing tools," *IEEE Transactions on Dielectrics and Electrical Insulation*, vol. 18, no. 5, pp. 1599–1608, 2011.

[77] J. Seshadrinath, B. Singh, and B. K. Panigrahi, "Single-turn fault detection in induction machine using complex-wavelet-based method," *IEEE Transactions on Industry Applications*, vol. 48, no. 6, pp. 1846–1854, 2012.

[78] M. T. C. F. T Hong and D. Hilder, "Pd classification by a modular neural network based on task decomposition," *IEEE Trans. Dielectr. Electr. Insul*, vol. 3, no. 2, pp. 207–212, 1996.

[79] A. K. P. U. Lahiri and S. Mukhopadhyaya, "Modular neural network-based directional relay for transmission line protection," *IEEE Trans. Power Systems*, vol. 20, no. 4, pp. 2154–2155, 2005.

[80] S. Das, P. Purkait, C. Koley, and S. Chakravorti, "Performance of a load-immune classifier for robust identification of minor faults in

induction motor stator winding," *IEEE Transactions on Dielectrics and Electrical Insulation*, vol. 21, no. 1, pp. 33–44, 2014.

# Publications

**Journal Papers Published:**

1. N. Rama Devi, D. V. S. S. Siva Sarma, P.V. Ramana Rao, Diagnosis and Classification of stator winding insulation faults on a three-phase induction motor using Wavelet and MNN, IEEE Transactions on Dielectrics and Electrical Insulation, Oct 2016, Vol. 23, No. 5, pp. 2543 - 2555 (DOI: 10.1109/TDEI.2016.005576).

2. N. Rama Devi, D. V. S. S. Siva Sarma, P. V. Ramana Rao, Detection and Identification of Stator Incipient Faults in Three-Phase Induction Motor - Simulation and Experimental Verification, IET Electric Power Applications, Sept 2015, Vol. 9, Iss. 8, pp. 540548 (doi: 10.1049/iet-epa.2015.0024, ISSN 1751-8660).

3. N. Rama Devi, D. V. S. S. Siva Sarma, P.V. Ramana Rao, Wavelet Based Stator Inter-Turn Faults Detection in Three-Phase Induction Motors Operated Under Noisy Condition, Journal of Electrical Engineering, Polytecnica Romenia, Vol 16, Issue 2, pp. 1 - 10 (article 16.2.2).

**Conference Papers:**

1. N. Rama Devi, D. V. S. S. Siva Sarma, P.V. Ramana Rao, Detecting and Identifying Stator Inter-Turn Faults in Three-Phase Induction Motor in Presence of Supply Unbalances, IEEE International Conference on Power Electronics, Drives and Energy Systems Conference 2014 held at IIT Bombay, Mumbai, 16th-19th December 2014.

2. N. Rama Devi, P.V. Ramana Rao, Shaik Abdul Gafoor , Wavelet ANN based Fault Diagnosis in Three Phase Induction Motor, IEEE conference on Engineering Sustainable solutions (INDICON 2011) held at BITS Pilani Hyderabad Campus, Andhra Pradesh, India December 16th-18th, 2011.

3. N. Rama Devi, Shaik Abdul Gafoor , P.V. Ramana Rao , Wavelet ANN Based Stator Internal Faults Protection Scheme for 3-Phase Induction Motor, 5th IEEE conference on Industrial Electronics and Applications held in Taichung, Taiwan on 15th 17th June 2010.